Polytechnic of Leiria
School of Technology and Management
Department of Electrical and Electronics Engineering
Master in Electrical and Electronic Engineering – Electronics and Telecommunications

DISSERTATION

SMALL ANTENNAS FOR 5G AND IOT

TIAGO EMANUEL DA SILVA OLIVEIRA

Leiria, November of 2021

This page is intentionally left blank.

Polytechnic of Leiria
School of Technology and Management
Department of Electrical and Electronics Engineering
Master in Electrical and Electronic Engineering – Electronics and Telecommunications

DISSERTATION

SMALL ANTENNAS FOR 5G AND IOT

TIAGO EMANUEL DA SILVA OLIVEIRA
Number: 2192599

Dissertation supervised by Professor Rafael F. S. Caldeirinha (rafael.caldeirinha@ipleiria.pt) and Professor João R. Reis (joao.reis@ipleiria.pt).

Leiria, November of 2021

This page is intentionally left blank.

ACKNOWLEDGMENTS

I would like to start by thanking my supervisors, Professor Rafael Caldeirinha and Professor João Reis for the time, guidance and assistance provided during this dissertation, which granted me the knowledge to complete the proposed objectives, and contribute to the knowledge and to the scientific community.

Likewise, I would like to acknowledge the School of Technology and Management of Polytechnic of Leiria and the Instituto de Telecomunicações - Leiria (IT-Leiria), for providing all the resources necessary to the development of this work, from materials to facilities and measuring equipment. I am particularly grateful to the Instituto de Telecomunicações for funding my developments realised in line with the project WSN-EM: Wireless Sensor Network for Environment Monitoring (PTDC/EEI-EEE/30539/2017).

I want to endorse the support, wisdom and tuition of my fellow colleagues at IT-Leiria Antennas and Propagation group with a special thanks to Mário Vala, Stefânia Faria and Luís Duarte for setting and maintaining an excellent work environment and friendship.

Finally, I want to dedicate this work to my family and girlfriend for their care, effort and counselling that motivated me to pursue my goals.

This page is intentionally left blank.

ABSTRACT

In this dissertation, the author's work on small form factor antennas for 5^{th} Generation of mobile network (5G), Internet of Things (IoT) and Wireless Sensor Network (WSN), is presented. After a dedicated literature review on the topic, several antennas were designed and further optimised utilising a full-wave electromagnetic solver (Computer Simulation Technology (CST)-Microwave Studio (MWS)). Three of the developed antenna designs were prototyped, tested and characterised in laboratory environment and, finally applied to a real-world scenario of a wireless sensor network.

In a first iteration, a high-gain wideband parasitic microstrip antenna, for 5G and IoT applications at 26 GHz, is presented. An antenna, composed of miniaturised parasitic patches, has been studied and optimised to operate at 26 GHz, aiming at the 5G New Radio (NR) Frequency Range 2 (FR2) band n258. The proposed antenna uses eight microstrip patches as parasitic elements, in a squared layout, surrounding a central probe-fed patch. The patches operating as parasitic elements are coupled by the magnetic and electric field created by the central active patch.

Subsequently, the development of directional antennas, for WSN Base Station (BS), is performed. In particular, two antenna designs have need studied: a microstrip Quasi-Yagi antenna followed by a enhanced lunar waning crescent Quasi-Yagi antenna. The latter, considered as a novel antenna design, follows the planar Quasi-Yagi concept and employs a microstrip dipole as the driven element and, waning crescent shaped reflector and directors, to manipulate the shape of the radiation pattern. The antenna is designed and optimised to operate in the 2.4 GHz ISM band, attending the ease of integration in a multi-sector BS antenna configuration.

A small differential slotted microstrip patch antenna to be implemented in a sensor node operating at 2.4 GHz, is also proposed. This particular antenna design takes advantage of slotted resonant elements to reduce its overall size. In particular, specific project requirements, such as: resonating frequency, gain, Half-Power Beam-Width (HPBW) are taken into consideration when dimensioning the antenna. Further studies on the impact of vegetation and fire on the antenna performance are carried out. The simulations were performed using CST-MWS mimicking several application scenarios: involved by soil, vegetation and fire, approximating the model to a real case scenario of a wildfire.

Finally, the implementation of a WSN based on WiFi protocol and using LoPy4 transceivers, is proposed. The WSN is composed of a multi-sector base station

and several sensor nodes used for environmental monitoring. The antenna previously developed have been used in the BS and sensor nodes implementation. The implementation and performance assessment of such network in real scenarios is presented, and metrics such as area coverage and max range are determined in the field.

Keywords: 5G, IoT, WSN, Base Station, Sensor node, Antenna, Wildfire.

TABLE OF CONTENTS

This page is intentionally left blank.

LIST OF FIGURES

LIST OF TABLES

This page is intentionally left blank.

LIST OF ACRONYMS

3GPP	3^{rd} Generation Partnership Project.
4G	4^{th} Generation of mobile network.
5G	5^{th} Generation of mobile network.
ACL	Asynchronous Connection-Less.
BLE	Bluetooth Low Energy.
BS	Base Station.
CPW	Coplanar Waveguide.
CPWG	Coplanar Waveguide with Ground.
CST	Computer Simulation Technology.
DC	Direct Current.
DUT	Device Unter Test.
EPC	Enveloped Packed Core.
ETSI	European Telecommunications Standards Institute.
FOV	Field of View.
FR2	Frequency Range 2.
Gbps	Gigabits per Second.
HPBW	Half-Power Beam-Width.
IEEE	Institute of Electrical and Electronics Engineers.
IoT	Internet of Things.
ISM	Industrial, Sientific and Medical.
LPWAN	Low-Power Wide Area Networks.
LTE	Long Term Evolution.
MAC	Media Acess Control.
Mbps	Megabits per Second.
MIMO	Massive Input Massive Output.
mm-Waves	Millimeter-Waves.
MWS	Microwave Studio.
NR	New Radio.

PCB	Printed Circuit Board.
PHY	Physical Layer.
Rel-15	Release 15.
Rel-16	Release 16.
Rel-17	Release 17.
RF	Radio Frequency.
RSSI	Recieved Signal Strength Indicator.
Rx	Receiver.
SCO	Synchronous Connection-Oriented.
SHF	Super High Frequency.
SN	Sensor Node.
TEM	Transverse Electro-Magnetic.
Tx	Transmitter.
URLLC	Ultra-Reliable Low Latency Communucations.
VNA	Vector Network Analyser.
WLAN	Wireless Local Area Network.
WSN	Wireless Sensor Network.

1

INTRODUCTION

1.1 BACKGROUND OF STUDY AND MOTIVATION

The 5^{th} Generation of mobile network (5G) has been the focus of research in the past few years and is nowadays being deployed worldwide [1], promising high data rates, low latency and the usage of new frequency bands. The key concept of 5G is to provide a highly flexible and scalable network technology for connecting everyone and everything, everywhere. Internet of Things (IoT), on the other hand, aims to connect every single device (or "Thing") over the internet, allowing the exchange of data between users and other devices. IoT is then well aligned with the 5G mindset [2], [3], with some 5G standards being developed promoting the interoperability with IoT.

Wireless Sensor Network (WSN), seen has an particular case of IoT networks, are nowadays widely implemented [4], due to the their versatility, often being offered as a solution for monitoring networks, in the field of: environmental monitoring [5], security [6], health [7], agriculture [8], hazard detection [9], among many others. A WSN comprises a collection of a large number of Sensor Node (SN), that are scattered in a certain monitoring area [10] and, a Base Station (BS) which collects the nearby environment data and forward it to higher layer network or upload to a Cloud service for further analysis. Such networks are typically arranged in a point-to-multipoint configuration. Due to their large scale deployments, the nodes are design to be low-cost and low-profile devices hence, the smaller the antenna the better [11]. With this in mind, microstrip antennas are often used, as they are known to yield relatively good electromagnetic performances, are rather easy to manufacture at low costs and easy to embedded into the main system Printed Circuit Board (PCB) [12, 13]. Typically, SN are stationary, being beneficial the use of high-directional and high gain antennas, since a larger coverage area is achieved. On the other hand, BS antennas should have equal radiation characteristics in all directions (*i.e.* exhibit an omnidirectional radiation pattern), hence a larger area is covered. Omnidirectional radiation patterns are easily achieved with dipoles. However, such antennas exhibit considerably low gains, which negatively impact on the overall system dynamic range, and consequently, the useful distance (range) between BS and SN.

To this extent, it is normally proposed to take advantage of antenna sectorisation in order to increase the overall gain at the BS while making it compact and light-weight [14]. Antenna sectorisation techniques consists of splitting the scanning plane in smaller sectors [15], further making use of directive antennas with higher gains. The number of sectors will ultimately depend on the antenna radiation characteristics and particularly on its Field of View (FOV), typically defined by the antenna Half-Power Beam-Width (HPBW).

1.2 OBJECTIVES

The antenna is an essential part of any wireless communication system, transforming electromagnetic energy from its guided form to free-space radiation, and vice versa [13]. In recent years, several antennas have been developed for 5G and IoT communication systems. Such antennas not only must fulfil strict requirements in terms of bandwidth and directivity, but also in terms of size (and form factor), so they can be easily integrated in the mobile handset and/or small cell base-stations, depending on the application.

To this extent, this dissertation aims at the development of small form factor antennas, for 5G and IoT devices. This work is particularly focused on the design, simulation and optimization of small antennas for WSN, following the antenna specifications of the WSN-EM project [16], operating at specific frequencies bands of interest, in particular 2.4 and 26 GHz, and subsequent implementation and experimental characterisation.

The main key objectives of this work are as follows:

- Literature review on small antennas and antennas designs for 5G, IoT and WSN;
- Familiarisation with Computer Simulation Technology (CST) Microwave Studio (MWS);
- Design, simulation and optimisation of small antennas for 5G, IoT and WSN, operating at specific frequencies of interest;
- Antenna prototyping and experimental characterisation in laboratory environment (anechoic chamber);
- Antenna testing in real IoT/WSN scenarios.

1.3 DISSERTATION LAYOUT

This dissertation is organised as follows:

Chapter 2, contains the literature review on 5G, IoT and wireless sensor networks, with emphasis on small antennas for WSN, as they are the focus of application of this dissertation.

In Chapter 3, a high-gain wideband parasitic microstrip antenna for 5G and IoT applications at 26 GHz is presented. The proposed design, utilises one microstrip patch as driving element and eight surrounding patches, that act as parasitical elements. These are coupled by the electric and magnetic fields generated by the driven patch. This configuration, is proven to enhance the overall gain of the antenna reducing its physical size. Simulations carried out in CST are present to validate and characterise the proposed antenna model.

Chapter 4, shows the development of directional BS antennas. Firstly a microstrip Quasi-Yagi antenna is presented, followed by a enhanced lunar waning crescent Quasi-Yagi antenna. Both antennas were designed, optimised and prototyped to operate at the 2.4 GHz Industrial, Sientific and Medical (ISM) band. Subsequently, the development of a WSN BS based on the latter antenna is also presented. The parametric studies on the impact of adjacent antennas is evaluated, as well as the proposed multiplexing mechanism. Finally, the prototyping of the BS antenna is presented, followed by a preliminary experimental characterisation including the antenna matching.

Chapter 5, is dedicated to the implementation of a balanced microstrip slotted patch antenna to be employed on a SN. The antenna with the small dimension of 45×45 mm, was optimised to operate at the 2.4 GHz band. A balun is also presented to assist with the measurements of the antenna characteristics. Both antenna and balun were prototyped for experimental characterisation, and a study to assess the antenna performance camouflaged under grassland fire was carried out.

Chapter 6 proposes a WSN architecture that utilises LoPy4 devices as the circuitry for the BS and SN. These devices were utilise to assess the performance of a WSN that employs the antennas proposed in Chapter 4 and Chapter 5, respectively. Firstly, it is presented the system architecture followed by the base station circuitry and the user interface. Moreover, the implementation and performance assessment of such network in real scenarios is displayed. The node antenna was further tested, to assess the impact of fallen leaves on its performance.

Finally, Chapter 7 is composed by the main conclusions of the work presented in this dissertation, listing the work contained in each chapter and concluding this thesis with proposal for future work.

2

LITERATURE REVIEW

2.1 INTRODUCTION

In this chapter, the literature review carried out on the main topics of this thesis is presented. Emphasis is given to 5G networks, IoT, and WSN systems and applications. Firstly a literature review on 5G is introduced, followed by the IoT concept. As integral part of IoT, WSN are then exposed focusing the literature review on its characteristics including: network architecture, BS and SN designs and, more specifically, antenna designs being used in WSN base stations and sensor node devices.

2.2 5TH GENERATION OF MOBILE NETWORK

The 5th Generation of Mobile Network, being deployed since 2018, is the successor of 4^{th} Generation of mobile network (4G) that is, today, the one which provides connectivity to the majority of mobile devices.

One of the biggest features posed for 5G is the use of the Millimeter-Waves (mm-Waves) spectrum for mobile communications. Millimetre-waves are electromagnetic waves that lie within the spectrum range from 30 to 300 GHz, corresponding to a wavelength of 10 mm and 1 mm, respectively [17]. The usage of mm-Waves grants to a wireless system, data-rates of Gigabits per Second (Gbps) [18]. Moreover, systems that operate with Radio Frequency (RF) mm-Waves benefit from a much larger absolute bandwidth [19]. Therefore, the addition of the New Radio (NR) Frequency Range 2 (FR2) (Table 2.1) to the 5G standards. Due to the short wavelength, antenna designs can be miniaturised has well as various wave components, reducing the overall system size. Other important factor is the decrease of interference with the increase of frequency, thus mm-Waves systems present a stable transmission channel [20].

Initially the 5G system, often referred has "5G Phase 1", was based on the Release 15 (Rel-15) version of the specifications developed by 3^{rd} Generation Partnership Project (3GPP) [21]. Rel-15 was the first full set of 5G standards, the scope was to cover 'stand-alone' 5G, enabling the rapidly progress of chip design and network implementation for the mobile providers.

Table 2.1: FR2 bands

Band	Common name	Uplink/Downlink (GHz)	Channel bandwidths (MHz)
n257	LMDS	26.5-29.5	50,100,200,400
n258	K-band	24.25-27.5	50,100,200,400
n259	V-band	39.5-43.5	50,100,200,400
n260	Ka-band	37-40	50,100,200,400
n261	Ka-band	27.5-28.35	50,100,200,400

Meanwhile, Release 16 (Rel-16) (or "5G, Phase 2") completed in December 2020, is focused on new features such has enhancement on ultra-reliable low latency communications, IoT, 5G location and positioning services, network slicing and so on [22].

Currently, 3GPP, is working on the specifications of Release 17 (Rel-17) with the intent to enhance previous features and introduce new ones. Various areas have been prioritised, between them is important to stand out the NR Massive Input Massive Output (MIMO), industrial IoT , a study on IoT over non terrestrial networks, NR quality experience and NR coverage.

The ambition for 5G is not only to enhance the mobile network specifications but also to extend the coverage in order to provide connectivity to everyone everywhere which workover with the IoT concept.

2.3 INTERNET OF THINGS

Mark Weiser was one of the first authors promoting the IoT [23], dating back to 1991. IoT is a concept for an intelligent network with an ambition to connect every single device over the internet, granting data exchange between users and devices everywhere [24]. The alluring IoT application scenarios for both business and consumer markets increased the interest and development of the concept in the 21^{st} century. Thus, industrial alliances and standards developing organizations, such as 3GPP, Institute of Electrical and Electronics Engineers (IEEE) and European Telecommunications Standards Institute, effort to standardize IoT solutions [25]. The developed standards encouraged the rise of industrial IoT systems, the initial purpose of these systems was to monitor the confection stages of a product. However, these systems quickly expanded to the automation of production.

The assimilation between operational and information technology is the core of industrial IoT aiming the improvement of business across a variety of market sectors by data analytics, WSNs, smart machines and factories [26]. The Industry

4.0 exploiting IoT guaranteed an revolution of product manufacturing, by applying intelligence among the industrial components and optimised production processes [27]. Among the applications scenarios of IoT in industry are applications such as: localization of objects by virtual tags, self-management chain of processes with no user intervention, wireless sensor networks, product and resources control in real-time and communication infrastructure for events and products advertisement.

Today, the consumer markets present a diverse set of IoT compatible devices with the intend to increase the quality of life of the consumer [28]. Home automation interest raised due to the opportunity to realize simple day tasks remotely e.g. control the temperature, lights, doorbell, security cameras and even being notified for various incidents when away from home [29, 30]. Health Care is another massive application scenario [31], employing wearable devices to monitor the user activities, pulse and sleep habits to notify and guide the user through the day [32, 33]. Thus the topics of applications of IoT for the consumer markets beeing: home automation, health care, automotive consumer gadgets, wearables (i.e. Smart Watch, Earbuds, Glasses, etc.) and devices (i.e. Smart TV, Fridge, Phone , etc.).

IoT network benefited from emerging RF technologies such has ZigBee, Bluetooth, Bluetooth Low Energy (BLE), Wi-Fi and, RFID for low-range communications, as well as LoRa and even GSM for long-range communications. Including different RF technologies is a huge advantage to this concept, thus comprise a superior number of devices.

2.4 WIRELESS SENSOR NETWORKS

Considered as a particular IoT case, a WSN is a network which employs dedicated sensors that acquire physical parameters of its surroundings. Wireless sensor networks, are typically composed by a collection of a large number of SN that are scattered in a certain monitoring area [10]. To collect the fetched data of the nodes, WSN typically recur to *e.g.* BS or sink nodes that send the data to a cloud storage. To enhance the robustness of these networks, general characteristics need to be taken into account when developing a WSN [34]. For instance the network should: be flexible enough to support different available communication services; be able to maintain the services when adding new nodes; grant the application requirements; be capable to maintain the network running when nodes present failure; be capable to maintain the consistent data with real-world events, taking into account factors such as space and time; support a broad field of applications; show a low-cost and finally be heterogeneous, meaning that is essential to tie different frameworks, models and hardware components in a WSN, ceasing technological disparities.

According with [35], wireless sensor networks can be divided in 6 categories. The geographic area of application is an important factor to distinguish the WSN. For instance, if the WSN was deployed above ground it is considered a Terrestrial Wireless Sensor Networks (TWSNs). However, for areas underground [36–38], the WSN is defined has Wireless Underground Sensor Networks (WUSNs). In underwater applications [39–41], the WSN will be categorise has an Underwater Wireless Sensor Networks (UWSNs). Finally, there is also a category for Space-Based Wireless Sensor Networks (SB-WSNs) [42, 43].Typically WSN are stationary (the SN is static), nonetheless mobile WSN are also present in the literature [44–46], thus the necessity of the Mobile Wireless Sensor Networks (MWSNs), in order to differentiate this networks from static ones. Another distinction is done by their functionalities, WSN which feature multimedia transmission i.e. image, audio and video [47–49] is recognise has a Wireless Multimedia Sensor Networks (WMSNs);.

In the literature, TWSNs are typically referred has WSN and are probably the most common type of WSN being deployed nowadays. For the sake of simplification, this dissertation will always employ the term WSN.

In the course of this section, wireless sensor networks are presented in detailed.

2.4.1 *Network Topology*

Any communication network is typically comprised by various "nodes", capable of data transmission and reception, either via cables or radio-waves (wireless). These communications are established by links which depend on the protocols (for communication and coverage) and the physical position of the nodes. Several network topologies are indentified in Fig. 2.1.

In particular, a WSN is typically arranged in a star configuration (Fig. 2.1), where every node is linked to the BS directly and independently. Therefore, if one SN goes down, the network will continue to be stable. This is an huge advantage, since WSN are unmaintained, hence prone to failure [50]. However, a larger coverage area can be obtained with the tree topology (Fig. 2.1) since the area of study is not limited by the range between BS and SN, as in the star topology. On the other hand, the SN which serve has repeaters will suffer a greater power consumption reducing the lifetime of the WSN. Mesh topologies are extremely reliable. These topologies are considered the most fault tolerant due to the multiple connections of the networks which can thrive even with the loss of some nodes. However, they become highly complex, each interconnection requires to be configured after deployment. Thus, these networks are not cost and energy effective since the nodes will be active for the majority of time on acknowledge routines. There is also the possibility to design an

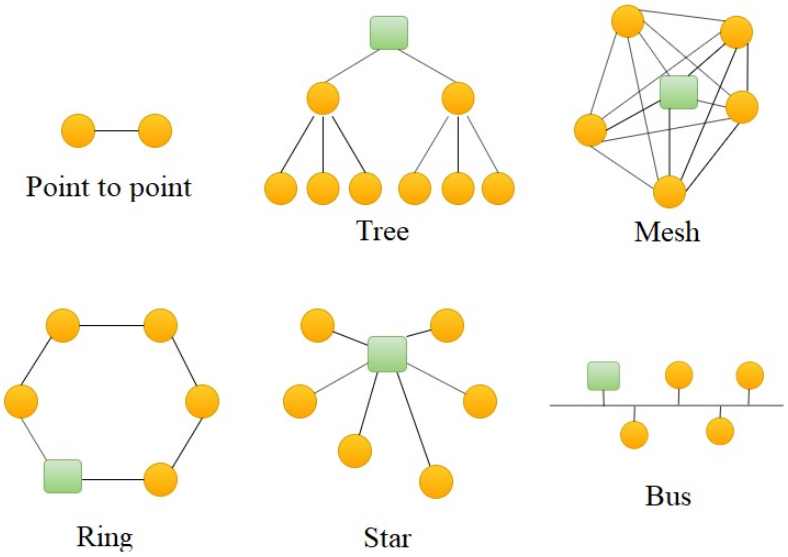

Figure 2.1: Diagram of basic network topologies.

network that exploits two, or more, topologies, these networks are usually described has hybrid.

The topology of the network will ultimately depend on the application of the WSN and the communication standard due the specification requirements established and standardised.

2.4.2 *Base Station*

The BS is tasked to request/receive the data from the nodes, the data can then be compressed and, saved locally or transmitted i.e. via Global System for Mobile (GSM). The data can then be analysed by the users to better understand the area / parameter of study.

Like the nodes, the BS can be stationary or mobile, depending on the application of the WSN. Studies such has [51, 52] dangle on increasing the overall efficiency of a mobile WSN by optimising the mobile base-station.

When designing a BS typically there is no limitation on size, implying the antenna dimensions too. These are stand-alone devices where one BS is connected to multiple SN, which are deployed on strategic places, granting the highest coverage possible. Therefore, the heigh of the antennas is critical to establish the maximum range and it depends on the scenario of the application. For instance, the need to study the vegetation of the area to determine the height of the BS antennae to achieve the desired results.

Figure 2.2: Size comparison between Mica2Dot SN and a quarter, extracted from [57].

2.4.3 *Sensor Node*

In 1975, Intel co-founder Gorden Moore predicted that "the number of transistors incorporated in a chip will approximately double every 24 months" [53], suggesting that electronic devices will double the speed and capability's every 2 years. This prediction is referred to as "Moore's Law", which hold for a long time [54–56]. For example, the first computer would fill an entire room, but today we all walk with a more powerful computer in our pockets, due to the size reduction of the electronic components. However, the Moore's Law didn't hold up in recent years since the number of transistors incorporated in a chip has increased but didn't double. Gordon Moore made his prediction for 5 years but it hold true to 35 years.

Chips with lower capabilities possess fewer transistors hence the smaller dimension and less power consumptions. An WSN take advantage of this by using multiple small devices, which have simple functions, for example, a periodic information extraction (using sensors) and transmission of data to the BS. In Fig. 2.2 is presented a compact SN commercial device, for educational proposes denominated by Mica2Dot. This particular node has a diameter of 2.54 cm and feature light, humidity, temperature, barometric pressure, acoustic and, magnetic sensors. According to the manufacturer with an AA battery the node presents a lifetime of approx. 1 year. A generalise sensor node architecture will be further review in the next section.

2.4.4 *Sensor Node Architecture*

Figure 2.3 depicts an generic block diagram of the main parts of wireless sensor nodes [58–60]. It is compose of a power unit, sensing unit, the RF-System on Chip (SoC), antenna matching and, the Microcontroller Unit (MCU) which is the main block of the device. The MCU is responsible the automatic control of the blocks in the node. Which can also be seen as a mediator between the sensing unit, the Radio Frequency System on Chip (RF-SoC), and when utilised, the actuator model.

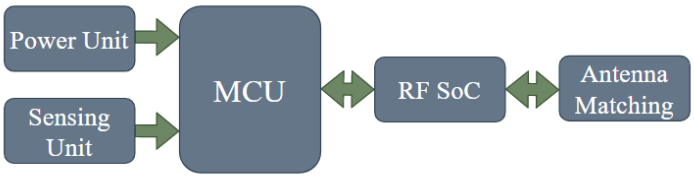

Figure 2.3: Block diagram of the SN main modules.

The sensing unit can be composed of multiple sensors (*humidity, temperature, pressure, tocity...*) that retrieve data from the area of study which is then sent in analog or digital form to the MCU. The data is then send to the RF-SoC to be modulated and transmitted to the BS. An antenna matching module is necessary in order to have the most efficiency possible, granting the maximum range of communication. The RF-SoC is in control of the communication part of the device, thus dictates the transmitted power. It is important to search the legal values for the maximum effective isotropic radiated power in order to better understand the capabilities of the network, and adapt the network if necessary. In Portugal, the effective isotropic radiated power for the 2.4 GHz ISM band cannot exceed 20 dBm, which means, if the antenna gain is 5 dBi the maximum transmitted power should be set to 15 dBm (considering a loss of 0 dB).

All the modules above need the energy to operate, which is managed by the power unit, that should be designed to be extremely efficient concerning the life span of the battery.

2.4.5 *Energy Consumption*

Energy consumption is the most important factor to dictate the lifetime of the WSN, particularly in the SN side. Thus, the importance on the power consumption when choosing hardware for a SN [61].

Typically, wireless sensor networks for environmental monitoring in remote areas, employ nodes that are active for small periods of time, coupled with a battery cell capable to sustain the SN through a few years. Therefore, the importance to study and manage the activity of the node, reducing it to the minimum as possible.

The SN activity can be described in five stages:

- Active - The microcontroller unit or sensor are functioning e.g. extracting data, processing;
- Tx - SN is transmitting data;

- Rx - SN is receiving data from the BS, typically acknowledgements from transmitted data;
- Idle - The SN is "awake", however unproductive, this stage normally occurs between stages;
- Sleep - Is the stage which the SN consumes less power, the microcontroller unit awaits an event to become active, until there all processes are blocked thus consuming less energy;

The module that is active for the majority of stages is the MCU however, it may not be the one that drain the most energy. Furthermore, the stage where the SN consumes more energy can not be generalised. For example, a WMSN that implements a camera with motion detection will consume more energy on the sensing unit since it is always active. However, if the camera is only active on remote occasions, the RF-SoC may be the module with the most energy consumption. Nevertheless, all modules should be designed to be the most power-efficient respecting the desired application while increasing the lifetime of the networks. In [62] the authors present a collection of lifetime maximization techniques for WSN, passing by their constraints, applications, and estimation life time models.

2.4.6 *Communication Standards*

WSN, like generic IoT networks, can utilise various communication technologies which have requisites that need to be complied. To this extent when scheming a WSN, the communication technologies should be chosen wisely in order to better accommodate the needs of the network. Hence, in this subsection, a brief description and discussion about the most common standards is provided. Prevalent RF-SoC in the market employ the following standards:

Bluetooth:

The specification for Bluetooth are dictated by the Bluetooth Special Interest Group (SIG). In 1998, an union with the name of Bluetooth was initiated by Intel, Nokia, Ericsson and IBM. Conceive to develop the specifications for an wireless communication network aiming interoperability between products. Today, according to SIG, there are over 36000 companies associated to it.

Operating at the 2.4 GHz ISM band, Bluetooth intent was to replace cable links between devices with a low-power wireless communication technology. It was defined as "an industry specification over short-range RF connectivity design for portable devices" in the IEEE standard 802.15.1 [63]. At first, Bluetooth invest on Asynchronous Connection-Less (ACL) links for file share, as it may be used for broadcasting data

on bursty transmissions (with symmetrical or asymmetrical traffic). However, to annex audio streaming capabilities, in version 1.2, Synchronous Connection-Oriented (SCO) links were included which provides symmetrical streaming links [64, 65].

Bluetooth specifications present 79 channels with 1MHz of bandwidth on the operating 2.4GHz band. To improve security and reduce interference in the communication, Bluetooth modulates data with frequency-hop spread spectrum, this technique alters frequencies in conform to the agenda set by the paired devices [66], typically is the Master device who sets the agenda in the initial stage of pairing.

Nowadays, it is specially used in consumer market for peripheral devices such has keyboards, headsets, smart-watches, auto-radios, and others.

Bluetooth Low Energy:

BLE was built under Bluetooth and it's been reformed for low energy operations. In substance, BLE target the reduction of RF transmissions to the minimum has possible [66], as well as, bit rate devaluation to attain an higher energy efficiency [67]. Therefore, BLE will constantly be on sleep mode unless when starting a connection.

Instead of the 79 channels available in Bluetooth, BLE provides 40 channels as a result of raising the channel bandwidth from 1 to 2 MHz. Even though there are 40 channels, only 37 are available for data transfer, since 3 channels are reserved for establishing the communication.

As a result of the low-cost and low-energy consumption, BLE is one of the best solutions for WSN, principally when deployed on small areas of study due to the short-range communication.

Wi-Fi:

Wi-Fi or IEEE 802.11 standards are created by the IEEE LAN/MAN Standards Committee (also known as IEEE 802), that specifies the Media Acess Control (MAC) and Physical Layer (PHY) protocols in Wireless Local Area Network (WLAN).

At the moment, 7 standards for Wi-Fi were released. The first standard, IEEE 802.11 [68], was released in 1997 and it is commonly referred has Legacy. Nowadays this standard its obsolete, however, it was ground breaking at the time, able to provide wireless connections with speeds of Megabits per Second (Mbps) at the 2.4 GHz band. After the Legacy success in 1999, IEEE 802.11a [69] and IEEE 802.11b [70] standards were launched. Concerning the noise at 2.4 GHz, IEEE 802.11a was design to operate at the 5 GHz band, showing theoretical connections speeds of 54 Mbps. IEEE 802.11b kept working at the 2.4 GHz ISM band, with a maximum data rate of 11 Mbps. 2003 was another year of Wi-Fi standards release, with the IEEE 802.11g [71]. The standard was massively accepted due to the usage of 2.4 GHz but with the increase of the maximum data rate to 54 Mbps, instead of the

11 Mbps provided in 1999. In 2009, 2013 and 2019, the standards IEEE 802.11n [72], IEEE 802.11ac [73] and IEEE 802.11ax [74] were released, respectively, operating at the 2.4 GHz and 5 GHz bands. However, the IEEE 802.11n standard supports multi-channel usage, with the maximum data rate of 600 Mbps. Meanwhile, IEEE 802.11ac, launched in 2013, added MU-MIMO and remarkably increased the Wi-Fi standards rates to 1.3 Gigabits per Second (Gbps). Finally the last reveal, made in 2019, presented the IEEE 802.11ax standard which upgraded various support capabilities from the previous standards, such has the MU-MIMO and promises, in theory, the capacity to provide connections of 10 Gbps.

Initially, with the Legacy standard it was possible to use hopping spread spectrum (technique used in Bluetooth), but that specifications were abandoned. Instead the IEEE 802.11b utilises a direct sequence spread spectrum technique called Complementary Coded Keying (CCK), while the others use Orthogonal Frequency Division Multiplexing (OFDM). The channel bandwidth is dictated by the standard chosen the minimum (and most used) value being 20 MHz, and the maximum (in the new standard) 160 MHz.

Wi-Fi was conceded for high-data rate communications, discarding the management of power consumptions. To this extent, Wi-Fi was rejected as a standard for low-power networks. Nonetheless, with the emergence of IoT new requirements needed to be fulfil. RF-SoC started to implement sleep modes allowing Wi-Fi to be use in low-power operations [75]. Thus making it suitable for IoT devices such has SN.

LoRa:

Lora is a communication protocol developed by LoRa Alliance, a non-profit organization compose of more then 500 company members. The committee aims to empower IoT Low-Power Wide Area Networks (LPWAN) with the envelop of LoRa open standard, for long-range communications with low data rates. It was first presented in 2015, and within 2 years the specification 1.1 was released.

To achieve longer distances of communications between devices, LoRa uses the 415 MHz, 868 MHz and 915 MHz bands, and the spread spectrum modulation technique derived from chirp spread spectrum technology. The payload should not be set for more then 100 bytes since that is the limited value for a reliable transmission, however for the majority of WSN is more then enough.

This standard enables inexpensive, long-range communications specially design for IoT in remote areas. Distance of kilometres between linked devices can be attain with a remarkable battery lifetime. One of the drawbacks of this standard remains on the missing liability for continued and real-time monitoring applications.

2.4.7 *Deployment*

For WSN, the deployment of the nodes is a critical issue. The principal requisite for node placement is to achieve the desired coverage and QoS for the network [76]. In such a manner, the usage of deterministic deployments based on studies and simulation of the terrain of the area of interest should be applied. This way, the node placement can be precisely attaining the desired coverage. However, this is not always possible by virtue of the terrain itself, i.e. remote locations, hard terrain, intolerable weather conditions, and others.

To answer these difficulties, stochastic deployments may be considered a viable alternative i.e. low-flying plane pallet deployments [77]. Yet, stochastic deployments raise another problem, it is impossible to predict the node position and orientation, which could resolve on a lower coverage area than expected [78, 79].

A comparative performance evaluation of four existing algorithms designed to solve the minimum cost coverage deployment problem is presented in [80]. The algorithms are based on stochastic optimization techniques and are compared in terms of scalability, computation cost, QoS, and convergence speed. The authors conclude that ant colony and integer encoded fixed length genetic algorithms shown the best results.

2.4.8 *Applications*

Considering the proficiency and low-cost of WSN, an increase of interest in industry and research was generated, resulting in various application scenarios for these networks.

Military applications:

Military applications demand high security and accuracy as the result of their essence, employing complex network architectures with particular protocols [81]. Intelligent surveillance and reconnaissance systems are fundamental to assess possible threats of a monitoring area hence the research reinforcement of WSN.

Applications for intrusion and presence of the enemy in the monitoring area are the most common application present in the literature: Authors in [6] propose the distribution of ground sensor nodes for military vehicle identification based on acoustic signal analysis. Although the identification method was successful, the system had difficulties distinguish two vehicle classes. For this reason, the authors suggest acquiring the vehicle speed for class differentiation. In [82], the authors focused on ship detection by the waves they create, since it was observed that ocean

waves and ship-generated waves have different energy spectrums. Thus, taking advantage of this by deploying the nodes on the sea surface with a three-axis accelerometer. To increase the reliability of the system, the authors also exploit spatial and temporal correlations of intrusion.

Though military applications also benefit from WSN with capabilities to detect Chemical, Biological, Radiological, Nuclear, and Explosive (CBRNE) and Toxic Industrial Material (TIM) [83], not only to prevent soldiers of the toxic and harmful environments but also to detect explosives conforming to the survey in [84]. WSN, also prosper with stealth unmanned aerial vehicles, on the one hand, can be used to deploy the nodes in the area. On the other hand, they can retrieve the data from the nodes acting like a mobile BS as contemplated in [85]

Industry applications:

The sector which benefited the most with WSN is, without a doubt, the industry. The vast number of applications of sensor networks are uncanny, and because of it, the growth of WSN development.

Just like the military applications, nodes that employ sensors capable of detecting toxic gas/materials are very effective in leakage detection and worker's safety, hence the work in [9,86]. Enduring the factory environment, authors in [87,88] use WSN for production monitoring proving a great advantage, increasing the speed of production as well as troubleshoot the various stages. An extensive list of applications for WSN in the industry are presented in [89], between many others, are the automated robots and vehicles, object identification, civil engineering applications and critical infrastructure protection and security applications.

One interesting use of WSN is in Unmanned merchant ships, these ships operate without any need for people on board. Even though applications are still in the testing phase, they can bring safety and economic advantages [90].

Health applications:

Health devices became popular in recent years, consumers have been specially interested in smartwatches that cant track various parameters such has number of steps, heart rate, oxygen level, and others. Thus, increasing the health conditions and losing sedentary habits. Such devices employ sensors that can be implemented on a node and distributed in the resident patients of an hospital creating an WSN. With a monitor network over critical patients is then possible to alert nurses and doctor in real-time, thus providing a rapid response to the patient in need.

Conventionally, these systems are present in hospitals and clinics, however the intention is to move them to nursing and patients homes [91]. Therefore, authors in [7] propose a complete system to support daily activities of elderly people. The

authors aim to deploy not only at the home of the elderly but also in crowded places to better asses and provide care to the patient.

Even though, these systems prove to be extremely useful for early health risk detection, authors in [92] perceived the need to address facilitators and barriers for WSN in smart home healthcare systems by identifying important sociotechnical, cognitive, affective, and contextual factors. A huge concern pointed by the authors, is the human detachment that the patient may face after the deployment as a result of the reduce interactions with nurses to access the patient health. Which can be potentially harmful for the patients mental health. Another drawback pinpointed is the possible lack of privacy. Thus, when developing and deploying these systems, various aspects need to be address facilitating both the mental and physical health of the patient.

Environment monitoring applications:

Environment monitoring is the most common application present in the literature, the low-cost, low-maintenance and capabilities of WSN are in good agreement with environment monitoring systems, thus the high interest in this field. The application is self-explanatory, the objective is to monitor the chosen environment, like the project Wireless Sensor Network for Environment Monitoring (PTDC/EEI-EEE/30539/2017) which objective is to elaborate WSN for temperature and humidity environmental monitoring over a wide area. In [93], which propose a environment monitoring system for indoor and outdoor aiming to attain the temperature, humidity and Co2 concentration of the area, displaying it in a dashboard for further analysis.

However it is not strictly necessary to study parameters such as sun exposure, air quality, temperature, etc. In fact, these networks are extremely useful in prevention systems, i.e. early detection of natural disasters and population control. In [94] the author employ a WSN in a conservation of illegal logging of forest trees system. Where foundation of the WSN are vibration sensors able to detect variation in vibration frequency. Another example is the work of [95], that propose a WUSN deployed in tunnels, chambers or earth air tunnels integrated in a smart cooling system. The WUSN monitor the ambient temperature around the node, with this information the system can then act to temperature fluctuations preventing underground area of becoming an hazard. The system utilizes 100 % fresh air and guide it on the conducts to the needed area. According to the authors, the results prove the system to be extremely energy efficient, 60-70 % energy costs are saved enabling long term savings.

Typically, these networks have an star topology and an stochastic deployment due to the areas of interest are located in remote places, or by the desire to study large areas. The low, or even none maintenance of the network, results on sensor

nodes designed to be active for smaller periods of time, so its achieved a higher life-time of the network. Withal, there is the need of redundancy to preserve the network on node failure.

2.5 ANTENNAS FOR WIRELESS SENSOR NETWORKS

In every wireless device, is essential to employ an antenna that transforms electromagnetic energy from its guided form to free-space radiation, and vice-versa, to transmit and receive information from the network.

The most simple antenna, monopole, can be created by a copper wire with a determined length that dictates the frequency of operation of the antenna. Theoretically, a monopole presents an omnidirectional radiation pattern, thus transmitting the same power in every direction.

However, in communication between static devices, is useful to focus the energy in the direction of the other device thus, increasing the communication range. Several devices take advantage of high gain antennas to reduce energy consumption since it is then possible to achieve the same range with less transmitted power.

2.5.1 *Base Station Antennas*

Typically, BS aim to achieve a omnidirectional radiation pattern, making possible the deployment of SN in a wider-area. Therefore, BS with directional antennas employ sectorization techniques to increase the overall gain and provide an omnidirectional radiation pattern (in the azimuth plane).

There are available various commercial antenna designs for BS Fig. 2.4 presents 4 commercial antennas which are thought to be suitable for WSN operating at the 2.4 GHz ISM band. In Table 2.2, there is a brief comparison on the characteristics of the antennas.

Even though, size is typically not a limitation when designing a BS antenna, it is important to maintain the low-cost of the WSN. Thus, PCB antennas are normally proposed in the literature to be integrated in the BS, since the production cost are lower while providing similar results of the commercial antennas.

In [96], the authors presented a wideband Vivaldi for 5G BS, to achieved dual-polarization the authors use two elements, that are placed in a cross-shape configuration. To cover the 690-960 MHz band, it is suggested the integration of the two elements in a lower band element as shown in Fig. 2.5a. A single Vivaldi antenna element is depicted in Fig. 2.5b, it is composed by two exponentially tapered flares

(a) (b) (c) (d)

Figure 2.4: Commercial antennas suitable for WSN at 2.4 GHz: (a) Tupavco TP541, (b) RF-Links AD-24SHS, (c) Tp-link TL-ANT2414B and (d) Shure PA805Z2.

Table 2.2: Comparative table of commercial BS antennas.

Antenna	Frequency (GHz)	Gain (dBi)	HPBW (°) (Az Plane)	Nº. of Antennas for 360º FOV
Tupavco TP541	2.4-2.5 ; 4.9-5.85	9	58	6
RF-Links AD-24SHS	2.4 - 2.483	6.5	360	1
Tp-link TL-ANT2414B	2.4 - 2.5	14	60	6
Shure PA805Z2	2.05 - 2.70	8	100	4

that transform the slot line impedance of 100 Ω to the air impedance. The length L and the width B dictate the lower cut-off frequency. The elliptical slots are used to better improve to attain a better matching as well as reducing the side-lobes. In order to feed the antenna, the authors take advantage of a balun that transforms the input unbalanced signal to a balance signal. For development of the antenna the authors choose a substrate with a dielectric constant of ε_r=2.2 and 0.3 mm thickness. According to the simulations, the antenna covers the band from 1.4 to 3.8 GHz, the radiation pattern present a 60° ± 25 symmetric beamwidth and its gain ranges from 7 to 10.4 dBi.

The authors in [97], used a different approach utilising an 1x4 array composed by improved inverted-F antennas to be implemented in a Wi-Fi BS. Although the

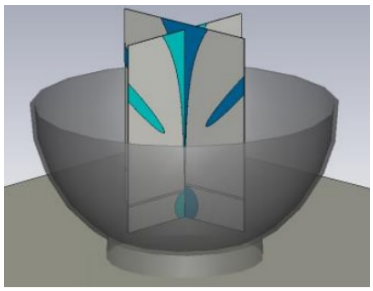

(a)

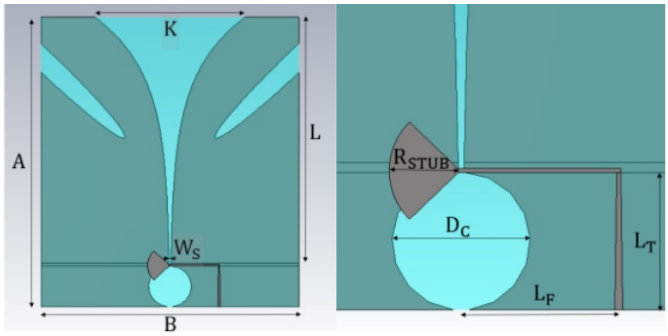

(b)

Figure 2.5: Wideband Vivaldi design for 5G BS, proposed in [96].

antenna was thought to be implemented in a Wi-Fi base station, the antenna is suitable for any technology operating at the 2.4 GHz band. The layout of the antenna is depicted in Fig. 2.6, where it can be seen that the four inverted-F antennas, which composed the array, face different directions. This method granted the authors, a radiated circular polarization to the array without the need of complex feeding networks to achieve the same result. The antenna employs a printed power divider that maintain consistent phases thought the array, as well as ground plane in a FR4 epoxy resin substrate with a ε_r=4.4. The authors also added an additional reflective board (represented in blue 2.6), which is placed beneath the array at a distance, providing a unidirectional radiation pattern. The simulation results, shown a bandwidth from 2.25 to 2.55 GHz, a gain of 12.07 dBi and an HPBW of 26° in the azimuth plane and 60° on the elevation plane.

Meanwhile, in [98] the authors present a broadband solar antenna element for base stations. The design, shown in Fig. 2.7, employs 4 solar cells that act like a radiation aperture which is excited by a wideband feeding system, creating a fairly complex antenna structure. It is composed by 3 substrates, substrate 1 acts as the radiator and integrates the solar cells with Direct Current (DC) lines that will then be connected to the DC lines present in substrate 2, where the ground plane of the antenna is based. Substrate 3 employs the feeding structure for substrate 1. The solar cells type chosen include a glue layer, grid electrodes, epitaxial and copper layers from the top down. DC energy is generated by the epitaxial layer, solar cells then exploit the usage of grid electrodes for DC energy transmission, while the

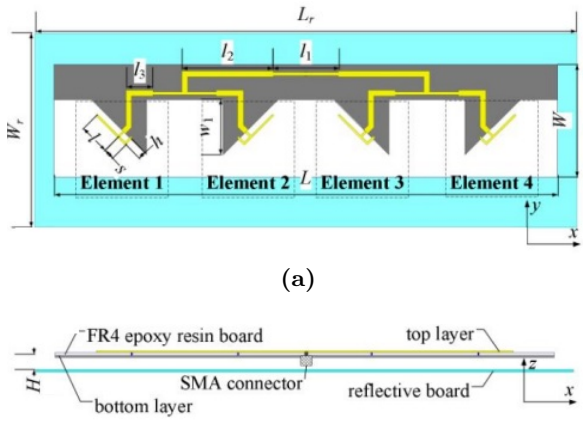

(a)

(b)

Figure 2.6: Antenna layout proposed in [97] (a) Top View and (b) Side View.

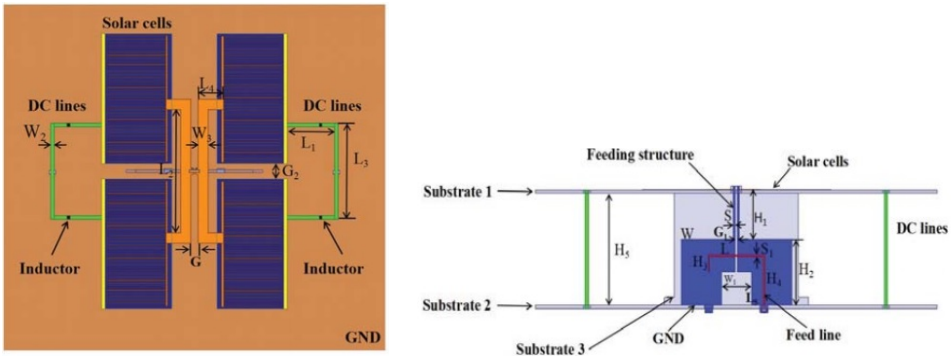

(a) **(b)**

Figure 2.7: Broadband solar antenna element layout proposed in [98] from: (a) Top View and (b) Side View.

cooper layer is used has the ground plane and as physical support for the solar cell, fixing it on the desired location. The authors ensure that the antenna has a gain of 8 dBi across the 1.66 to 3.08 GHz band, while the simulation results at the 2.4 GHz ISM band ensure a gain of approx. 8.5 dBi and a HPBW of approx. 50° on the azimuth plane. To achieve this results the authors choose FR4 substrates with a relative permittivity of 4.4

Finally, in [99] a filter antenna was design to be implemented on a BS. The filtering is used for decoupling improving the isolation while ensure the stability of the radiation pattern of the antenna. Therefore, the design presented in Fig. 2.8, integrate a main radiator, two vertical feed structures and a reflector, etched on F4b substrate with a ε_r=2.55 and a thickness of 0.8 mm. The main radiator, depicted in Fig. 2.9a, has two dipoles with a ring-slot each to generate band-notched effect the opening direction of the slot faces the feeder. To feed the main radiator, two vertical substrates are used, shown in Fig. 2.9b. On the backside, are located L-shape balun patches that are connected to the dipoles and the reflector. In the front side there is a C-shape resonator, that combined with the slot in the main radiator, forms a sharp band-notched and a transmission line. To facilitate the assembly of the

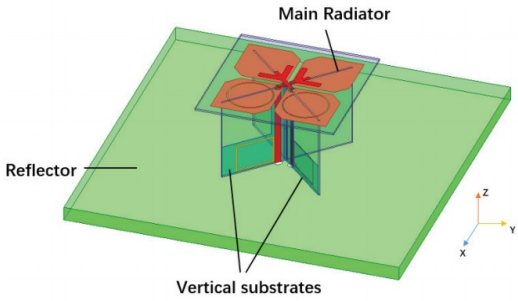

Figure 2.8: 3D view of the filter antenna layout proposed in [99].

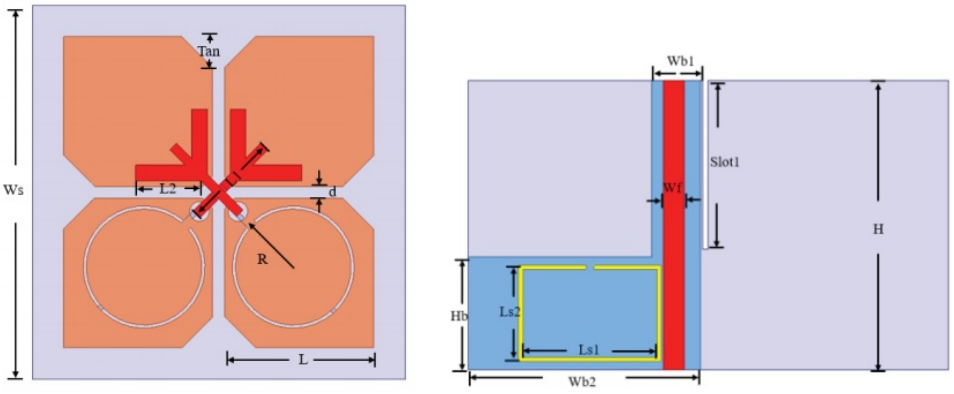

Figure 2.9: Filter antenna element layout: (a) Main radiator and (b) Vertical substrate, proposed in [99].

antenna structure, each vertical substrate employs a slot represented as slot1, in Fig. 2.9b. According to the simulation results the antenna operates from 1680 to 2940 MHz, however it filters the band from 1920 to 1980 MHz. The gain of the antenna at the 2.4 GHz is around. 9 dBi and an HPBW of approx. 40° on the azimuth plane.

2.5.2 *Sensor Node Antennas*

Sensor node antennas, on contrary to the BS ones, have more restrict limitations aiming to achieve a lower cost of production while presenting the smallest size possible.

Small antennas such has ceramic chip and inverted F antennas (IFAs), are often used on commercial devices operating at 2.4GHz, due to their ease of integration in the circuitry. Ceramic chip antennas operating at 2.4 GHz (Fig. 2.10a), normally present a gain varying from 0 to 2.6 dBi (depending on the manufacturer). When it comes to the HPBW (in the azimuth plane), ceramic chip antennas typically achieve a near omnidirectional radiation pattern, thus having a 360° FOV. In a different matter, inverted F antennas (in Fig. 2.10b) are PCB antennas comprised of a metallic trace drawn directly onto a PCB, posing lower costs of production.

(a) (b)

Figure 2.10: Commercial antennas for small devices at 2.4 GHz: (a) Ceramic Chip Antenna ,from Johanson Technology (2450AT42A100) and (b) F inverted antenna, from Texas Instruments (DN0007)

(a) (b)

Figure 2.11: Commercial external antennas for small devices at 2.4 GHz: (a) Whip antenna, from Necables (400103) and (b)Button Antenna, from Taoglas (WCM.01.0111)

For example in [100], Texas Instruments presents an antenna with a peak gain of 3.3 dBi with a size of 25.7×7.5 mm^{32} and, with a radiation pattern, in the main plane (azimuth) near to omnidirectional. In another example, Texas Instruments presented the design note AN043 which employ a peak gain of 5.3dBi while loosing the omnidirectional radiation pattern. However, any change to the circuitry may result on the need to rearrange the antenna placement.

There is also de possibility to integrate external antennas into the SN. Commercial whip antennas, as the one depicted in Fig. 2.11a, are commonly used in devices for low-range / indoor communications due to their low gain (0 to 2dBi). But there are many other options in the market that provide directional radiation patterns with a considerable gain, suitable for mid to long-range application. One example is the button antenna depicted in Fig. 2.11b. The antenna as dimensions of 19.8x14.3x16.4 mm^3 and, when employing a 20x20 mm^2 centred ground plane, attain a peak gain of 5.40 dBi.

The antennas previously described are unbalanced, meaning that have one element being fed and its potential is referenced to ground. Balanced antennas on the other hand, have two elements being fed, where one of the elements is 180° out-of-phase of the other. The usage of differential RF signals present the advantage of suppressing the common mode current [101], eliminating the need of filtering processes on the circuitry. Thus, RF-SoC with such characteristics are a perfect solution for devices like the SN that have tight size restrictions.

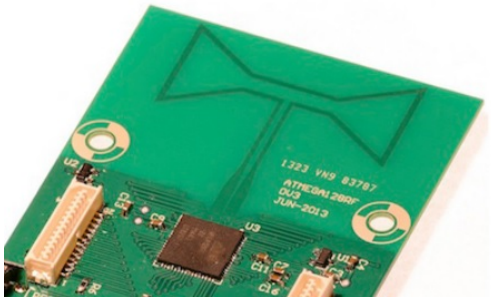

Figure 2.12: BSFD antenna proposed in [102].

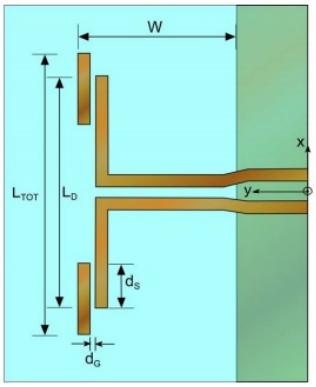

Figure 2.13: End-loaded printed dipoles antenna proposed in [103].

In [102], the authors designed an antenna to be integrated into an agricultural sensor node operating on 2.4 GHz ISM band. The antenna, depicted in Fig. 2.12, is a differential Bowtie-Shaped Folded Dipole (BSFD), with a differential input impedance of 100 Ω. The proposed design was build upon a folded dipole, followed by the optimisation of each section's connecting angles, lengths and the trace width in order to attain the maximum performance. Measurement results shown that the proposed BSFD antenna have a gain of 2.3 dBi, with a bandwidth of 401.8 MHz. This results were achieved with the antenna etched on a FR4 PCB substrate with 0.8 mm thickness.

Furthermore, in [103] the authors simultaneously lay three balanced planar antenna designs for WLAN applications. The proposed antennas are dual band, able to operate at the 2.4 GHz and 5.2 GHz bands, printed on a Roger RO4003C substrate with a thickness of 0.5 mm and ε_r=3.38. According to the authors, the end-loaded printed dipoles presented in Fig. 2.13 attain the best performance of the three, with a peak gain of 4.5dBi with a bandwidth from 2.41 to 2.48 GHz.

Meanwhile the authors in [104], opted to design an small cubic antenna design for WSN. The proposed antenna, represented in Fig. 2.14a, has a dimension of 12.5x11.2x10mm^3 using a meandered microstrip half-wave dipole design (Fig. 2.14b) with folded arms to reduce the side dimension of the structure. To attain a higher current near the excitation, it is necessary to reduce the usage of the meander

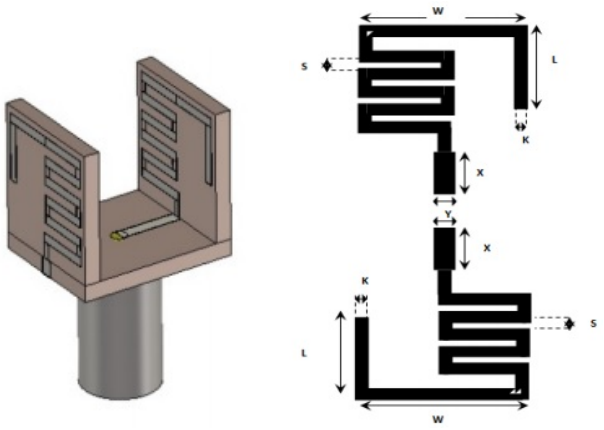

(a) **(b)**

Figure 2.14: Proposed (a) antenna design and (b) layout for the meandered microstrip line, in [104].

technique of the microstrip in the proximity of it. Since the antenna is bottom fed, it can be attach to the top of the circuitry, withdrawing the need of extra space on the PCB. Simulations result ensure a realised gain of 1.87 dBi with an bandwidth of 70 MHz (2.41 to 2.48 GHz) and showing a omnidirectional radiation pattern in the azimuth plane. These results were obtain with the chosen substrate Roger/Duroid TMM 10i that have a ε_r of 9.8 and a thickness of 1.27 mm.

Finally, like the work of [104], the authors in [105] proposed an alternative bottom fed antenna, with beamstearing capabilities. The radiation pattern is controlled by changing the phase difference between the feeding points. The antenna, depicted in 2.15, is composed of two branched radiators, a reflecting plate with an artificial magnetic conductor structure, and a power divider with a switched-line phase shifter. In addiction, the power divider with a switched-line phase shifter is not necessary when attached to a RF-SoC that outputs a differential signal. When acting like a balanced antenna, the two branched radiators can be seen as two crossed dipoles since they generate a equivalent radiation. Finally the artificial magnetic conductor is utilise as a reflecting plate granting a short distance between reflecting plate and antenna. The authors measured results guarantee that the antenna operates on the bandwidth from 2.37 to 2.49 GHz, with a peak gain of 6.62 dBi and an approx. HPBW of 30°. These results, were achieved when the branched radiators are etched on a FR4 substrate with 4.5 relative permittivity and 0.4 mm thickness. Even though the results shown to be promising, the antenna dimensions are 100x100 mm², which is a major hitch for SN.

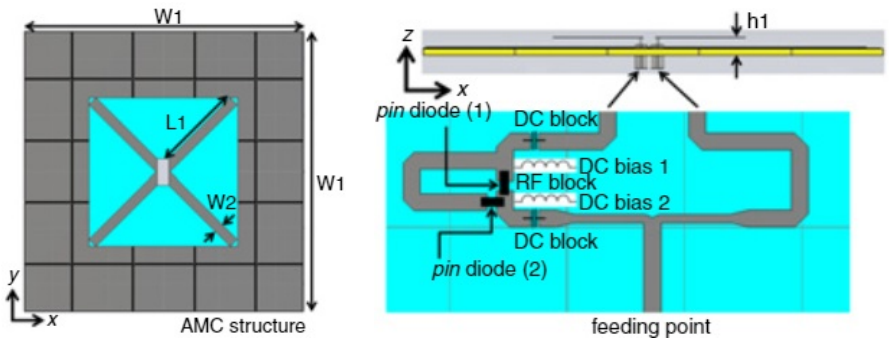

Figure 2.15: Proposed antenna layout in [105] (a) Top View and (b) Side View with feeding structure.

2.6 INTERIM CONCLUSIONS

In this chapter it is presented the literature review on 5G and IoT technologies, with emphasis on WSN, considered as the core of the work realised in this dissertation. For WSN, the BS and SN are presented in detailed, followed by a general hardware architecture and the importance of managing energy consumption in the nodes. It is also exposed the variety of solutions for WSN topologies, communication standards, coverage problems and deployments. Subsequently, an extensive review on WSN applications takes place. Finally, a literature review on BS and SN antennas is performed, with special attention given to their electromagnetic characteristics and commercial designs.

3

HIGH-GAIN WIDEBAND PARASITIC MICROSTRIP ANTENNA FOR 5G AND IOT AT 26 GHZ

3.1 INTRODUCTION

In this chapter, a high-gain wideband parasitic microstrip antenna, for 5G and IoT applications at 26 GHz, is presented. A single antenna, composed of a miniaturised parasitic patch antenna, is studied, characterised and optimised to operate at 26 GHz, aiming at the 5G new radio, frequency range 2 (FR2), band n258. After the optimisation the results are analysed and compared to others present in the literature.

3.2 ANTENNA CONFIGURATION

The proposed antenna configuration, depicted in Fig. 3.1, follows the initial layout introduced in [106]. The antenna in consideration is composed of a central microstrip patch element, in a probe fed configuration and, eight surrounding microstrip patches acting as parasitic elements. While the central element is responsible for the feeding, the eight surrounding elements are coupled via electric (E) and magnetic (H) fields, to enhance the overall gain and reduce the physical size of the antenna, when comparing with a traditional microstrip patch antenna. The antenna was modified

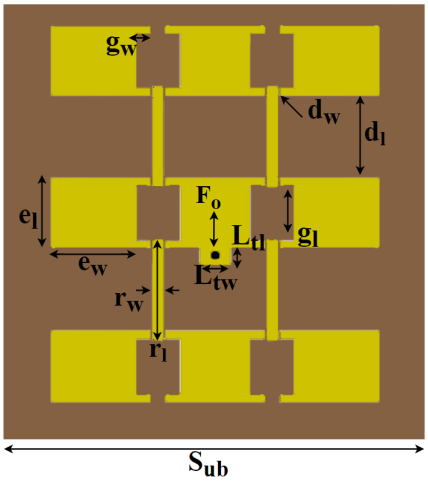

Figure 3.1: Parasitic microstrip antenna element layout.

and further optimise to operate in the frequency band defined between 23.5 and 27.5 GHz, aiming at the 5G new radio (NR), frequency range 2 (FR2) band.

Following the layout of Fig. 3.1, the frequency of operation is defined by size of the patches represented by e_w and e_l, while the feeding point offset F_O is used to match the input impedance of the antenna. To accommodate the F_O, the extra space set by $l_{tw} \times l_{tl}$ is considered. The microstrip lines, defined by r_l, r_w, are used next to the patches to perform the coupling on the E-plane, whereas for the H-plane the coupling is adjusted from the spacing between elements d_l and d_w. Additionally, the gaps defined by $g_w \times g_l$ are used to adjust the overall impedance of the patch set. Due to the parasitic patch elements disposition, this particular antenna stands out from the several other designs as the coupling between the central patch and the parasitic elements occurs for the two planes (H and E) in a single substrate layer, while most of the designs found in the literature are coupling the two planes using independent layers.

To redesign the proposed antenna for the frequency of interest (26 GHz band), several aspects were taken into consideration: the feeding point offset (F_O) is critical to adjust the impedance and keep the current distribution uniform throughout the various patches. If the feeding point is not set correctly, the antenna radiation pattern will offset from boresight. Moreover, the values of r_l, r_w, d_l and d_w need to be optimised to ensure that all elements are excited in phase. Throughout the process of re-designing the antenna, parametric studies were carried out, to ascertain how each design parameter affects the gain, directivity, bandwidth and the radiation diagram of the antenna. The results of these studies are presented in the next section.

3.3 DESIGN AND OPTIMISATION

To implement the proposed antenna (Fig. 3.1) a double side Rogers RT/Duroid 5880 substrate, with $\varepsilon_r = 2.2$, loss tangent of 0.0009 and a substrate thickness $h = 1.5$ mm, has been considered. Moreover, a parametric study was performed to tune the proposed antenna for the desired frequency band, defined from 23.5 to 27.5 GHz.

As a starting point, the initial values and layout parameters, provided by [106] and detailed in Table 3.1, for an antenna operating in the 18 to 21 GHz band, have been taken into consideration. A parametric study on e_w and e_l parameters was firstly carried out to adjust the operating frequency of the antenna. According to an initial set of simulations, depicted in Fig. 3.2a, an antenna with patch dimensions of $e_w = 4$ mm and $e_l = 3$ mm is resonating around 26 GHz, with a bandwidth of

Table 3.1: original design parameters for an antenna operating in the 18 to 21 GHz frequency band [106] .

Parameter	Values	Unit
e_w	5.3	mm
e_l	4.4	mm
d_w	0.15	mm
d_l	3.2	mm
r_w	0.4	mm
r_l	5.4	mm
g_w	0.6	mm
g_l	2.3	mm
S_{ub}	3.2	cm
F_O	1.6	mm

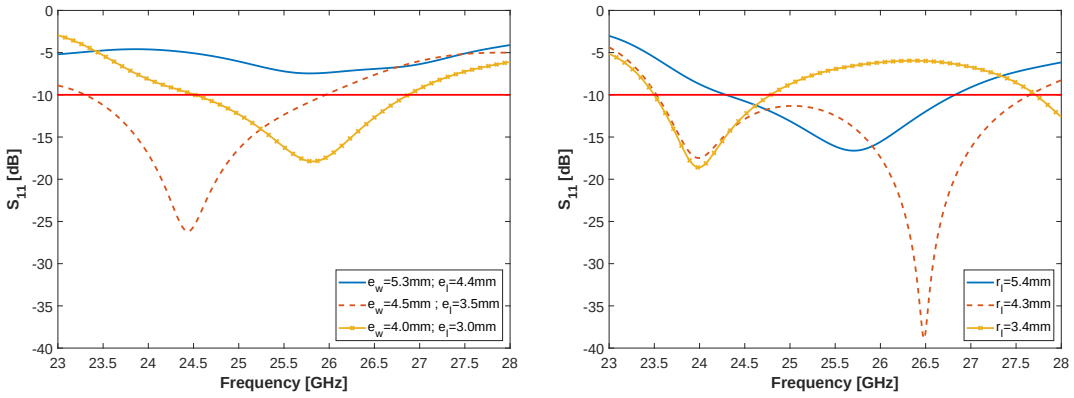

(a) **(b)**

Figure 3.2: S_{11} results from the parametric study on: (a) e_w and e_l, (b) r_l, respectively.

2.3 GHz, defined from 24.5 GHz to 26.8 GHz (considering a S_{11} < -10 dB). However, the radiation pattern at 26 GHz presents an undesired offset angle from broadside of -5° on the elevation plane, as a consequence of this original tuning. This offset occurs since value of F_o has not been taken into consideration on e_w and e_l parametric study. The feeding point offset defined by F_o is critical for the behaviour of the antenna. Therefore, to reduce the offset, the value of F_o was changed from 1.6 mm to 1.8 mm.

In order to enhance the antenna bandwidth, a subsequent parametric study on r_l was performed, as this parameter not only controls the E-field coupling, but also the current distribution for the parasitic patches. The simulation results of this parametric study can be seen in Fig. 3.2b, where a bandwidth of 4 GHz (from 23.5 GHz to 27.5 GHz) can be observed when considering $r_l = 4.3$ mm.

So far, the optimisation process only assessed the frequency band of the antenna, which was obtained from the S_{11} on each parametric study. Considering that the antenna has been optimised to operate in the target frequency band (23.5 to

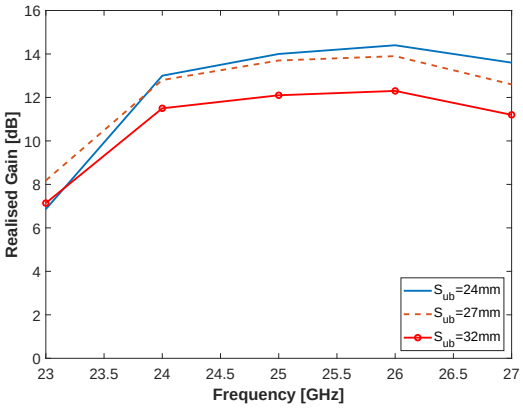

Figure 3.3: Overall realised gain achieved with different S_{ub} values.

Table 3.2: Optimised values.

Parameter	Values	Unit
e_w	4.0	mm
e_l	3.0	mm
d_w	0.15	mm
d_l	3.2	mm
r_w	0.4	mm
r_l	4.3	mm
g_w	0.6	mm
g_l	2.3	mm
S_{ub}	2.4	cm
F_O	1.8	mm

27.5 GHz), the next step of the optimisation process was to enhance the antenna gain. This can be improved by adjusting the size of the ground and substrate (S_{ub}), as shown in Fig. 3.3, which depicts the overall gain of the antenna achieved with for different values for S_{ub}. From the simulation results, it can be observed that by decreasing S_{ub}, the overall gain of the antenna increases. However, this only occurs until the optimal value is reached, which is at S_{ub}=24 mm.

According to the presented parametric study, table 3.2 presents the optimised dimensions for the antenna operating in the 5G frequency band n258, whilst maximisin the highest gain possible within the band.

The final S_{11}-parameter of the optimised antenna is depicted in Fig. 3.4 (optimised dimensions in table 3.2). For completeness, the radiation patterns at specific spot frequency within the desired operating band, in particular at 24, 26 and 27 GHz, are depicted in Fig. 3.5. From the radiation pattern at 24 GHz, a HPBW in the main plane (azimuth) of 33.8° and a realised gain of 13.3 dBi were achieved. Remarkably at 26 GHz (Fig. 3.6), the antenna reached its peak performance with a realised gain of 14.4 dBi and an HPBW of 32.4°, which stands out for similar designs present

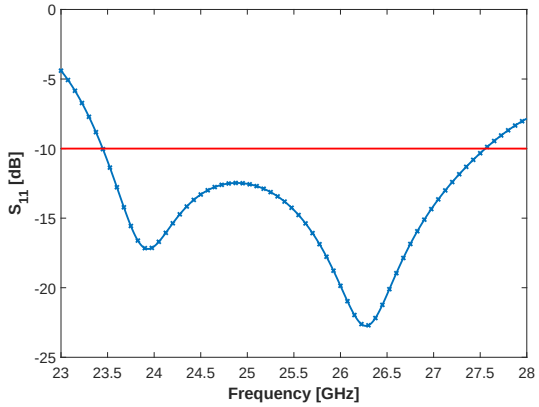

Figure 3.4: Simulated S_{11} of the optimise antenna.

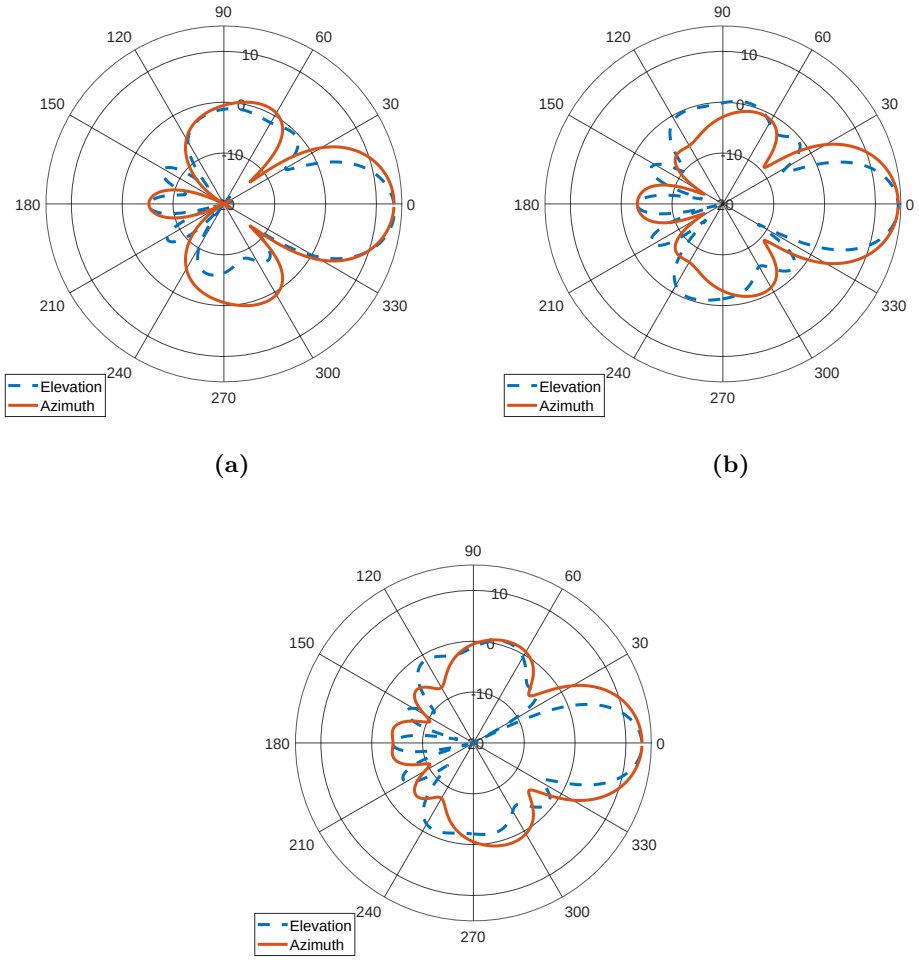

Figure 3.5: Radiation pattern on azimuth and elevation plane at: (a) 24 GHz, (b) 26 GHz and, (c) 27 GHz.

Table 3.3: Comparison table (at 26 GHz).

Antenna	Layers	Elements	Size (λ_o)	Bandwidth (%)	Gain (dBi)
[108]	4	16	1.85×1.85	17.7	16.4
[111]	2	5	0.63×0.63	20	5.2
[112]	2	4	2.43×3.04	3.1	4.79
[107]	1	4	3.63×0.9	6	13.1
[109]	2	42	6.4×7.7	6.3	21.8
[110]	3	64	4.3×4.3	15.2	21.5
Proposed Antenna	1	9	2.1×2.1	16.29	14.4

in the literature (Table 3.3). Lastly, at 27 GHz, the antenna presented a gain of 13.5 dBi and an HPBW of 32.5°.

Table 3.3 compares the antenna element developed herein with other antennas present in the literature (operating in a similar band), in terms of dimensions, number of layers and elements, gain and bandwidth achieved by each design (λ_o represents the wavelength of the central frequency of each antenna). The proposed design is sought to be the one from the Table 3.3 that generally outperforms in terms of performance, less complexity and ease of implementation, since is comprised of only one layer in addition only 1 active element, which is probe fed, while for example in [107], all the 4 elements are fed. The gain of the proposed design falls behind when compared to the more complex designs such as [108–110]. However, this design stands out due to its simplicity and ease of production, since it can be printed on the node PCB, with minor changes (feed probe). Unfortunately, was not possible to develop a prototype of the proposed antenna due to the low resolution (0.5 mm) of the PCB manufacture facilities of Polytechnic of Leiria. Utilising such low resolution compromise the optimised value of the parameter r_w and the gaps between the lines and patches, interfering with the E-field coupling and the current distribution of the antenna.

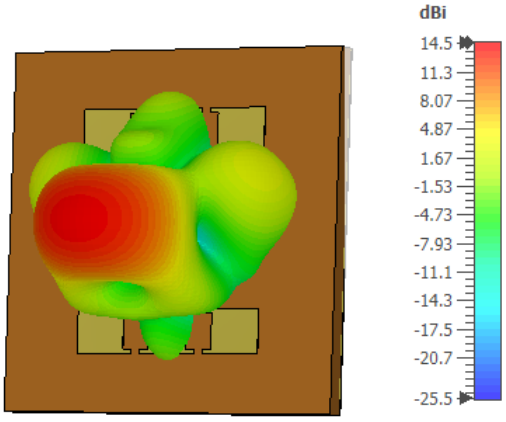

Figure 3.6: 3D representation of the radiation pattern at 26 GHz.

3.4 INTERIM CONCLUSIONS

In this chapter, a high-gain wideband parasitic microstrip antenna was designed, characterised and optimised to operate at the 5G new radio (NR), frequency range 2 (FR2), band n258. Various parametric studies were carried out in order to optimise the antenna to operate from 23.5 to 27.5 GHz while achieving the highest gain possible. Simulation results ensured a realised gain of 14.4 dBi (at 26 GHz) and a total bandwidth of 4.15 GHz, after optimisation in CST-MWS. The proposed antenna design stands out due to its small dimension, simplicity (only 1 layer) and, relatively high gain, when compared to the state-of-art designs. This is in-line with the need to achieve small-form factor and ease of integration on the same PCB as the other electronic circuitry, using a small printing area of 24×24 mm², particularly for sensor node antennas, which makes it a suitable candidate for wearable 5G and IoT applications.

The contents of this chapter resulted in the following conference paper:

- T. E. S. Oliveira, J. F. Goncalves, J. R. Reis, M. Vala and R. F. S. Caldeirinha, **"High-Gain Wideband Parasitic Microstrip Antenna for 5G and IoT at 26 GHz"**, *Conf. on Telecommunications - ConfTele*, Leiria, Portugal, February, 2021, pp. 1-5, doi: 10.1109/ConfTELE50222.2021.9435457.

This page is intentionally left blank.

4

DIRECTIONAL ANTENNAS FOR WSN BASE STATIONS AT 2.4 GHZ

4.1 INTRODUCTION

This chapter presents the design, optimisation and measurement of antennas to be implemented in a WSN base station. In particular, two antenna designs are presented, which were studied and optimised utilising the CST-MWS, to operate in the 2.4 GHz frequency band. Firstly, a microstrip Quasi-Yagi antenna is studied and characterised, followed by a noval microstrip Quasi-Yagi design based on lunar waning crescent elements. Further studies on the latter antenna are performed aiming its implementation in a WSN base station.

4.2 A MICROSTRIP QUASI-YAGI PATCH ANTENNA

The first antenna design to be studied was a microstrip Quasi-Yagi antenna. This antenna type explores the concept of the well-known Yagi antennas, adapted to microstrip technology. The Yagi antenna is a directional antenna model consisting of multiple parallel elements in a line, usually half-wave dipoles, made of metal rods and separated by multiples of the wavelength. Therefore, the antenna design of [113] was considered. Following redesign and optimisation processes, using the FR4 substrate that is commonly utilised on the circuitry PCB. The antenna was successfully modified to operate from 2.27 to 2.83 GHz, aiming at the 2.4 GHz ISM band.

The work presented on this chapter follows the specifications imposed in the WSN-EM project [16], for the base station antenna, In particular, the antenna must have a gain higher or equal to 8 dBi, operate at the 2.4 GHz ISM band, with an HPBW higher or equal to 60° and display a minimum front-to-back ratio of 20 dB.

4.2.1 *Antenna Layout*

The antenna layout, depicted in Fig. 4.1, is based on planar Quasi-Yagi layout in which metallic parasitic elements are added as directors, in order to focus the

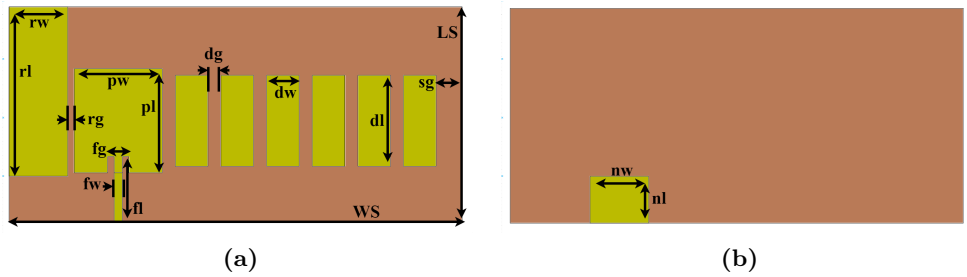

Figure 4.1: Quasi-Yagi microstrip antenna layout: (a) top view and (b) bottom view.

radiated energy in one direction. The design proposed by [113], which operates from 2.74 to 4.25 GHz, is composed of: a microstrip patch ($p_w \times p_l$), acting as active element, which defines the frequency of operation; a reflector ($r_w \times r_l$) and six directors ($d_w \times d_l$), separated by d_g, that are responsible for providing the end-fire radiation pattern. The reflector element, in addition to the directors, helps to shape the antenna radiation pattern, which provides the design with the possibility to redirect the main lobe direction on the elevation plane. The addition of directors increases the overall gain of the antenna, which as a consequence, reduces the HPBW.

This particular antenna design is light-weight, low-profile with a planar configuration, but relatively high gain when compared with other microstrip antenna designs.

4.2.2 *Design and Optimisation*

To implement the proposed antenna, design of Fig. 4.1, a double sided FR4 substrate, with $\varepsilon_r = 4.4$ and a loss tangent of 0.014 was considered. The substrate has a thickness of $h = 1.6$ mm.

The initial parameters of the design are shown in Table 4.1. The first step of the optimisation phase was to change the patch dimensions, since it dictates the frequency of operation for the antenna. With this consideration, a detailed parametric study on p_w and p_l parameters was carried out. The simulation results are presented in Fig 4.2, where the S_{11} is shown for different parameter combinations. The results ensure a frequency band of operation from 2.27 to 2.6 GHz, when $p_l = 38$ mm and $p_w = 27$ mm. However, the radiation pattern shows a main lobe magnitude of 5.8 dBi, at 2.44 GHz. In order to further optimise the radiation pattern of the antenna, parametric studies on the reflector length (r_l) and the directors dimension (d_w and d_l) were also performed.

Table 4.1: Original values from [113], for the microstrip Quasi-Yagi antenna(in mm), operating from 2.74-4.25 GHz.

p_w	p_l	d_w	d_l	r_w	r_l	f_w	**fl**
18.0	23.0	5.0	21.0	18	35	2.5	20.0
W_s	L_s	n_w	n_l	r_g	d_g	f_g	**sg**
98.0	54.5	15.0	14.44	2.0	4.0	5.0	8.0

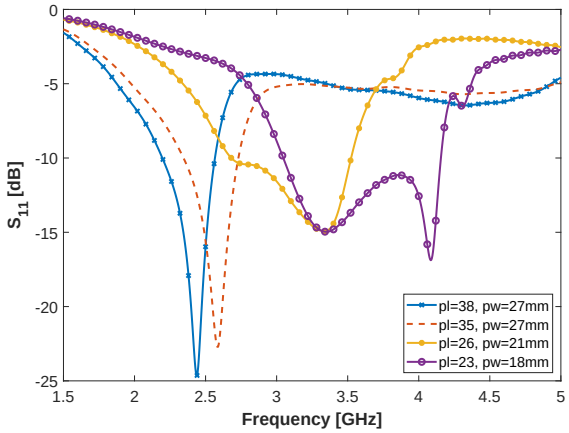

Figure 4.2: S_{11} results for the parametric study on p_l and p_w.

The simulated radiation patterns obtain for different combinations of r_l, d_w and d_l are depicted in Fig. 4.3, where it can be seen that the antenna has a main lobe magnitude of 8.32 dBi, when $r_l = 52$ mm, $d_l = 31$ mm and $d_w = 12$ mm.

Due to the changes performed in the design, the resonating frequency shifted 100 MHz from the previous results in Fig. 4.2, therefore adjustments of the patch dimension were made.

After subsequent optimisation on the S_{11}, the antenna has an operating frequency band from 2.27 to 2.83 GHz, coffering a bandwidth of 21.96%, Fig. 4.4. The radiation pattern for both main planes, as depicted in Fig. 4.4b, presents a realised gain of 9.41 dBi, an HPBW of 70° on the azimuth plane. The optimised values for the design can be seen in Table 4.2.

Table 4.2: Optimised values for the proposed antenna design (in mm), operating at 2.4 GHz.

p_w	**pl**	d_w	d_l	r_w	r_l	f_w	f_l
27.0	34.0	12.0	31.0	18.0	52.0	2.5	20.0
W_s	L_s	n_w	n_l	r_g	d_g	f_g	s_g
150.0	60.0	15.0	14.44	2.0	4.0	5.0	8.0

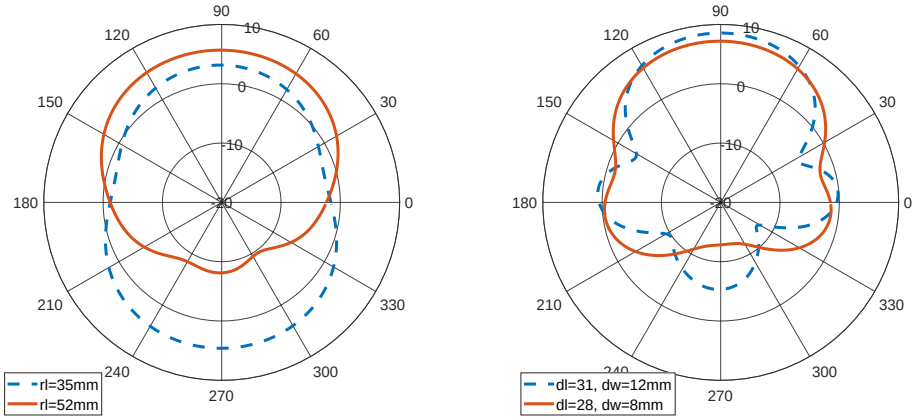

(a) **(b)**

Figure 4.3: Parametric results of the radiation pattern, at 2.44 GHz, for: (a) r_l ,(b) d_w and d_l, in the azimuth plane

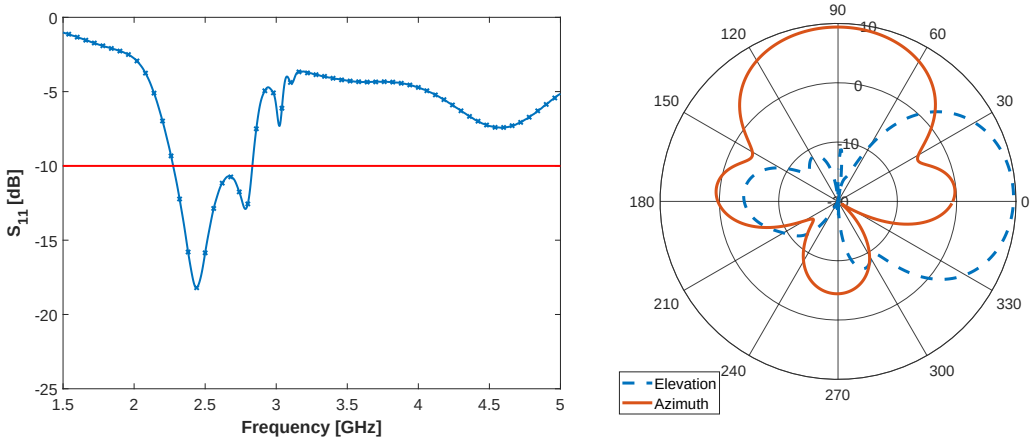

(a) **(b)**

Figure 4.4: Simulation results: (a) S_{11}, (b) Radiation pattern on azimuth and elevation plane at 2.44 GHz.

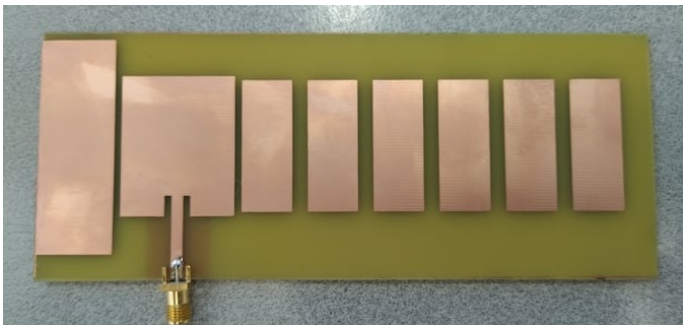

Figure 4.5: Microstrip Quasi-Yagi antenna prototype.

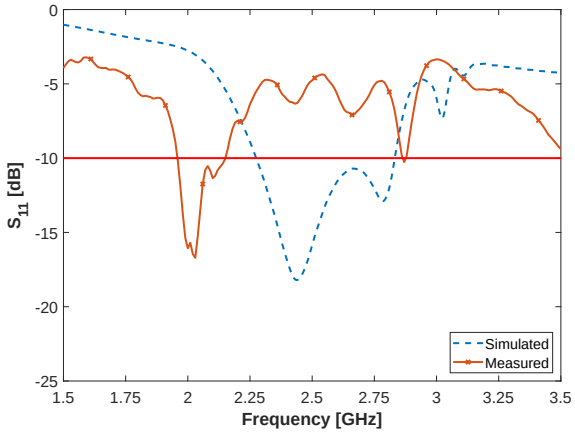

Figure 4.6: Simulated and measured S_{11} results of the microstrip Quasi-Yagi antenna.

4.2.3 *Experimental Characterisation*

With the antenna design optimised, a prototype of the antenna has been produced. A photograph of the prototype is depicted in Fig. 4.5.

In order to measure the S_{11}, the antenna was connected to a Vector Network Analyser (VNA) (R&S ZVM). This two ports model, can measure the S_{11}, S_{12}, S_{21} and S_{22} of a Device Unter Test (DUT), with the possibility to retrieve informations such has the insertion loss and the matching of a DUT.

Analysing the results in 4.6 is observed that simulations are inconsistent with measured results, appraising the low matching of the antenna. A potential cause for such discording results, is the small ground plane proposed for the design. Two prototypes were developed to test a possible shift on the resonating frequency between results however without success. Therefore, the design is not suitable to be integrated in a cylindrical-base configuration. For this reason, it is proposed a Lunar Waning Crescent Quasi-Yagi Antenna, for the BS antenna.

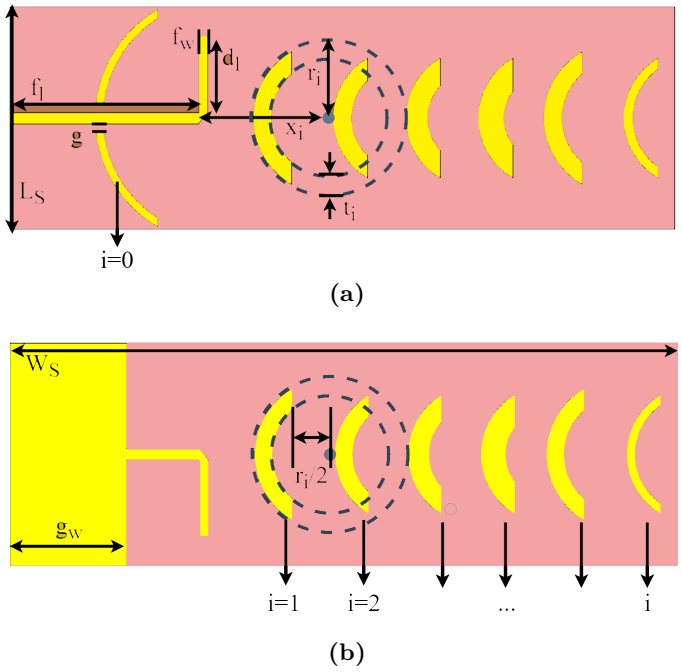

Figure 4.7: Proposed Lunar Waning Crescent Quasi-Yagi antenna layout, (a) top view and (b) bottom view.

4.3 A LUNAR WANING CRESCENT QUASI-YAGI ANTENNA FOR WSN BASE STATION

To overcome the design/implementation issues of the previous antenna, a novel microstrip Quasi-Yagi design based on lunar waning crescent elements has been introduced. In particular, the new design employs a bigger ground-plane to attain a better antenna matching and a dipole as driven element (instead of a patch). Both reflector and directors have a semi-circular shape, mimicking the lunar waning crescent shape. The same substrate (FR4) will be used for the new design. Details about the antenna design are further described next section.

4.3.1 *Antenna Layout*

The proposed antenna layout is depicted in Fig. 4.7. The antenna is composed of a microstrip dipole, a waning crescent reflector over a ground plane (defined by g_w) and, six waning crescent directors. The waning crescent shaped for the reflector and directors was chosen, since it outperform other shapes studied (higher gain). As can be seen in Fig. 4.8, which depict the results of a study on the performance of a dipole with a single director.

The proposed shape, should be seen as a quarter of a circle centred at x_i, with radius (r_i) and thickness t_i, where $i = 0, 1, 2, ...$ represents the number of the of the

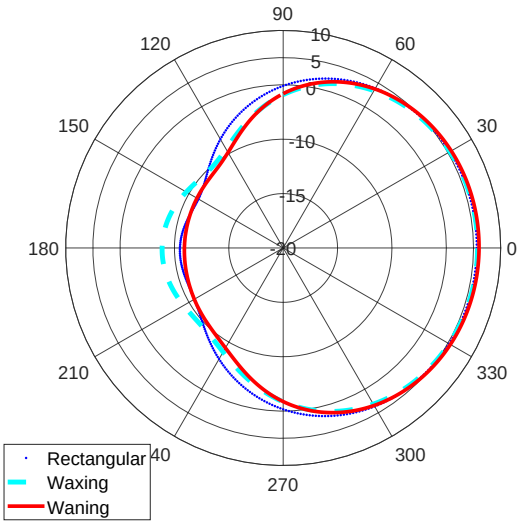

Figure 4.8: Radiation pattern on the azimuth plane for different director shapes.

reflector/director. The overall antenna dimensions are dictated by the parameters $W_S \times L_S$.

The feeding line width and length dictates the input impedance of the antenna. Aiming to attain a 50 Ω impedance, the width of the feeding line was calculated by [13]:

$$Z_o = \frac{120\pi}{\sqrt{\varepsilon_e}\left[\frac{W}{H}+1.393+\frac{2}{3}ln\left(\frac{W}{H}+1.4444\right)\right]}, \tag{4.1}$$

where,

$$\varepsilon_e = \frac{\varepsilon_r+1}{2}+\left[\frac{\varepsilon_r-1}{2\sqrt{1+12\left(\frac{H}{W}\right)}}\right], \tag{4.2}$$

and W is the width of the feeding line and H the thickness of the substrate. Notice that these equations can only be applied if $W > H$.

The frequency of operation is defined by the dimensions of the dipole arms (d_l), to achieve a better efficiency the dipole arm should have a length equal to half of the wavelength propagating in the microstrip line, $\lambda_g/2$ [13]. However, at 2.4 GHz, λ_g is 22.8 cm, according to the Eq. 4.3 [114]. Therefore, to keep the size of the antenna moderated, it was opted to start the design with the total length of $\lambda_g/4$, reducing the size of the substrate.

$$\lambda_g = \frac{c}{f\sqrt{\varepsilon_e}}, \tag{4.3}$$

The dipole arms are perpendicular to the feeding line thus, creating a 90° bend which can cause an unnecessary signal reflection to the source. To overcome this

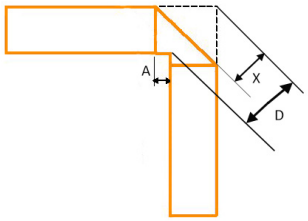

Figure 4.9: Microstrip mitred bend, (extracted from "everythingrf").

issue the bend was mitred (Fig. 4.9) following Eq. 4.4 to Eq. 4.6, to reduce the capacitance of the line, maintaining the desired impedance [115].

$$D = W \times \sqrt{2}, \tag{4.4}$$

$$X = W \times \sqrt{2} \times \left(0.52+0.65 \times e^{\left(-1.35\times\frac{W}{H}\right)}\right), \tag{4.5}$$

$$A = X \times \sqrt{2} \text{ - } W, \tag{4.6}$$

The antenna was designed in a double-sided FR4 substrate, with $\varepsilon_r = 4.4$, a $tan\delta = 0.014$ and a thickness of 1.6 mm. The optimisation of the antenna dimensions and the number of directors are further analysed and discussed next section.

4.3.2 *Antenna Design*

In a first iteration, the microstrip dipole with ground plane of Fig. 4.10a was designed and simulated, in order to assess the length of the dipole arm needed to attain an antenna resonating of 2.445 GHz (target frequency). Therefore, a parametric study was carried out on d_l, with the initial value being set at $\lambda_g/8$ and, by fixing g_w at 32 mm, $L_S = 61$ mm and $f_l = 52$ mm. While L_S was defined to accommodate at least the arms length (i.e. $2\times$ $\lambda_g/8$), f_l and g_w were deliberately defined to further accommodate the reflector shape. Additionally, f_w was set at 3.1 mm corresponding to a 50Ω impedance line for the proposed substrate. The simulation results of the parametric study are depicted in Fig. 4.11. The simulation ranged from 20.5 to 28.5 mm, with 2 mm step. From the results, it can be observed that a $d_l = 20.5$ mm ensures the antenna is resonating at the desired frequency (*i.e.* 2.445 GHz).

With the dipole arms length already defined, the next step in the antenna design is to evaluate the impact of adding the directors in antenna performance. Therefore,

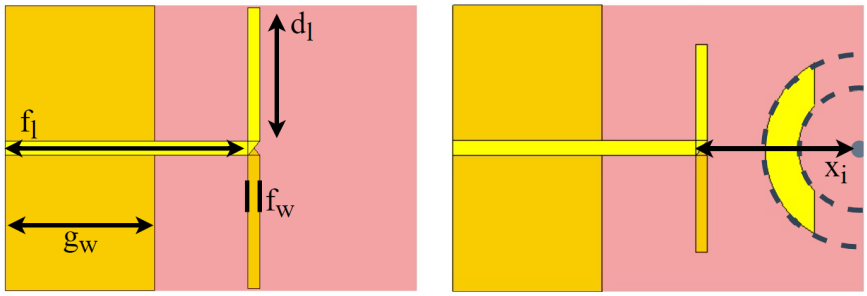

Figure 4.10: CST-MWS model of: (a) the microstrip dipole and (b) inclusion of a single waning crescent director.

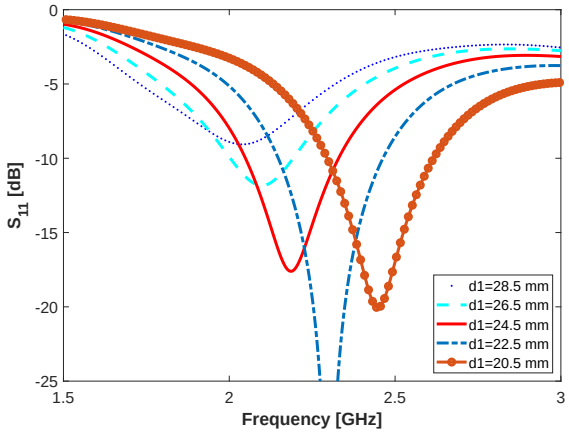

Figure 4.11: Simulated S_{11} results for the parametric study of d_l.

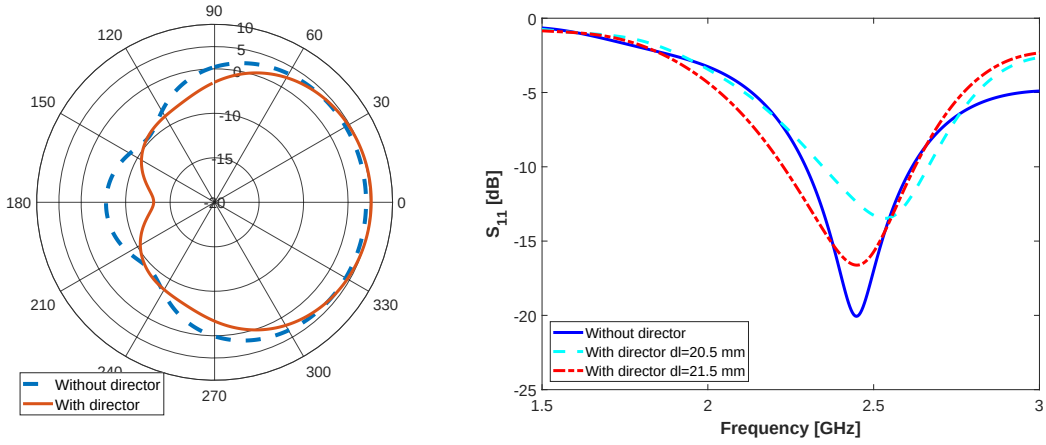

(a) **(b)**

Figure 4.12: Impact of the addition of a single waning crescent director in (a) radiation pattern, at 2.445 GHz, and in (b) antenna S_{11}.

a single waning crescent director was added to the feeding antenna, at the position $x_1 = 32$ mm, as depicted in Fig. 4.10b. At this point, no reflector has been considered. The initial values of $t_1 = 8$ mm and $r_1 = 22$ mm where considered as starting point for the optimisation. The addition of the director caused two effects: an increase in the overall antenna gain and an undesirable deviation of the antenna's resonating frequency, as depicted in Fig. 4.12. While the first effect was expected (in line with the Yagi antenna concept [116]), the latter is associated with mutual coupling effects between the driven element (dipole) and the added director. To compensate for this frequency shift, the length of the dipole arms (d_l) were readjusted for 21.5 mm (Fig. 4.12b).

After ensuring the antenna was re-tuned for the desired frequency, a parametric study was carried out in all parameters (r_1, x_1 and t_1) of the first waning crescent director ($i = 1$). The study aimed to optimise the waning crescent director dimensions to achieve the best antenna gain possible. To this extend, the following methodology was been considered: a parametric simulation run for a single parameter at the time, while the others are assigned a fixed value. After discovering the value that would provide the highest gain, it becomes fixed, and a new parametric simulation on a different parameter is carried out. At the end of the study, this process is repeated once again, to ensure that the defined values are, in fact, the optimised ones (double confirmation).

In particular, Fig. 4.13 presents the radiation patterns obtained for different values of t_1, with x_1 and r_1 fixed at 32 mm and 22 mm, respectively. With $t_1 = 4$ mm the antenna presents a gain of 5.4 dBi (Fig. 4.13a), for $t_1 = 5$ mm the gain is of 5.5 dBi (Fig. 4.13b), for $t_1 = 6$ mm is 5.58 dBi (Fig. 4.13c), and finally, for $t_1 = 7$ mm the gain stabilises at 5.55 dBi (Fig. 4.13d).

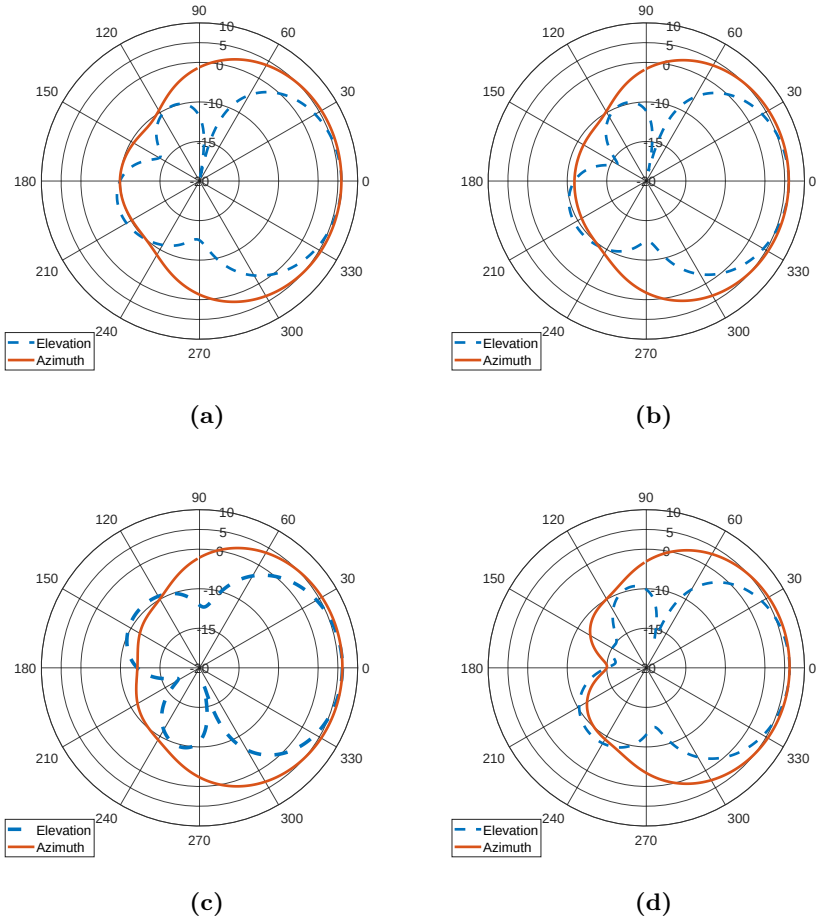

Figure 4.13: Radiation pattern on azimuth and elevation planes, at 2.445 GHz, for (a) $t_1 = 4$ mm, (b) $t_1 = 5$ mm, (b) $t_1 = 6$ mm and, (d) $t_1 = 7$ mm.

In line with the methodology described above, further studies were carried out in the parameters x_1 and r_1, individually. From the final optimisation realised on the first director, it was found that the parameters which best favour the antenna performance in terms of gain are: $x_1 = 36$ mm, $t_1 = 5$ mm and $r_1 = 21$ mm, yielding a realised gain of 6.02 dBi. This results in an increase of 1.65 dBi in gain, when comparing to the antenna without a director.

Aiming to design an antenna with a higher gain, the process of adding directors has been studied. Thus, a parametric workout was carried out to access the gain improvement against the number of directors (with the same dimensions). The directors were added progressively to the layout, at the position $x_i = x_{i-1} + 18$ mm. Note that in this particular study, all directors have the same dimensions. The maximum gain at the antenna boresight has been obtained, and it is plotted against the number of directors (up to 8) in Fig. 4.14. From the analysis of the results, it can be seen that after the addition of 6 waning crescent directors, the ratio between gain and number of directors decreases. The difference from 6 to 8 directors is 0.81 dB, while the difference from 4 to 6 is 1.24 dB. Thus, for the best trade-off

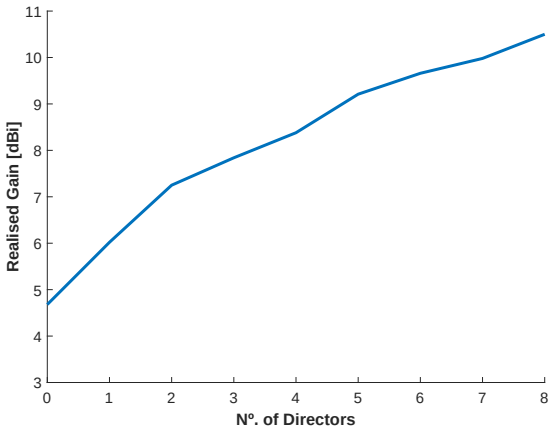

Figure 4.14: Variation of the realised gain of the antenna with the number of directors.

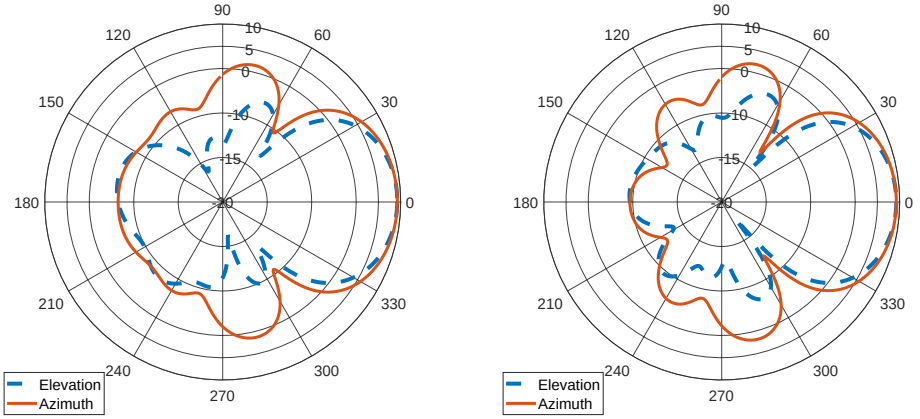

(a) **(b)**

Figure 4.15: Radiation pattern in azimuth and elevation planes at 2.44 GHz, on the (a) without and (b) with the reflector.

between antenna dimensions and gain, it was opted for 6 director design which achieves the target gain of 9.6 dBi. This represents an additional gain of 3.6 dB, when comparing with the configuration of a single director.

To further improve the front-to-back ratio of the antenna (already considering 6 directors), an additional waning crescent reflector was added to the design. The element was added prior to the feeding line (at the position x_o 8 mm), over the ground plane. The dimensions of the reflector were also optimised using CST MWS with the goal of improving the front-to-back ratio. From the parametric workout, it was found that the best front-to-back ratio is of 18.63 dB, achieved with $r_o = 34.5$ mm, $x_o = 8$ mm, $t_o = 5$ mm and $g = 2$ mm, as depicted Fig. 4.15, which improves 4.28 dB, from the case without reflector, Fig. 4.15a.

In this configuration the antenna gain is also slightly improved by 0.1 dB. Simulation results ensure a realised gain of 9.7 dBi, at 2.44 GHz, a front-to-back ratio of 18.63 dB, and a HPBW of 60°. Not satisfied with the achieved front-to-back

ratio, an optimisation process took place, by studying the effect of different director dimensions in the antenna performance. The entire process is described in the next section.

4.3.3 *Antenna Director/Reflector Optimisation*

Using the double confirmation technique described before, all the parameters of each director (r_i, x_i and t_i) are optimised, individually, with the goal of achieving the highest gain possible whilst keeping the S_{11} < -30 dB, in the resonance frequency. Therefore, a parametric study was carried out to access the curve of the gain improvement with the addiction of the optimised directors to the design. The directors were added progressively to the layout, at the position $x_i = x_{i-1} + 20$ mm, and further optimised for best antenna gain and impedance matching. The results of the parametric study, depicted in Fig. 4.16, ensure that the best trade-off between antenna dimensions and gain, is also attained with 6 director's. Since the difference from 6 to 8 directors is 0.6 dB, while the difference from 4 to 6 is 1.45 dB. With six directors the antenna achieves the gain of 9.45 dBi. Representing a decrease of 0.1 dB when compare to the antenna that utilises equal directors.

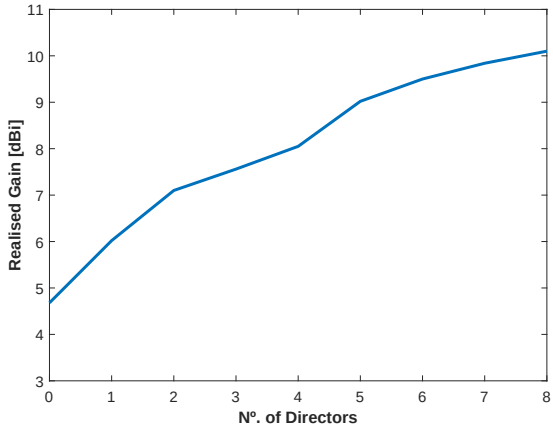

Figure 4.16: Variation of the realised gain of the antenna with the number of directors.

An additional waning crescent element was added as a reflector, to further improve the front-to-back ratio of the Quasi-Yagi antenna element, as previous. Using the same methodology, the reflector dimensions were optimised, where it was found that the best front-to-back ratio is of 20.16 dB, obtained for r_o = 34.5 mm, x_o = 6 mm, t_o = 2.1 mm and g = 2 mm, being improved in 5.68 dB when compared with the case without reflector (Fig. 4.17). With the values presented above, the HPBW of the antenna increases 3° and, consequently, the gain decays to 9.45 dBi, causing a difference of 0.25 dB to the previous design. However, the new design presents an additional 1.53 dB front-to-back ratio, which thought compensate the gain difference between the designs.

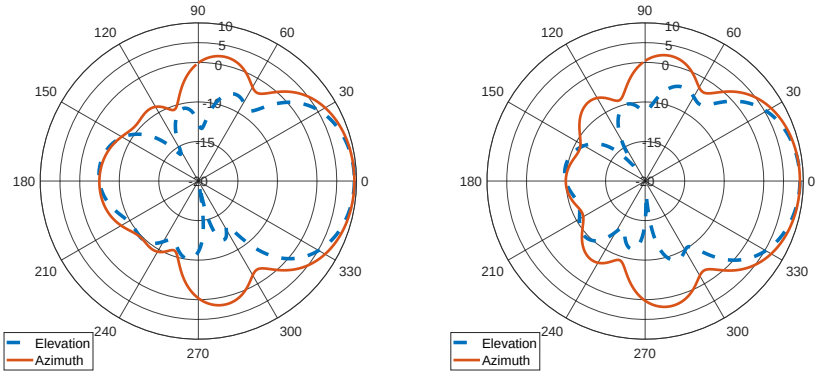

Figure 4.17: Radiation pattern in azimuth and elevation planes at 2.445 GHz, on the (a) without and (b) with the reflector.

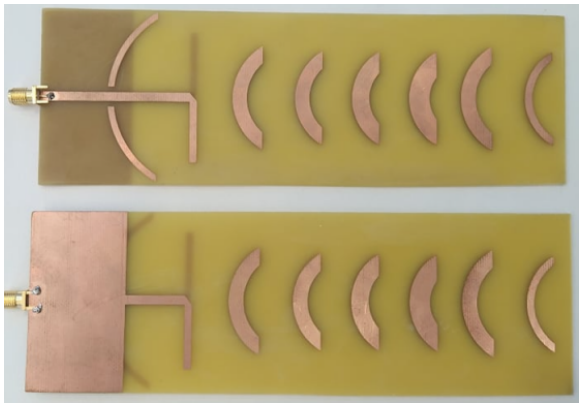

Figure 4.18: Lunar Waning Crescent antenna prototype (with different director dimensions).

Finally, after all the design optimisation in the proposed layout, an antenna with overall size of 183×61 mm², and dimensions of (in mm): $L_S = 61$, $W_S = 183$, $f_l = 52$, $g = 2$, $g_w = 32$, $d_l = 21.5$, $f_w = 3.1$, and director dimensions of: $x_0 = 6$, $r_0 = 34.5$, $t_0 = 2.1$, $t_1 = 5$, $r_1 = 21$, $x_1 = 36$, $t_2 = 5$, $r_2 = 19$, $x_2 = 56$, $t_3 = 6$, $r_3 = 19$, $x_3 = 76$, $t_4 = 7$, $r_4 = 19$, $x_4 = 96$, $t_5 = 5$, $r_5 = 21$, $x_5 = 116$, $t_6 = 2.5$, $r_6 = 1$ and $x_6 = 136$, presents a realised gain of 9.45 dBi at 2.445 GHz, with a bandwidth of 450 MHz, a front-to-back ratio of 20.16 dB, and a HPBW of 63°. The final antenna radiation pattern can be seen in Fig. 4.17b.

4.3.4 *Experimental Setup*

In order to experimentally characterise the developed antenna (Fig. 4.18), both antenna matching (S_{11}) and radiation patterns, in the two main antenna planes, *i.e.* in azimuth and elevation, have been obtained. While the S_{11} was measured using a two port VNA (R&S ZVM), the setup of Fig. 4.19 was assembled inside an anechoic

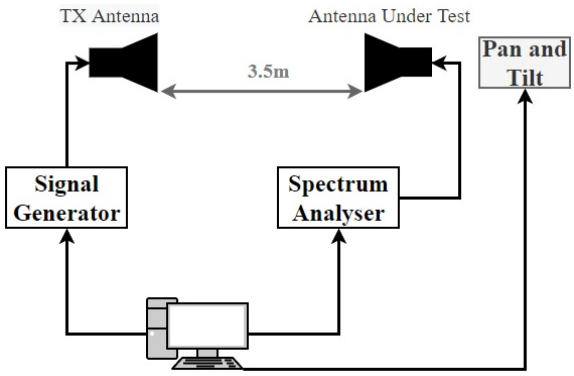

(a)

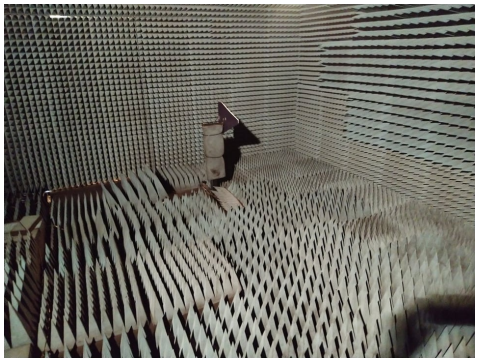

(b)

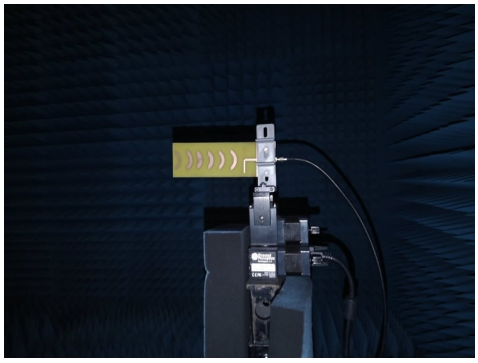

(c)

Figure 4.19: Radiation pattern measurement setup: (a) block diagram; (b) photography of Transmitter (Tx) antenna and (c) close up of the antenna under test, inside the anechoic chamber.

chamber, to measure the antenna radiation patterns. The anechoic chamber was used for indoor measurements enabling experiments to be performed in a controlled, electromagnetically quiet and reflection free radio environment.

In particular, a well characterised *Aaronia Hyperlog 30100* antenna was used as the Tx antenna (Fig 4.19b). It is connected to a signal generator that generated a single tone (continuous wave), with a transmission power of 0 dBm. At the receiver end, a well characterised *Aaronia Hyperlog 60100* antenna was connected to the spectrum analyser to be used as reference, later replaced by the antenna under test (AUT). The antennas were placed 3,5 meters apart, ensuring that the measurement took place in the far-field region of the antennas. The Tx antenna was kept fixed throughout the measurements, while the AUT was rotated around its axis with the assist of motorised pan/tilt head unit, Fig. 4.19c. The received power was acquire utilising a spectrum analyser (Agilent E4408B) for each angular step with 1° of resolution, within the range defined between -180° and 180° (in the azimuth plane). Both Tx and Receiver (Rx) antennas were further rotated 90° to measure the radiation pattern in the elevation plane, using the same physical setup. The received power acquisition and movement control were executed in real-time and post processed in MATLAB, using a software developed for the effect.

4.3.5 *Experimental Characterisation*

In Fig. 4.20, it is depicted the simulated and measured results for the S_{11}. From the analysis of the results, its concluded that both results are in relatively good agreement, even though a small deviation, in the resonating frequency of 46 MHz, is observed. When comparing the radiation pattern at 2.44 GHz (Fig. 4.21), for both simulations and experiments, it is observed that: the shape of the radiation patterns are in good agreement; the prototype attain a gain of 8.9 dBi, which is less 0.55 dB from the simulated results (9.45 dBi) and finally, the HPBW for the prototype is of 60°,in the azimuth plane, representing a difference of 3° from the simulated results.

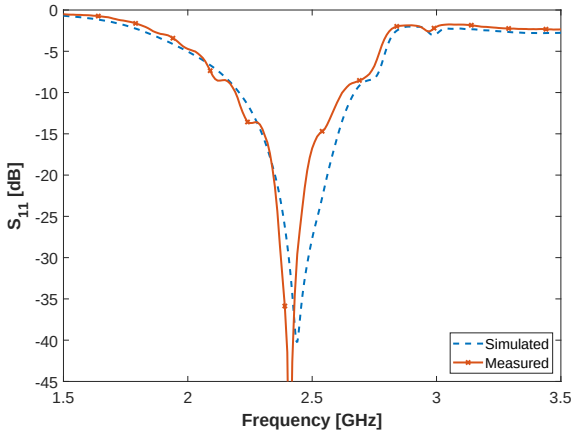

Figure 4.20: Simulated and measured results of the S_{11}, for the Lunar Waning Crescent Quasi-Yagi antenna.

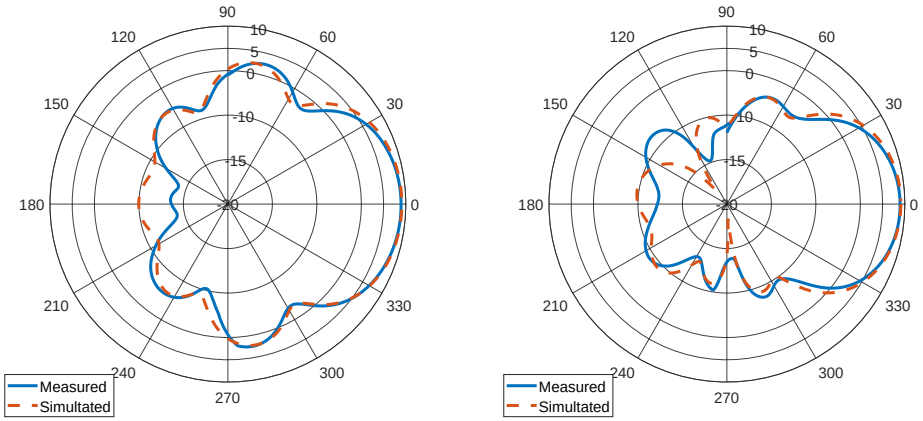

(a) **(b)**

Figure 4.21: Simulated and measured results of the radiation pattern at 2.44 GHz, on the (a) azimuth and (b) elevation plane, for the Lunar Waning Crescent Quasi-Yagi antenna.

4.4 DEVELOPMENT OF A WSN BASE STATION

As mentioned before, the developed antenna is though to be implemented in a cylindrical configuration, with a multiplexing mechanism as a solution for the desired omnidirectional pattern. However, such configuration may be vulnerable to parasitical effects from the adjacent antennas. Thus, the simulation scenario, in Fig. 4.22, was created. Six antennas are equally placed 60° apart in a circular shaped with a diameter defined by a_g, creating the desired 360° FOV. A parametric study on a_g, was carried out aiming to assess the impact of adjacent antennas, on the matching and radiation pattern of the driven antenna.

The simulated results of the impact of adjacent antennas on the radiation pattern, exposed in Fig. 4.23, ensure that at 2.445 GHz the configuration: with $a_g = 10$ cm presents a peak gain of 8.88 dBi and an HPBW of 62.4°; with $a_g = 12$ cm the peak gain is 8.89 dBi and an HPBW of 70.3°; for $a_g = 14$ cm the gain increases to 9.13 dBi with an HPBW of 71.8°; a gain of 8.5 dBi and an HPBW of 75° its achieved with $a_g = 16$ cm. Analysing the radiation patterns, it comes clear that the adjacent antennas act as parasitical elements, creating an small dip on the main lobe for values of a_g inferior to 16 cm. For the sake of the overall size of the configuration, it was opted for $a_g = 14$ cm.

It was opted for the "SKY13418-485LF" RF-switch as the multiplexing mechanism, which operates from 0.1-6.0 GHz and can employ up to 8 antennas. To characterise the RF-switch, the insertion loss and isolation between ports was measured with "Port 1" active. It was also taken into account the RF cables used between switch and antennas. The results, depicted in Fig. 4.24, are in good agreement to the data-sheet given by the manufactured, with a typical isolation $<$ -30 dB and $S_{11} <$ -1.7 dB at the 2.4 GHz ISM band.

To accommodate the antennas and RF-switch, a structure towards the cylindrical configuration was design, Fig. 4.25. Simulation results ensure that only the adjacent antennas have an impact in the radiation pattern of the driven antenna. Therefore the structure was produced in a 3D printer using Polylactic acid (PLA), Fig. 4.26. The matching of the antenna when employed on this structure is presented on

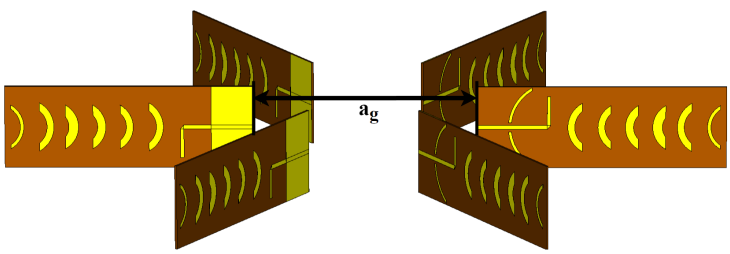

Figure 4.22: Simulation model for the study on the impact of adjacent antennas.

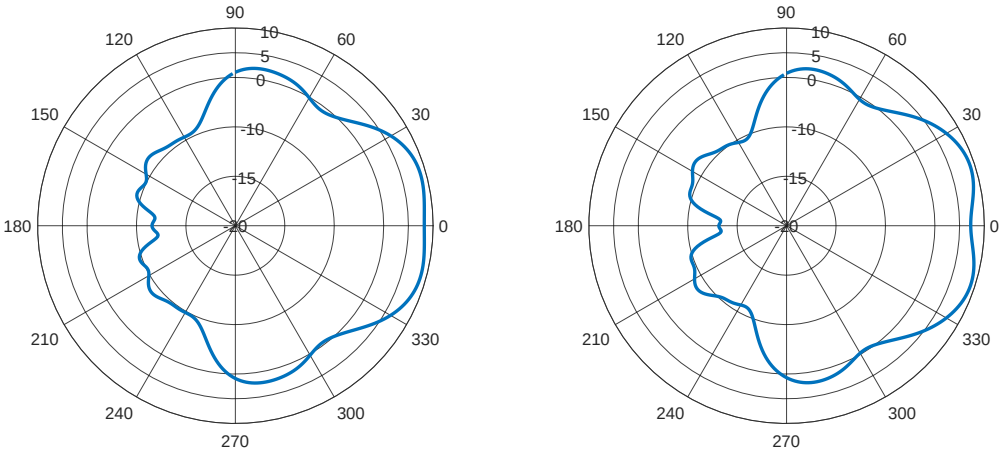

(a) **(b)**

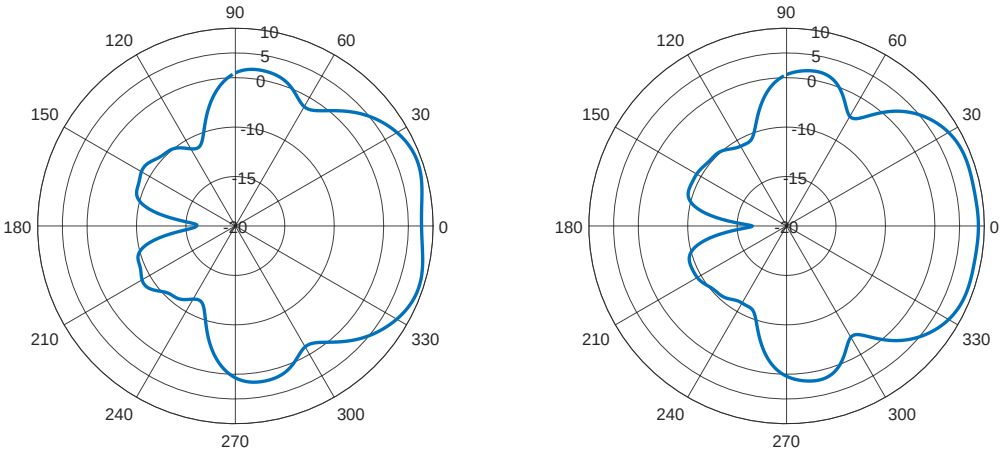

(c) **(d)**

Figure 4.23: Impact of the adjacent antennas on the radiation pattern (azimuth plane) with: (a) $a_g = 10$ cm , (b) $a_g = 12$ cm , (c) $a_g = 14$ cm and (d) $a_g = 16$ cm.

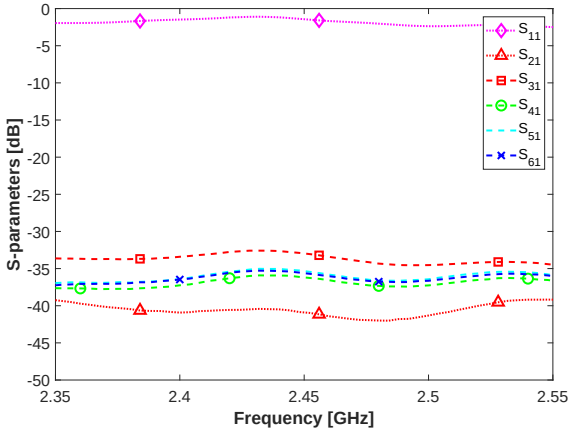

Figure 4.24: Measured isolation and insertion loss, on the RF-switch.

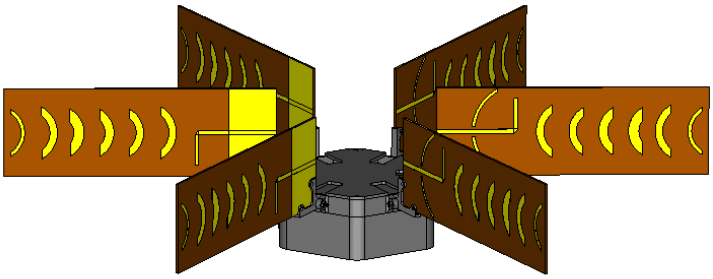

Figure 4.25: Proposed BS structure.

Figure 4.26: Base station prototype.

Fig, 4.27, where can be seen that when mounted, the antenna presents a small shift on the resonating frequency. However, the antenna continues to operate at the 2.4 GHz band, granting the integrity of the system.

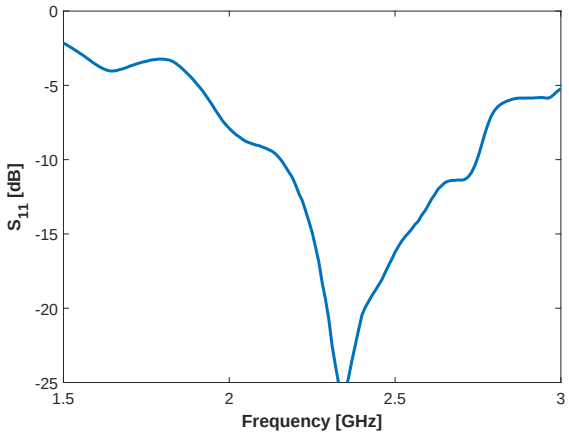

Figure 4.27: Reflection coefficient of an Antenna in the proposed BS

4.5 INTERIM CONCLUSIONS

This chapter expose a study on the design, optimisation, development and prototyping of antennas for a WSN BS operating at the 2.4 GHz ISM band. Firstly a microstrip Quasi-Yagi patch antenna built upon [113] was redesigned and optimised to operate at 2.4 GHz, however simulated and measured results diverge thus, it was succeeded by a Lunar Waning Crescent Quasi-Yagi antenna design. The latter design, achieved a measured peak gain of 8.9 dBi and HPBW of 60° at 2.445 GHz. The proposed antenna was proceeded with the development of an WSN BS, employing a RF-switch, to achieve a 360° FOV. Further simulations and measurements were made to assess impact of the adjacent antennas in the driven antenna.

The contents of this chapter resulted in the following conference papers:

- T. E. S. Oliveira, J. R. Reis, M. Vala and R. F. S. Caldeirinha, **"A Lunar Waning Crescent Quasi-Yagi Antenna for WSN Base-Stations at 2.4 GHz"**, *16th European Conference on Antennas and Propagation - EUCAP*, Madrid, Spain, January, 2022 **(submitted)**;
- T. E. S. Oliveira, J. R. Reis and R. F. S. Caldeirinha, **"A Waning Crescent Quasi-Yagi Microstrip Antenna for Wireless Sensing Networks"**, *15th Congress of the Portuguese Committee of URSI "Environmental sustainability in use of the radio spectrum"*, Leiria, Portugal, November, 2021 **(presented)**;

This page is intentionally left blank.

5

A DIFFERENTIAL MICROSTRIP SLOTTED PATCH ANTENNA FOR WSN SENSOR NODES AT 2.4 GHZ

5.1 INTRODUCTION

In this chapter, a differential microstrip slotted patch antenna for WSN sensor nodes, operating at 2.4 GHz ISM band, is proposed. The antenna is design, optimise and prototyped, aiming for a small form factor while granting a relatively high gain. Furthermore, a balun is developed to have a differential signal as the input of the antenna when considering only one port. Allowing the analysis of some antenna characteristics that could not be obtained while using only the antenna (S_{11}). The impact of vegetation and fire on the radiation pattern of the antenna is also studied aiming to assess the antenna performance in a critical scenario. Electromagnetic simulations are carried using a full-wave EM solver (CST MWS) considering several application scenarios.

The work present on this chapter follows the specifications imposed in the WSN-EM project [16], for the sensor node antenna. The project requires a balanced antenna of small dimensions that operates in the 2.4 GHz band, with a relatively high-gain and HPBW, with ease of integration in the node PCB.

5.2 SENSOR NODE ANTENNA

5.2.1 *Antenna Layout*

The proposed design built upon [117] consists of a squared patch printed on a RF substrate, with two etched resonating slots. Two feeding pins are used to proceed with differential excitation. The size of the proposed antenna design is only about 45% that of the traditional microstrip antenna, making it suitable for the envisaged application.

This design stands out since the antenna can be used on top of the SN while the ground plane provides shielding over possible electromagnetic noise created by the circuitry. Therefore the size of the antenna can now be the same as the PCB of the SN instead of a reduced reserved area which is typically the case.

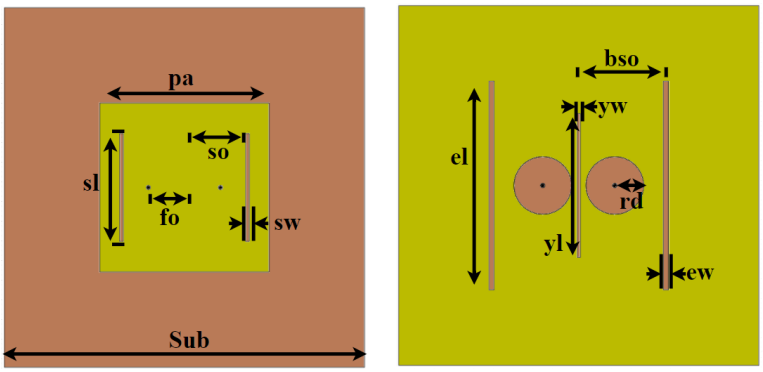

Figure 5.1: Proposed antenna layout for SN (a) top view (b) bottom view.

Table 5.1: Initial values of the parameters used in the SN antenna design (in mm).

S_{ub}	p_a	f_o	s_o	**sw**	**sl**
50.0	20.3	5.0	8.2	0.5	15
e_w	e_l	y_w	y_l	r_d	b_{so}
0.7	27.0	20.0	0.4	3.0	11.75

The layout, depicted in Fig. 5.1, is composed by a slotted patch ($p_a \times p_a$) and a slotted ground plane ($S_{ub} \times S_{ub}$).

The resonating slots on the patch ($s_l \times s_w$) and ground ($e_l \times e_w$), are used to reduce the size of the overall antenna, shifting the resonant frequency of the antenna below the traditional patch antenna. The frequency band can be adjusted by changing the distance between the feeding points (f_o), the size of the patch ($p_a \times p_a$) or even the distance between slots ($_so$ and b_{so}). However the distance between the feeding pins ($2\times f_o$) not only shifts the resonant frequency but also the input impedance of the antenna. Two circular slots around the feeding pins, whose radius are defined by (r_d) were added to facilitate the adjustment of input impedance.

5.2.2 *Antenna Design and Optimisation*

Similarly to the BS antenna, the chosen substrate for this layout is FR4, with $\varepsilon_r = 4.4$, a loss tangent of 0.014 and a thickness of $h = 1.6$ mm. However, the antenna proposed in [117], used a different substrate thus, the need to redesign and optimise the antenna. The initial parameter values used in the layout are presented in Table 5.1.

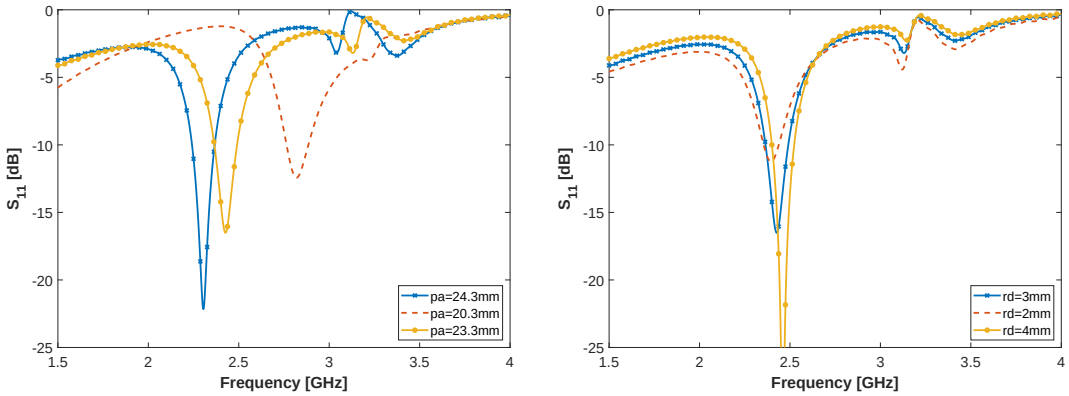

(a) **(b)**

Figure 5.2: S_{11} results for the parametric study on: (a) p_a and (b) r_d

Table 5.2: Optimised values (in mm) of the SN antenna (with a dimension 50×50 mm²).

S_{ub}	p_a	f_o	s_o	s_w	s_l
50.0	23.5	5.0	8.5	0.5	15.0
e_w	e_l	y_w	y_l	r_d	b_{so}
0.7	29.0	20.0	0.4	4.0	11.75

To adjust the frequency of operation, a parametric study on p_a was carried out. The results depicted in Fig. 5.2a ensure that the antenna reaches the desired frequency band when $p_a = 23.3$ mm.

In order to increase the total efficiency of the antenna, the parameter r_d, which defines the size of the circular slots, was studied. Figure 5.2b shows the simulation results, where it can be seen that the antenna reaches its peak performance when $r_d = 4$ mm. The values achieved with the optimisation steps are presented in Table 5.2 and the simulation results depicted in Fig. 5.3. According to the simulations, at this stage, the antenna reached a gain of 4.15 dBi and an HPBW of 85.5° on the azimuth plane.

Even though the simulation results satisfy the needs of a SN antenna, it is desirable to optimise the antenna in terms of size. Thus, the parameter S_{ub} was changed from the 50 to 45 mm. This modification created a shift on the frequency of operation of the antenna, as shown in Fig. 5.4. To this extent, a new parametric study on p_a and b_{so} was carried out, the results depicted in Fig. 5.5a, show that with the $p_a = 23.2$ mm and $b_{so} = 15.75$ mm, the antenna is operating at the desired frequency band. However, to attain a larger bandwidth as well as a better efficiency, a new parametric study for small tuning of the antenna occur. The antenna reaches its peak performance for p_a=22.2 mm, y_w=22 mm and s_o=8.0 mm, as can be seen in Fig. 5.5b. For such antenna, simulation results in Fig. 5.6, ensure a gain of 5.27dBi with an HPBW of 80° in the azimuth plane, 60° in the elevation plane and

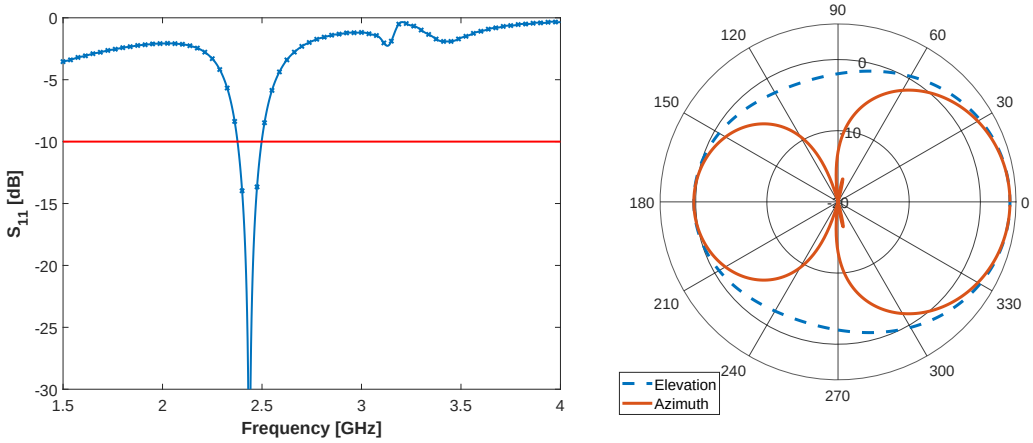

(a) (b)

Figure 5.3: Simulation results: (a) S_{11} and (b) radiation pattern on azimuth and elevation plane at 2.44 GHz.

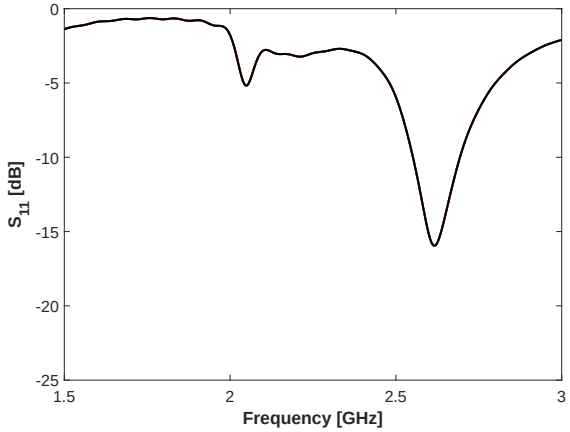

Figure 5.4: S_{11} results for $Sub = 45$ mm

a frequency of operation from 2.32 to 2.49 GHz. These results were attain with the final values for the parameters of the antenna presented in Table 5.3.

5.2.3 *Balun Layout*

The antenna is though to be added on a node that utilises an RF-SoC that outputs a differential signal. Therefore, to test the antenna a balun was design and optimise to operate at 2.445 GHz.

A balun, which stands, for "balanced-to-unbalanced", is RF device responsible to transform an unbalanced line to a balanced line and vice-versa. The proposed balun, presented in Fig. 5.7, is composed by a quarter-wave impedance transformer, a T-Junction power divider and a 180° phase shifter. For our application the balun was designed aiming a 50 Ω impedance in Port 1 (P1), while presenting a differential impedance of 100 Ω between Port 2 and 3 (P2 and P3). Thus, to calculate the

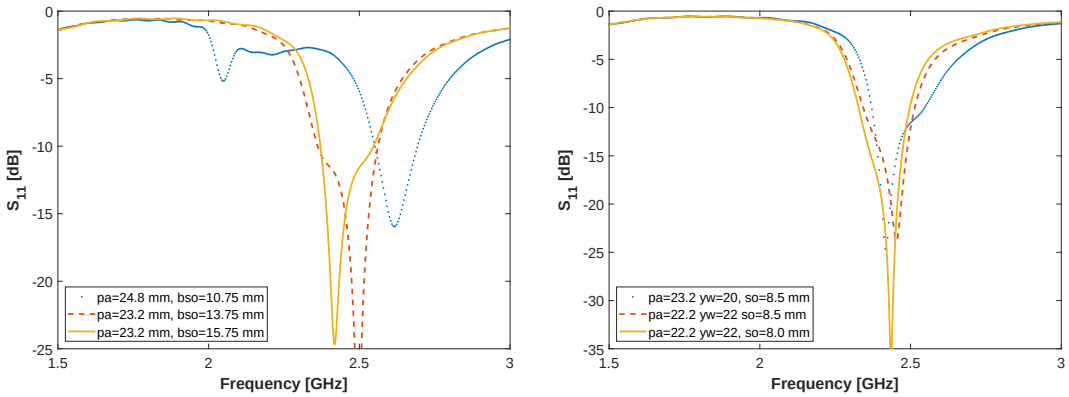

Figure 5.5: Simulation S_{11} results for the parametric studies on: (a) *pa* and *bso*, (b).

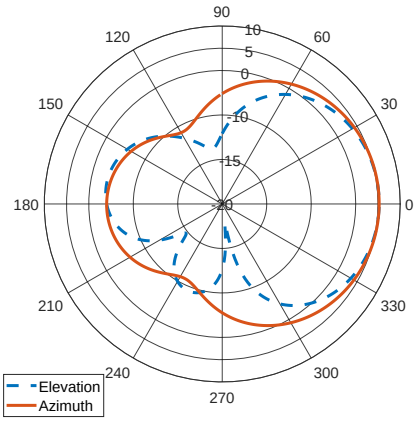

Figure 5.6: Simulated of the radiation pattern for the proposed SN antenna at 2.44 GHz.

Table 5.3: Optimised values of the parameters used in the SN antenna design (in mm).

S_{ubo}	p_a	f_o	s_o	s_w	s_l
45.0	22.2	5.0	8.0	0.5	15.0
e_w	e_l	y_w	y_l	r_d	b_{so}
0.7	28.0	22.0	0.4	4.0	15.75

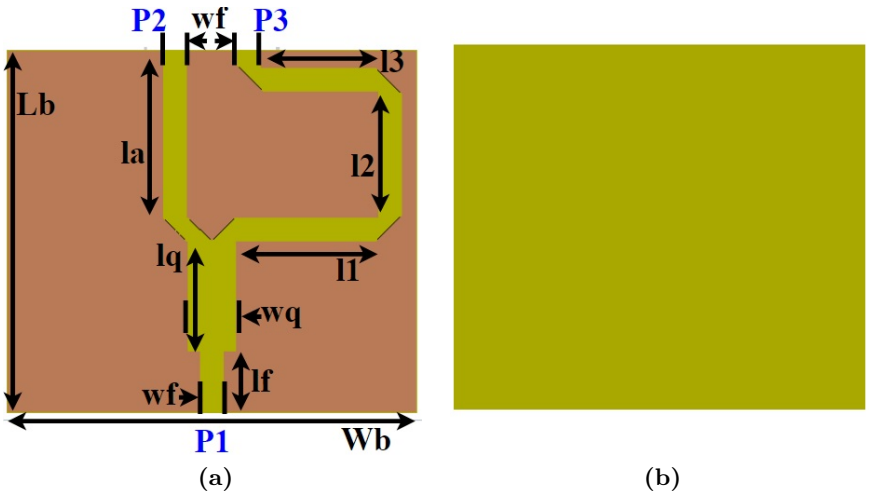

Figure 5.7: Proposed balun layout (a) top view (b) bottom view.

width of the microstrip in P2 and P3, Eq. 5.1 is utilised [118]:

$$Z_d = 2 \times Z_0 \left(1\text{-}0.48 \times e^{\left(-0.96\frac{d}{H}\right)}\right), \tag{5.1}$$

where, H is the height of the substrate, d the distance between traces (fixed at 7 mm) and Z_0 being the single ended impedance of the microstrip, which when calculated is 50 Ω, thus $w_f = 3.1$ mm (According to Eq. 4.1).

To attain a differential signal between P2 and P3, it is necessary that the signals reach the ports with a 180° phase difference. Therefore, a 180° phase shifter is employed, creating a shift of 180° by increasing the length of one of the traces by $\lambda/2$.

With the goal to split the power from P1 to P2 and P3 evenly, a T-junction power divided is developed. To attain an higher efficiency, the impedance of the unbalanced port was calculated by:

$$Z_{unb} = \frac{Z_2}{2} = \frac{Z_3}{2}, \tag{5.2}$$

where, Z_{unb} is the impedance of the unbalanced port, while Z_2 and Z_3 represent the impedance of the Port 2 and 3, respectively (50 Ω). However, the impedance given by Eq. 5.2 is 25 Ω which needs to be transformed to 50 Ω to match the output line. For this reason, a Quarter-wave impedance transformer was studied and added to the design. With the combination of Eq. 4.1 and Eq. 5.3, it is then possible to calculate the values for wq, lf and lq.

$$Z_{quarter-wave} = \sqrt{Z_{unb} \times Z_{in}}, \tag{5.3}$$

Finally, all the 90° bends were mitred, following the rational as in section 4.3.1.

Table 5.4: Optimised values of the parameters of the balun (in mm).

L_b	W_b	w_f	l_f	w_q
49.36	55.70	3.1	8.42	6.4
l_q	l_a	l_1	l_2	l_3
15.0	22.84	19.13	16.4	15.36

5.2.4 *Experimental Characterisation and Discussion of the Balun*

An ideal balun will present an equal insertion loss between from Port 1 to Port 2 and Port 1 to Port 3, meaning that when analysing the transmission coefficients (S_{21} and S_{31}) should present half of the power from P1 (-3 dB). However in a real-world scenario there are losses that may affect the expected performance. Therefore, to assess the performance of the balun, a prototype was constructed and measured utilising the setups depicted in Fig. 5.8, after a proper design optimisation in CST-MWS. Table 5.4 presents the dimensions for the optimised balun, using FR4 substrate, with $\varepsilon_r = 4.4$, a $tan\delta = 0.014$ and a thickness of 1.6 mm.

Since the VNA present in our facilities, only employs 2 ports to measure the transmission coefficients with accuracy, one of the balun ports, was terminated with a 50 Ω load. The results in Fig. 5.9 shown that the balun attains a phase difference (between P2 and P3), of 180±6° and a loss of 0.75 dB, in the desired 2.4 GHz frequency band. Although, the insertion loss measurement shown a small limitation of the design, the results proven to be suitable for measuring and testing purposes.

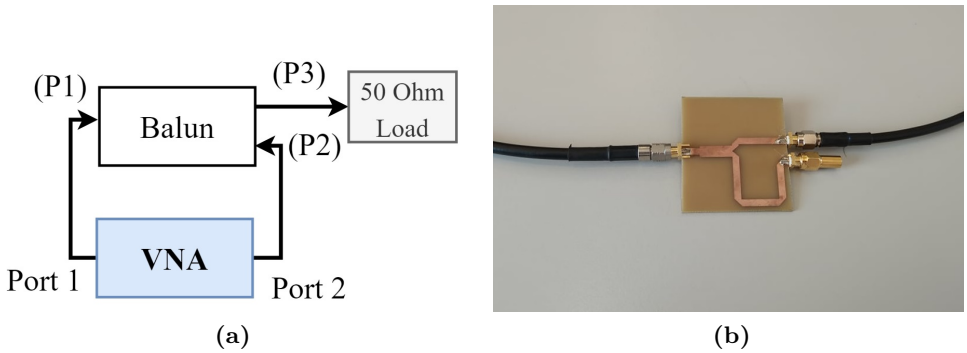

Figure 5.8: Measuring setup for the transmission coefficients: (a) diagram and (b) used setup for measuring S_{21}.

5.2.5 *Experimental Characterisation and Discussion*

After the optimisation, the prototype in Fig. 5.10 was produced to assess the antenna experimentally. Using the setup described in the subchapter 4.3.4, measurements

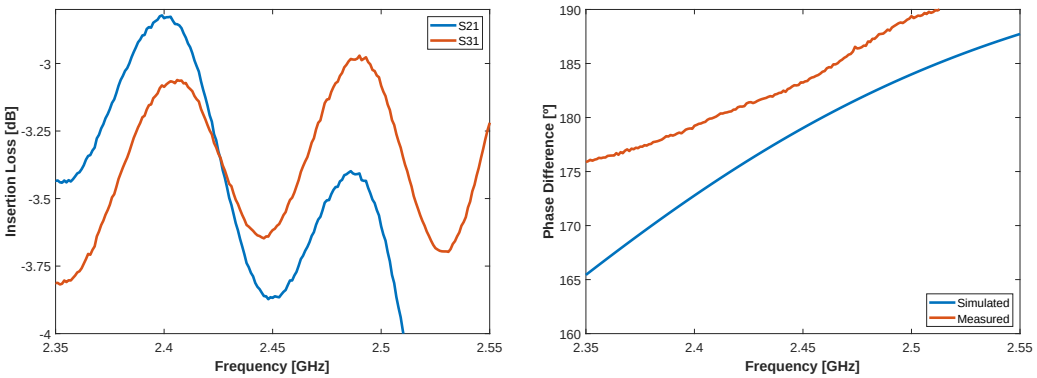

Figure 5.9: Simulated and measured results: (a) insertion loss and (b) phase difference between Port 2 and Port 3.

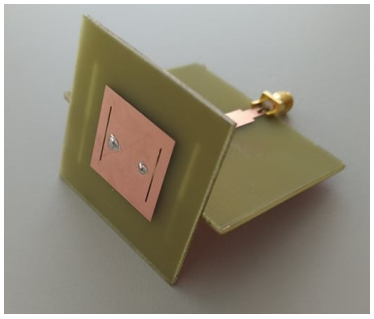

Figure 5.10: Antenna prototype attached to the balun.

of the S_{11} and the radiation pattern of the prototype were obtained. Figure 5.11, presents the simulation and measurement results side-by-side. Both simulated and measured results are in good agreement. the S_{11} presents an frequency band from 2.39 to 2.485 GHz, while the radiation pattern of the prototype ensured a gain of 4.4 dBi, an HPBW of 84° in the azimuth plane and 62° in the elevation plane. Table 5.5 compares the proposed antenna with different designs present in literature, at the same frequency of operation. When analysing Table 5.5, it is possible to conclude that the antenna presents a lower gain that [105] and it shows equal characteristics for the antenna proposed in [103]. Yet, in [103], the antenna was design to be added to the circuitry PCB while the proposed SN antenna just like the antenna proposed in [105], can be mounted directly on top of the SoC node in a stack mode configuration. Thus, eliminating the need to reserve space near the circuitry of the SN for the antenna and matching network, significantly reducing the PCB area of the node. Also, the size of the proposed antenna on this thesis, is more then half of the one proposed in [105] which, as mentioned before, is an important factor for nodes on WSN.

In the next section, the antenna performance will be study when camouflaged under grassland fire mimicking real case scenarios, since many WSN environmental applications involve the placement of the SN near the soil.

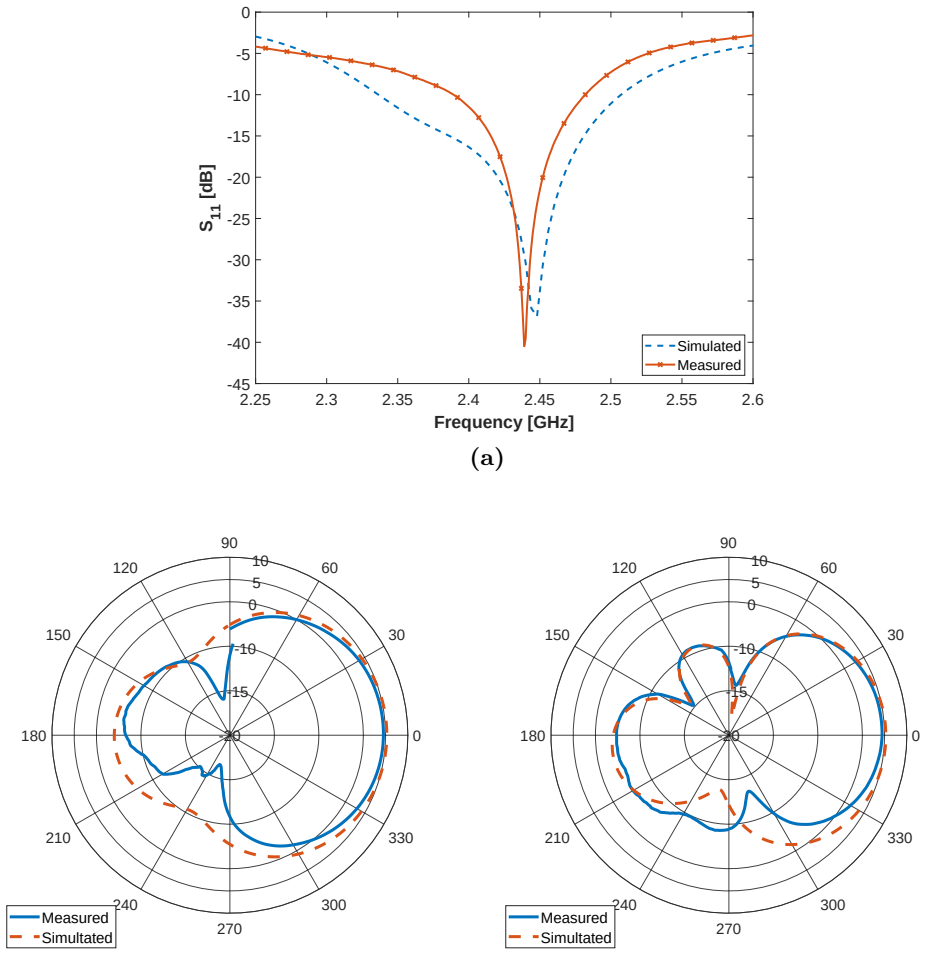

(a)

(b)

(c)

Figure 5.11: Measured and simulated (a) S_{11} results and, radiation pattern at: (b) the azimuth plane and (c) elevation plane.

Table 5.5: Comparative table of the designs present in the literature with the proposed antenna.

Antenna	Size (mm^3)	Frequency (GHz)	Peak Gain (dBi)	HPBW (°) (Az Plane)
[102]	30×35×1.6	2.25 - 2.7	2.3	-
[103]	75×29.5×0.5	2.41 - 2.48	4.5	80
[104]	12.5×11.2×10	2.41 - 2.48	1.87	360
[105]	100×100×0.4	2.37 - 2.49	6.62	30
Proposed Antenna	45×45×1.6	2.39 - 2.485	4.4	84

5.3 A STUDY ON THE ANTENNA PERFORMANCE CAMOUFLAGED UNDER GRASSLAND FIRE

Following the full characterisation of the SN antenna, the next step was to assess its performance in critical scenarios. Thus, the desire of building the simulation environment to be as close to reality as possible in the event of the start of a wildfire in the vicinity of the antenna.

5.3.1 *Scenario Definition and Case Studies*

The first simulation was performed considering forest soil below the antenna. For this simulation a 50 x 50 cm^2 (4λ x 4λ) square, with a depth of 20 cm was used as soil, considering the material already resent in CST Material Library, *Loamy Soil (wet)*, with an $\varepsilon_r = 13.8$ and $tan\delta = 0.18$. The antenna was placed 5 mm above the centre, as shown in Fig. 5.12a. These dimensions are thought to be enough since only the elements near the antenna will have a significant impact on its radiation pattern.

Following this simulation, a layer of vegetation was added above the soil and surrounding the antenna. A 3D model of tall grass was used as depicted in Fig. 5.12b. The dielectric properties were taken from [119], for a moisture content of 45%, where $\varepsilon_r = 10$ and $tan\delta = 0.4$ were considered for simulation purposes.

Lastly, fire was introduced in the simulation to ascertain how it would impact the antenna performance. In order to obtain the dielectric characteristics of fire, another simulation tool, Fire Dynamic Simulator (FDS), which is a computational fluid dynamics solver released by the National Institute of Standards and Technology (NIST) [120], was used. In FDS, it is possible to realistically simulate a fire environment and obtain some parameters such as gas densities and temperature profiles. In post-processing, from this data, it is possible to obtain the electron density and collision frequency that can subsequently be used to calculate the permittivity, as described in [121]. The fuel and burner characteristics were introduced and temperature and density profiles of the environment were extracted in order to calculated the electrical permittivity in a fire region [122]. Even though the fire is a turbulent media, characterised by fast and random variations (fire plumes) overtime, a single frame (single time instant) has been considered, for simulation purposes only. For such frame, several permittivity and conductivities ranging from air characteristics $\varepsilon_r = 1$ and $tan\delta = 0$ to $\varepsilon_r = 0.9535$ and $tan\delta = 0.1343$ were obtained in FDS software and imported to CST, resulting in the 3D scenario presented in Fig. 5.12c.

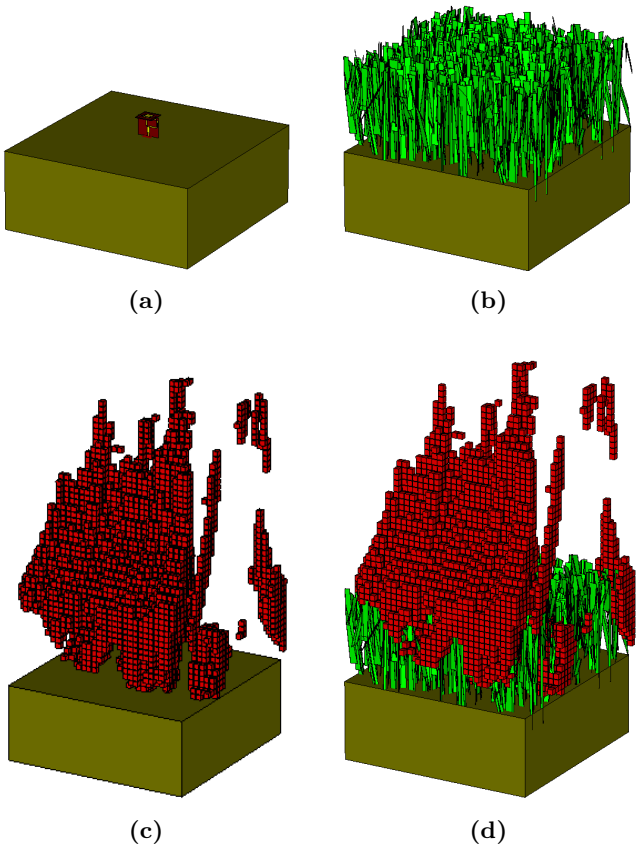

Figure 5.12: CST simulation environments: (a) soil only, (b) grass, (c) fire and (d) full scenario.

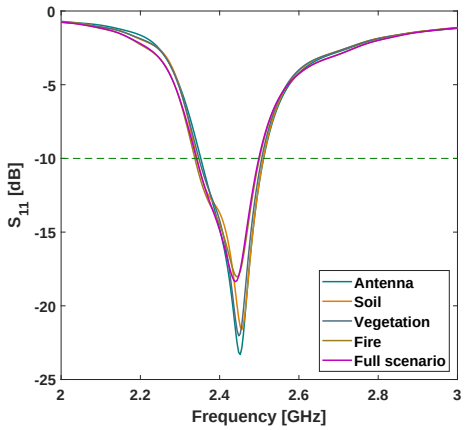

Figure 5.13: Antenna S_{11} for all scenarios considered.

5.3.2 *Simulation Results and Discussion*

In each one of the scenarios described above, both the S_{11} and radiation pattern of the antenna were analysed to infer how these would be affected with the presence of the soil, vegetation and fire, individually. The simulated S_{11} is depicted in Fig. 5.13, from the results, it can be seen that by adding the soil to the simulation, a degradation of 1.7 dB (from -23.3 dB to -21.6 dB) in antenna matching is observed. On the other hand, when vegetation is considered, the S_{11} almost remains unchanged. However, when the fire is taken into consideration, the S_{11} value decreases to -18 dB, presenting a difference of 5 dB from the case with only the antenna. This indicates that the fire has a significant impact in the antenna performance. Lastly, for the complete scenario, there is not a large difference in the S_{11}, when compared to the previous set of simulations.

In terms of the radiation pattern of the antenna, in its main planes, *i.e.* azimuth and elevation, presents some differences for the various scenarios, as shown in Fig. 5.14. Note that to match the coordinate system of the simulation (CST MWS) the bore-sight direction is set to +90° in azimuth and elevation. The first and most visible difference occurs when the soil is introduced in the model. Due to the high ε_r and tanδ of the considered material, the back lobe is severely attenuated (with consequent front to back lobe level enhancement), also verifying a small decrease in gain of 0.6 dB, i.e. from 5.2 to 4.49 dBi. Moreover, it can also be noticed a decrease in the realised gain of around 2 dB, when vegetation is included in the simulation model. For this particular case, it can also be seen a slight deformation in the shape of the radiation pattern, also visible in the 3D radiation patterns of Fig. 5.15. The simulation with fire also resulted in a decrease in the gain of around 0.8 dB, when comparing with the radiation pattern of Fig. 5.6. Lastly, with the scenario containing both vegetation and fire, the antenna gain decreases from 5.2 to 3.01 dBi (a difference of 2.2 dB). These results show that the fire still has an

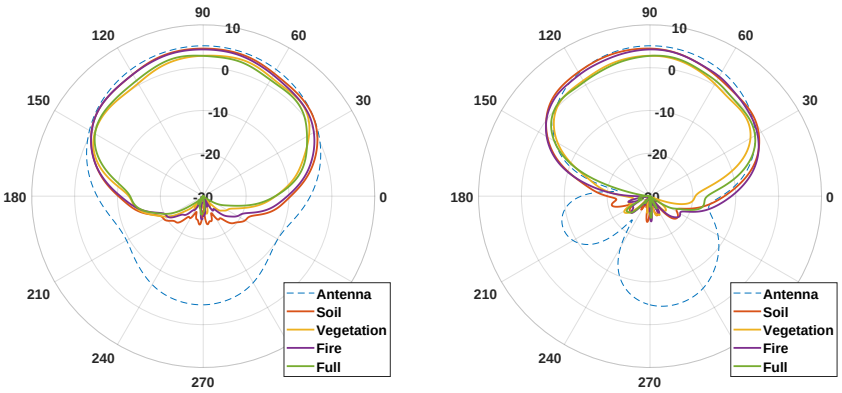

Figure 5.14: Antenna radiation patterns for the different scenarios: (a) azimuth and (b) elevation.

impact on the gain of the antenna even when vegetation is present. However, the decrease observed in the full scenario is smaller than that of the superposition of the vegetation and fire scenarios (Figs. 5.15b and 5.15c), due to the overlapping of the fire with the vegetation.

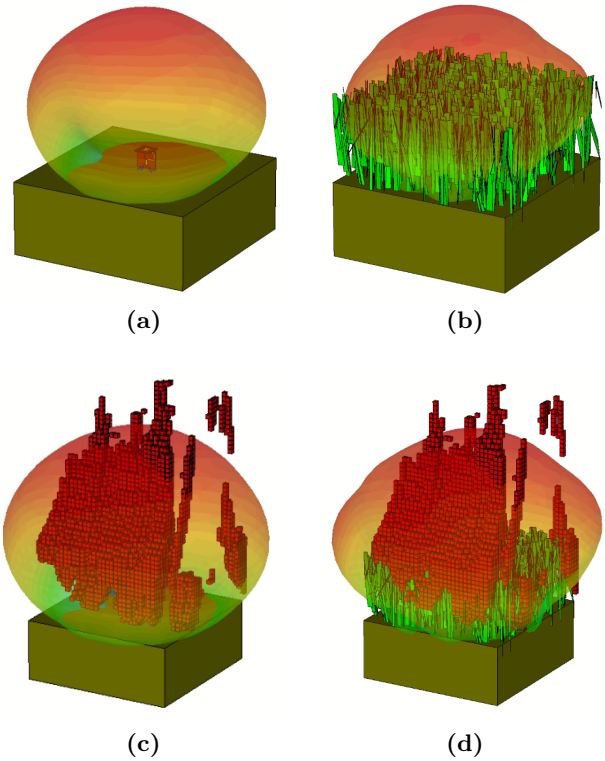

Figure 5.15: 3D radiation patterns: (a) soil only, (b) grass, (c) fire and (d) full scenario.

5.4 INTERIM CONCLUSIONS

In this chapter, a differential microstrip slotted patch antenna to be implemented on a SN, is presented. The antenna can be mounted on top of the circuitry in order to dismiss the reserved area for it in the PCB. For the size of 45×45 mm², the antenna achieved relatively good performance, measuring a gain of 4.4 dBi at 2.44 GHz while providing a wide HPBW (84° in the azimuth plane). Furthermore, the impact of vegetation and fire on the radiation pattern of the antenna, was also studied and presented. The antenna was involved by soil, vegetation and fire, approximating the model to a real case scenario of a wildfire. From the simulation results, it was observed that all these factors have impact in the performance of the antenna, deteriorating both the S_{11} and the radiation pattern. Next section will address the deployment of a wireless sensor network, operating at the 2.4 GHz frequency band, using both the SN and BS antennas proposed in this dissertation.

The contents of this chapter resulted in the following conference papers:

- T. E. S. Oliveira, M. Vala, S. Faria, J. R. Reis, N. Leonor and R. F. S. Caldeirinha, **"A study on small sensor node antenna performance camouflaged under grassland fire"**, *International Federation for Information Processing IFIP International Internet of Things Conference IFIP IOT*, Amsterdam, Netherlands, November, 2021 **(presented)**;
- T. E. S. Oliveira, M. Vala, J. R. Reis and Rafael Caldeirinha, **"High Performance Antennas for Early Fire Detection Wireless Sensor Networks at 2.4 GHz"**, *IEEE IEEE-APS Topical Conference on Antennas and Propagation in Wireless Communications APWC2021*, Honolulu, USA, August, 2021, pp. 158-163, doi: 10.1109/apwc52648.2021.9539629;

6

IMPLEMENTATION OF A WSN OPERATING AT 2.4 GHZ

6.1 INTRODUCTION

In this chapter, the implementation of a WSN operating at 2.4 GHz, is proposed. The WSN is composed of a base station and several sensor nodes that will be used for environmental monitoring. In particular, both base station and sensor node devices are implemented using the antennas developed in Chapter 4 and Chapter 5, respectively, and use LoPy4 transceivers with Wi-Fi protocol for communication. Details about the development of a multi-sector base station antenna with 360° FOV are also discuss in this chapter. The user interface created for controlling/ monitoring the Wi-Fi communication, within a specific sector is described. Finally, the implementation and performance assessment of such network in real scenarios is presented.

6.2 SYSTEM ARCHITECTURE

6.2.1 *Wi-Fi Transceivers*

The work developed in this dissertation seek to full-fill the requirements of the project Wireless Sensor Network for Environment Monitoring (PTDC/EEI-EEE/30539/2017) [16]. The main goal of the project is the development of a wide range wireless sensor network for temperature and humidity environmental monitoring, as depicted in Fig 6.1. The project specifies a point-to-multipoint (star) network topology to simplify the network management and reduce the overall communication energy consumption. The specified communication protocol is based on Bluetooth Low Energy (at 2.4 GHz), and it will be assured by the radio transceiver to be implemented within the project. The same chip is envisage to be employed in both BS and SN.

Considering that the WSN-EM [16] transceiver is under development and not readily available in time for the final tests of the prototypes developed in this dissertation, it was decided to test the proposed antennas with a commercial of-the-shelf solution, while maintaining the main radio parameters (*e.g.* bandwidth, sensitivity, transmitted power). Once the transceiver become available for field

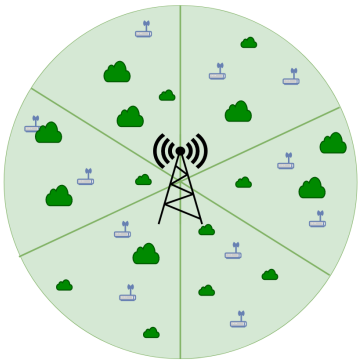

Figure 6.1: Representation of a WSN.

tests, it is though that the antennas will perform likewise. Therefore, this work proposes an alternative communication architecture, based on LoPy4 devices [123]. The LoPy4 depicted in Fig. 6.2, is a micro python programmable board that can use the following communication standards: LoRa, SigFox, Wi-Fi and Bluetooth. The device incorporate a ESP32 dual core microcontroller to operate with Wi-Fi and Bluetooth communication standards, including an internal antenna (ceramic antenna) and a connector for possible external antenna integration. According to the manufacture, utilising a data rate of 1 Mbps and a Direct-sequence Spread Spectrum Modulation, the LoPy4 has a sensitivity that can go down to -98 dBm and a maximum output power of 20.5 dBm, with an adjacent channel rejection of 37 dB. This makes these devices suitable to be employed as a SN or BS, on a WSN.

In order to replicate characteristics of the project (namely the frequency of operation), Wi-Fi was chosen as communication protocol. Therefore, the Lopy4 employed as the BS, will create an Wi-Fi network, utilising the 802.11b standard, with a channel bandwidth of 20 MHz and the Modulation Coding Scheme 0 [123]. With this configuration, the manufacture ensures that the Lopy4 attain a sensitivity of -93 dBm, being close to the one expected for the RF System-on-Chip to be developed in WSN-EM, which aims a sensitivity of -92 dBm [16]. The use of Wi-Fi open the possibility of the creation of a user interface to control, for example, the sectors of the base station antenna or display collected data from the sensor node in a webpage, as demonstrated in section 6.2.4.

6.2.2 *Multi-Sector Base Station Based on the Lunar Waning Crescent Quasi-Yagi Antenna*

The proposed BS adopts the structure presented in section 4.4, composed by a two deck 3D printed structure, to conceal the circuitry. The first deck, will sustain the LoPy4 with an Universal Serial Bus (USB) input port for the power supply, the second will hoard the RF-switch and its connections to the antennas. The

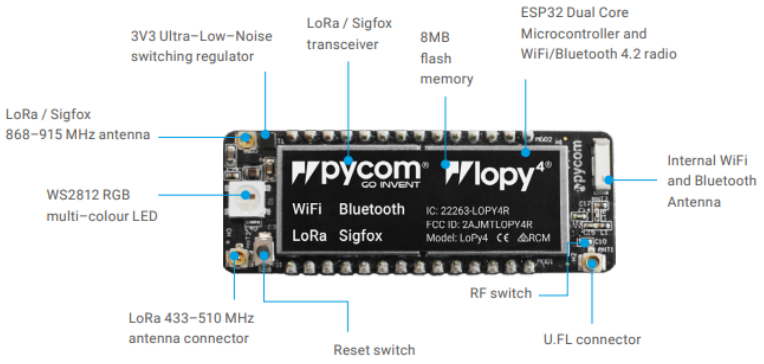

Figure 6.2: Lopy4 features diagram (source: core-electronics.com.au).

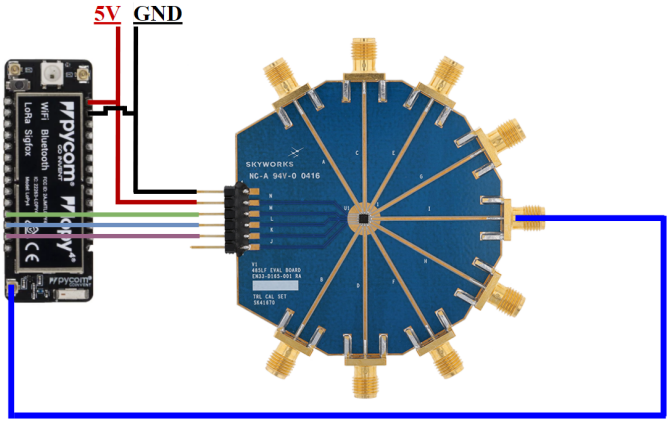

Figure 6.3: BS circuitry diagram.

LoPy4, which serves as access point of the network, also controls the RF-switch by applying the necessary logical voltage levels to the input controls of the RF-switch, as depicted in Fig. 6.3 and Fig.6.4. The switch can integrate up to 8 antennas, however, for the presented application, it is only needed 6 to achieve the desired results (360° FOV), thus the remaining two ports are terminated with a 50 Ω load, protecting the RF-switch circuitry.

6.2.3 *Sensor Node*

The Lopy4 that serves as sensor node, depicted in Fig 6.5, employs a PyTrack shield that contains an integrated Global Positioning System (GPS) receiver to attain its location. Afterwards, the node sends its current coordinates and the Recieved Signal Strength Indicator (RSSI) to the BS, which is then displayed in the user interface. The balanced microstrip slotted patch antenna developed in section 5.2 is connected to the node with the balun, since the LoPy4 RF-SoC outputs an unbalanced signal.

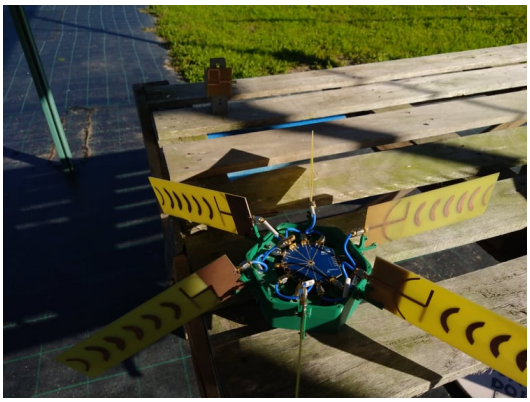

(a)

Figure 6.4: Photography of the BS circuitry.

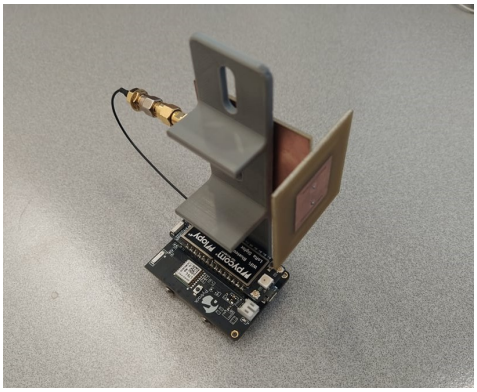

Figure 6.5: Photography of the Lopy4 device attached to the PyTrack and SN antenna.

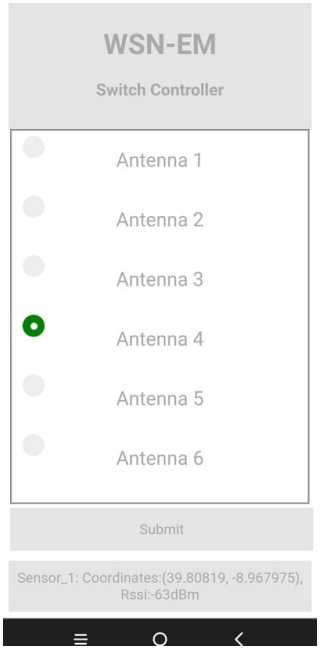

Figure 6.6: Screenshot of the user interface

6.2.4 *User Interface*

With the purpose of controlling the RF-switch active antenna of the BS and monitor the WSN, an user interface was developed. The user interface is available only when connected to the closed network, and can be accessed by a web browser. A screenshot of the interface is depicted in Fig. 6.6. The interface was developed in HTML and CSS reducing the usage of memory resource. To handle the communication between the devices the http protocol is used. The BS creates a socket defining it self as the web server, while the remaining devices (nodes, user device) are clients. When the user creates a request in the socket ("GET"), the BS respond with a string that contains all the information for the user interface site. To change the active antenna, the user simply select the antenna to be active and click, the "Submit" button. The interface also informs the user of the last data received on the BS, shown in the bottom of the site, listing the node identification, current coordinates and its RSSI. Several other information such as temperature, humidity, air pressure and others, can also be added to the interface.

6.3 IMPLEMENTATION AND EXPERIMENTAL CHARACTERISATION

6.3.1 *LoPy4 RSSI Characterisation*

The measurements, presented in the following sections, were based on the LoPy4 RSSI, which is an indicator of the received power in the device. To characterise the

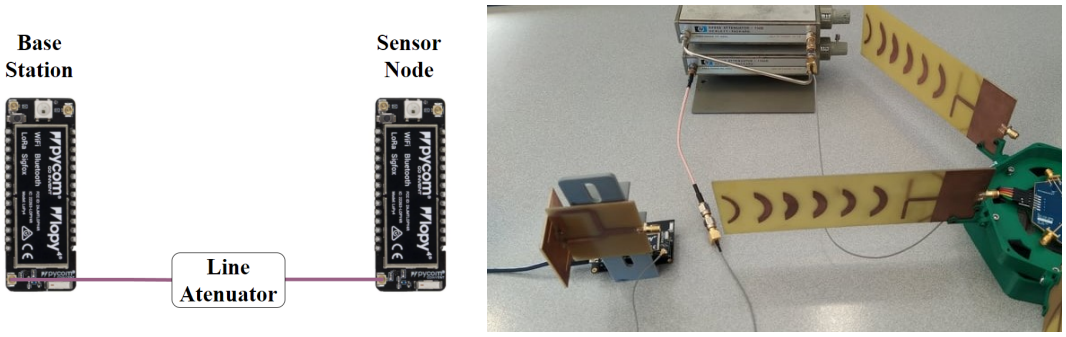

(a) (b)

Figure 6.7: Measurement Setup for the Lopy4 characterisation, (a) diagram and (b) photography.

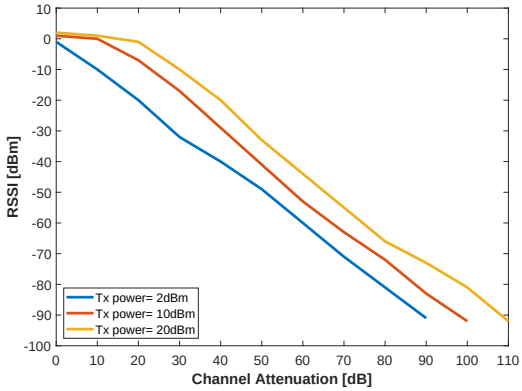

(a)

Figure 6.8: Measured results of the LoPy4 RSSI characterisation.

RSSI of the LoPy4, the BS and SN were connected back-to-back with a variable inline attenuator, aiming to attain the RSSI for different values of attenuation, as presented in Fig. 6.7. Three values were utilised for the transmission power: 2 dBm; 10 dBm and 20 dBm, while the attenuation varied from 0 to 120 dB, with a step of 10 dB. From the results, depicted in Fig. 6.8, it can can be observed that with a 2 dBm transmission power, the LoPy4 lost its connection with a line attenuation of 100 dB, while with 10 dBm, the link was maintain until 110 dB of attenuation. For a transmission power of 20 dBm, the LoPy4 could communicate with 110 dB, loosing its bind when the line attenuation was of 120 dB.

6.3.2 *Coverage Study*

As previously mentioned, a WSN typically benefit of having a omnidirectional radiation pattern (360° FOV), in the azimuth plane of the base station, to cover all its surroundings. Thus, the development of the proposed structure in Chapter 4, which utilises a sectorisation technique by a multiplexing mechanism (RF-Switch).

(a) **(b)**

Figure 6.9: Measurement Setup for the BS FOV, (a) proposed base station and (b) sensor node placement.

A measurement campaign was then carried out, to validate the proposed sectorisation technique, the FOV of each sector of the BS was studied. This measurements was done in *Campos do Liz, Leiria*. The location is characterised by vast and large agriculture fields with short vegetation. The BS and SN were placed at a height of 1.6 meters (in Fig 6.9). With the BS stationary and utilising only one sector for each measurement, the SN moved around the BS in random pattern, at a maximum distance of 82 meters. Due to the small area of study, the Tx power was set to 2 dBm and an attenuator of 20 dB was employed between the Lopy4 and RF-switch the base station, reducing the transmitted power. After connecting with the BS, the node sends its RSSI and GPS coordinates using the serial port to a computer, every second. This data is then processed in real time using MATLAB. The MATLAB script associates the measured RSSI, with the respective GPS coordinates obtained by the PyTrack shield, and saves it in a ".txt" file for further analysis. In Fig. 6.10, it is depicted the coverage results attained for the sector 2 and sector 5, respectively. From the results, it can be observed that the proposed BS configuration acts as desired, covering each sector (of 60°) when demanded.

6.3.3 *Maximum Range Assessment*

After studying the coverage, the maximum range obtained with the presented architecture was assessed. In order to have a partial Line-of-Sight between BS and SN, an area affected by fires of 2017 near *Poço do Inglês, Marinha Grande* was the chosen place for this measurement, Fig. 6.11. This location is characterised by sand dunes, with low vegetation and remaining burned trees.

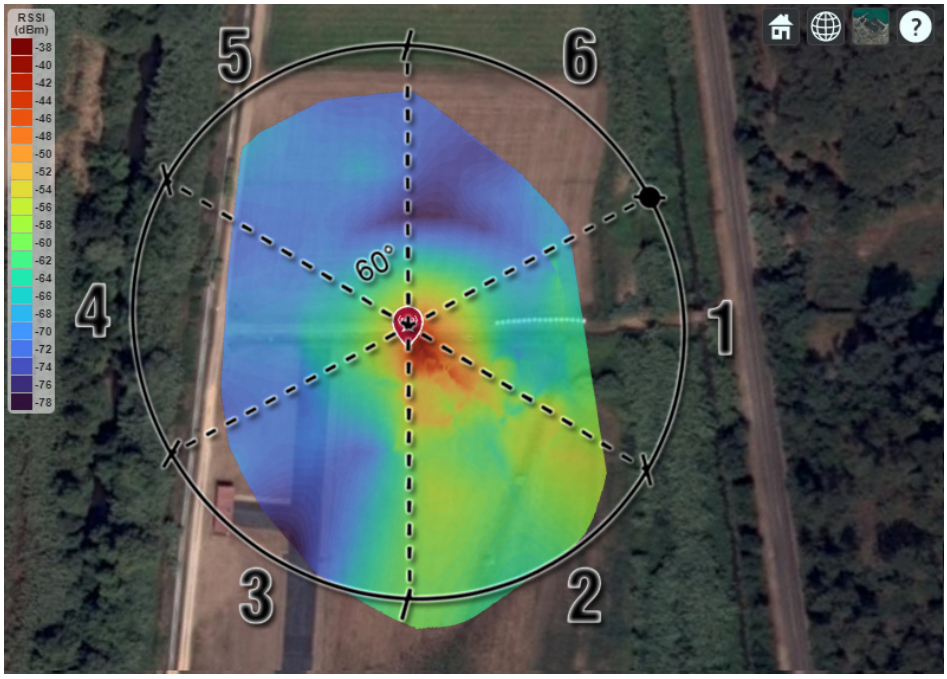

(a)

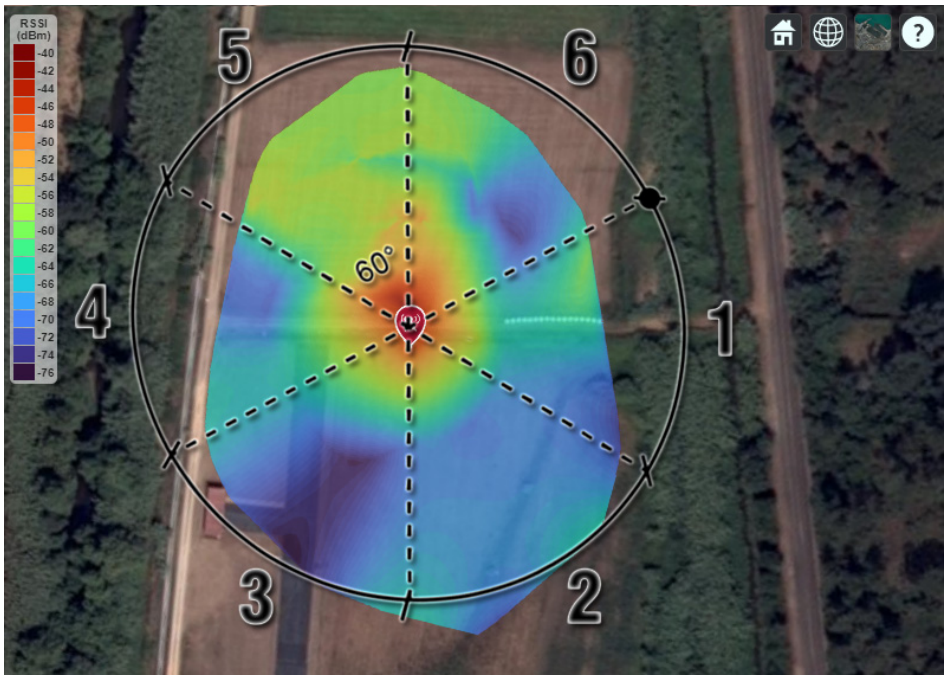

(b)

Figure 6.10: Measurement results for the BS FOV of: (a) Sector 2 and (b) Sector 5.

(a) (b)

Figure 6.11: Photography of the (a) BS placement on the WSN range campaign and (b) a close-up of the BS, *Poço do Inglês, Marinha Grande.*

The BS was placed at an altitude of approximately 65 meters (above the sea level) while the SN, attached to the 3D printed support (Fig. 6.5), was placed on a roof car (1.6 meters heigh). The road altitude used varies from 53 to 65 meters. The BS was set to have a maximum transmission power of 10 dBm.

Two measurements were made with a maximum distance, between the BS and SN, of 3.85 km, limited by the total length of the road where the measurements were performed. In both measurements, the 3.85 km were travelled without loosing the connection stablish by the Wi-Fi protocol. At the farthest distance tested (3.85 km), the node presents a RSSI of -92 dBm, Fig. 6.12, still ensuring Wi-Fi connectivity.

Theoretically, following the Friis transmission equation (Eq. 6.1) [13], a range of 5.5 km can be attained with the developed system:

$$\mathrm{P_{rx}} = \mathrm{P_{tx}}+\mathrm{G_{tx}}+\mathrm{G_{rx}}+20 \times \log_{10}\left(\frac{\lambda}{4\pi \mathrm{d}}\right) \tag{6.1}$$

when, the transmitted power is of 10 dBm (P_{tx} = 10 dBm), the received power P_{rx} = -92 dBm, G_{tx} =8.9 dBi and G_{rx} = 4.4 dBi which represent the gain of the transmitter and receiver antennas, respectively, and d the distance between Tx and Rx.

An estimation of the RSSI was also accomplished, by utilising the Free-Space Path Loss model (FSPL), to assess the channel loss on the campaign site. The RSSI is estimated by extrapolation of the curves obtained in the RSSI characterisation (Fig. 6.8), and the calculated channel loss (with FSPL), Fig. 6.13. After analysing the measured and estimated RSSI results, it can be concluded that both are in good agreement. However, at 3 km occurs the most noticeable difference between the results (approx. 4 dB), which is though to be due by the irregular terrain of the site.

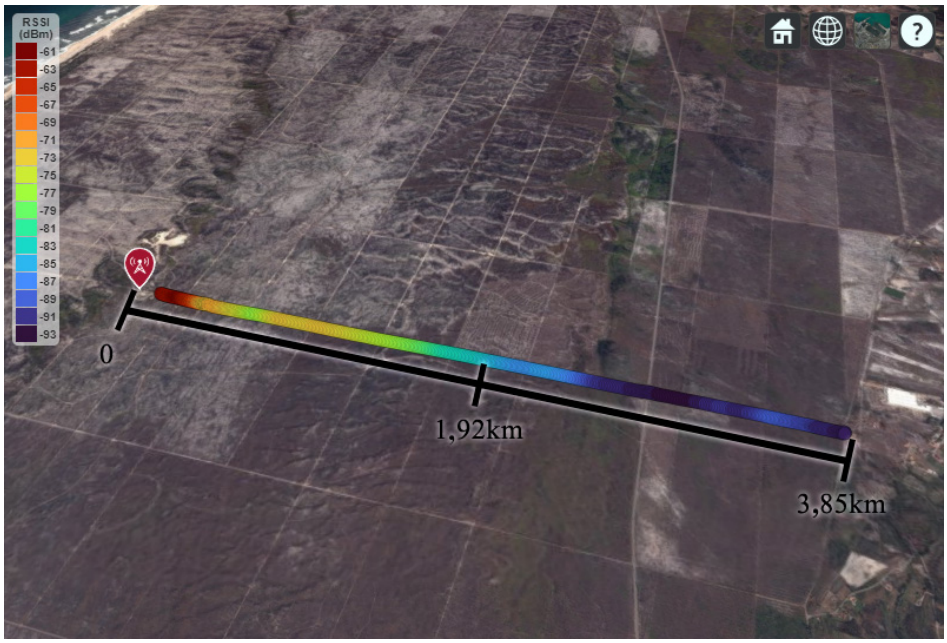

(a)

Figure 6.12: Measured RSSI of the WSN max range campaign.

(a)

Figure 6.13: Estimated RSSI of the max range campaign site.

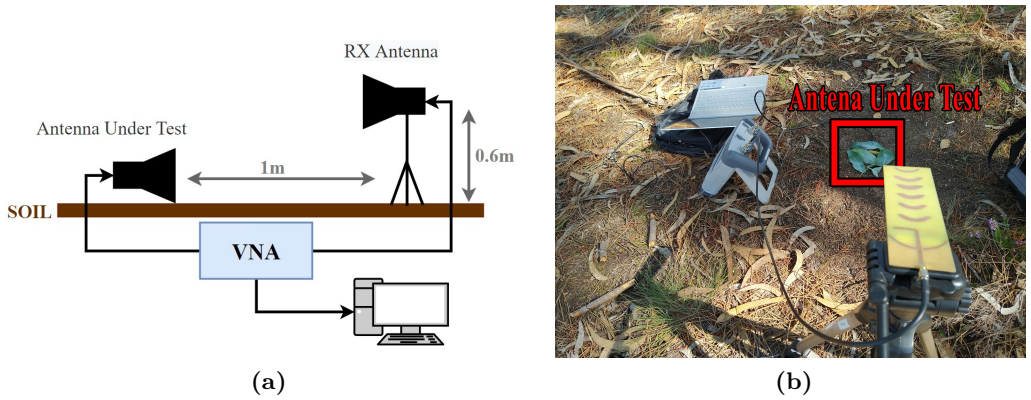

Figure 6.14: Measurement setup of the node antenna performance under fallen leaves, (a) diagram and (b) implementation.

6.3.4 *Sensor Node Antenna Performance Under Fallen Leaves*

A WSN is design to have a lifetime of years, throughout its lifetime many environmental and seasoning changes occur. Focusing on the seasons, autumn can be seen has the one that outputs the most significant impact on the node antenna performance. When sitting on top of the antenna, the discarded leaves from the trees, may influence the antenna characteristics thus, affecting the communication between sensor node, and base station. To this extent, the following campaign targeted the node antenna performance, when covered by fallen leaves. Therefore aiming to assess the impact of the fallen leaves on the antenna matching (S_{11}) and transmission (S_{21}), the measurements resorted into the setup depicted in Fig. 6.14. The node antenna was placed on the ground, 1 meter apart of the proposed BS antenna, which height is of 0.6 meters. With the described setup, eight measurements were performed, firstly, to serve as reference, the antenna with only the soil around was tested, followed by the antenna covered with fern, dry cork oak, juvenile eucalyptus, eucalyptus, dry eucalyptus, pine and dry pine leaves. The leaves position is completely random, emulating a real-world scenario.

From the results, depicted in Fig 6.15a, it can be concluded that the matching of the antenna is greatly impacted by the eucalyptus and pine trees, at 2.45 GHz. In particular, the antenna matching when covered by pine leaves degrade 5.96 dB from the reference scenario results (from -20.78 dB to -14.82 dB). This results in a transmission loss of 3.3 dB (decaying from -30.1dB to -33.4dB), as depicted in Fig. 6.15b. From the transmission coefficient results, it can also be observed that the dry leaves have a much smaller impact on the performance of the antenna when compared to green leaves, which is sought to be associated to the water content of the leaves. These results demonstrate that the performance of the antenna can be affected when covered leaves, but such impact will decay with the dehydration of

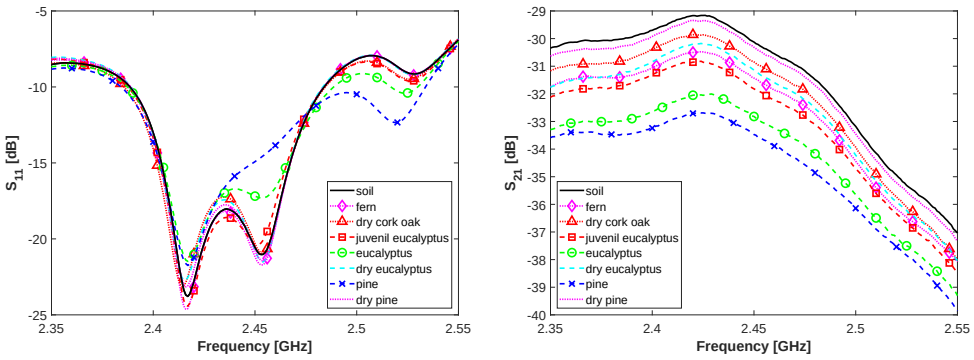

(a) **(b)**

Figure 6.15: Measurement results of (a) S_{11} and (b) S_{21}, for the node antenna under fallen leaves.

the leaves, approximating, on the limit, the antenna performance to the original characteristics.

6.4 INTERIM CONCLUSIONS

In this chapter, a implementation and validation of WSN which employ the proposed lunar waning crescent Quasi-Yagi and the differential microstrip slotted patch antennas is presented. Firstly the system architecture is proposed, followed by the BS circuitry and user interface. The coverage and range of the proposed architecture was also studied where the results confirm a 360° FOV and range of 3.85 km between the sensor node and base station. It is though, however that this range can be increased when utilising a dedicated RF system on chip for each of sector of the BS (working in different channels). Due to the large lifetime of an WSN, the proposed node antenna (differential microstrip slotted patch) was studied when covered by the fallen leaves (a phenomena that typically occurs in autumn). The antenna was covered by dry and green leaves of different specimen and its performance was assessed by its matching and the transmission coefficient. From the results, it was concluded that the green leaves have an higher impact on the antenna performance with the pine leaves creating a loss of 3.3 dB in the transmission between the antennas.

7

CONCLUSIONS

7.1 INTRODUCTION

This chapter contains the conclusion of the presented work. Firstly, a summary of the dissertation is introduced, followed by the contributions to science that arise from this dissertation. Finally, proposals for future work are addressed.

7.2 DISSERTATION REVIEW

Fundamentally, the focus of this work was to design, develop and prototype small antennas for 5G and IoT, including for WSN (here, seen as a particular case of a IoT network). To this extent, a thorough literature review on 5G and IoT with emphasis on WSN systems and antennas, was carried out. Five antenna designs were studied and characterised, of which: one was dedicated to 5G and IoT systems operating at 26 GHz; two were developed to integrate a WSN base station, operating at 2.4 GHz, and finally, one was conceived for a WSN sensor node also operating at 2.4 GHz. All the mentioned antennas, developed at 2.4 GHz, were designed and optimised following specific project requirements defined by the WSN-EM project [16]. Preliminary characterisation of the developed antennas, in a WSN based LoPy4 network (WiFi), allow to apply the BS and sensor node prototypes in a real-world scenario. In detail, the work of this thesis can be summarised as follows:

Chapter 1 exposes the background study and motivation, the main objectives and the structure of this thesis.

In Chapter 2, a literature review on 5G and IoT is presented. WSN systems are highlighted due to the major advantages and low-cost of implementation of these systems. Several aspects such has: topology; architecture; communication standards and deployment are extremely important when developing the mentioned networks. To complete this chapter, a thorough review on state-of-the-art antennas for BS and SN operating at 2.4 GHz, is presented.

Chapter 3 contains the steps for redesign and optimisation of a high-gain wideband parasitic microstrip antenna built upon [106]. The antenna was successfully modified

to operate at the NR, FR2, n258 band. Simulation results assure a 14.4 dBi with a total bandwidth of 4.15 GHz.

Chapter 4, is focused on the development of directional antennas for application in WSN base stations. Two antennas designs were studied and optimised to operate at the 2.4 GHz ISM band. The lunar waning crescent Quasi-Yagi antenna, which design is though to be novel, presents a measured gain of 8.9 dBi, HPBW in the azimuth plane of 60°, and a front-to-back ratio of 20.16 dB at 2.445 GHz, obtained in a constructed prototype. Parametric studies on a cylindrical configuration for six antennas were carried out, towards the implementation of the antenna in a WSN BS. A structure was built to accommodate both the antennas and multiplexing mechanism.

The contents of Chapter 5 are related to the design and optimisation of a balanced microstrip slotted patch. The measured results of the antenna, which counts with a dimension of 45 × 45 mm², ensure a gain of 4.4 dBi and an HPBW of 84°, in the azimuth plane, at 2.44 GHz. Subsequently, a study on the performance impact when camouflaged under grassland fire, was presented. The antenna was tested in four different scenarios, using full-wave electromagnetic solver (CST MWS) and, to obtain the dielectric characteristics of fire, the simulation tool Fire Dynamic Simulator (FDS), was used. The antenna was then involved by soil, vegetation and fire, approximating the model to a real case scenario of a wildfire. It was observed that all these factors have impact in the performance of the antenna, deteriorating both the S_{11} and the radiation pattern. When considering only a single frame of a propagation fire it was observed a decrease of 2 dBi in the gain characteristics of the antenna.

In Chapter 6, the antennas proposed in Chapter 4 and Chapter 5, respectively, were employed on a WSN utilising Lopy4 devices for both SN and BS. A experimental campaign was carried out to assess both coverage and range of the proposed network solution. The measured results of the WSN coverage, that employs the proposed antennas, ensured a 360° FOV, by a sectorisation technique, with an range of 1.2 km, in the 2.4 GHz ISM band. The performance of sensor node antenna, of Chapter 5 was further studied when covered by fallen leaves, a phenomena that may occur during the WSN lifetime. From the results it was concluded that the antenna performance is specially affected by green leaves however, due to the dehydration of the leaves, after a relatively small period of time, the antenna will present a performance close to the its original characteristics.

7.3 CONTRIBUTIONS TO THE KNOWLEDGE

The work developed during this thesis contributed to the knowledge and for the scientific community with five publications in international peer-reviewed conferences and a practical demonstrator. A future journal publication is under consideration.

- T. E. S. Oliveira, J. R. Reis, M. Vala and R. F. S. Caldeirinha, **"A Lunar Waning Crescent Quasi-Yagi Antenna for WSN Base-Stations at 2.4 GHz"**, *16th European Conference on Antennas and Propagation - EUCAP*, Madrid, Spain, January, 2022 **(submitted)**;
- T. E. S. Oliveira, J. R. Reis, M. Vala and R. F. S. Caldeirinha, **"Wireless Sensor Network for Environmental Monitoring: From Multi-beam Base Station to Small Radio Node "**, *15th Congress of the Portuguese Committee of URSI "Environmental sustainability in use of the radio spectrum"*, Leiria, Portugal, November, 2021;
- T. E. S. Oliveira, J. R. Reis and R. F. S. Caldeirinha, **"A Waning Crescent Quasi-Yagi Microstrip Antenna for Wireless Sensing Networks"**, *15th Congress of the Portuguese Committee of URSI "Environmental sustainability in use of the radio spectrum"*, Leiria, Portugal, November, 2021 **(presented)**;
- T. E. S. Oliveira, M. Vala, S. Faria, J. R. Reis, N. Leonor and R. F. S. Caldeirinha, **"A study on small sensor node antenna performance camouflaged under grassland fire"**, *International Federation for Information Processing IFIP International Internet of Things Conference IFIP IOT*, Amsterdam, Netherlands, November, 2021 **(presented)**;
- T. E. S. Oliveira, M. Vala, J. R. Reis and R. F. S. Caldeirinha, **"High Performance Antennas for Early Fire Detection Wireless Sensor Networks at 2.4 GHz"**, *IEEE IEEE-APS Topical Conference on Antennas and Propagation in Wireless Communications APWC2021*, Honolulu, USA, August, 2021, pp. 158-163, doi: 10.1109/apwc52648.2021.9539629;
- T. E. S. Oliveira, J. F. Goncalves, J. R. Reis, M. Vala and R. F. S. Caldeirinha, **"High-Gain Wideband Parasitic Microstrip Antenna for 5G and IoT at 26 GHz"**, *Conf. on Telecommunications - ConfTele*, Leiria, Portugal, February, 2021, pp. 1-5, doi: 10.1109/ConfTELE50222.2021.9435457;

7.4 FUTURE WORK

Future work will address the conception of a prototype for the high-gain wideband parasitic microstrip antenna presented in Chapter 3, for further experimental characterisation. Furthermore, the slotted patch antenna, developed in Chapter 4, need to be tested with a RF-SoC that outputs a differential signal, as envisaged for the WSN-EM project, in order to attain the characteristics of the antenna without the interference and loss generated by the developed balun.

As for the study on the proposed SN antenna performance when camouflaged under grassland fire, further work should address simulations with different vegetation densities and types, different time instants of fire, as well as an increase in the overall simulation environment size in order to ascertain at which distance the surroundings of the antenna will not have an impact on its performance. Testing in a real scenario is also thought to be done in the near future.

Finally, testing and measurements on a WSN that employs the lunar crescent Quasi-Yagi antenna and the microstrip slotted patch antenna with multiple sensor nodes is desired to be carried. LoPy4 is desired to be replaced by dedicated transceivers. Final coverage tests should also be carried out in such circumstances.

BIBLIOGRAPHY

[1] A. Tikhomirov, E. Omelyanchuk, and A. Semenova, "Recommended 5G Frequency Bands Evaluation," in *2018 Systems of Signals Generating and Processing in the Field of on Board Communications*, 2018, pp. 1–5.

[2] M. Shaik, A. Kabanni, and N. Nazeema, "Millimeter Wave Propagation Measurments in Forest for 5G Wireless Sensor Communications," in *2016 16th Mediterranean Microwave Symposium (MMS)*, 2016, pp. 1–4.

[3] H. M. Rahim, C. Y. Leow, T. A. Rahman, A. Arsad, and M. A. Malek, "Foliage Attenuation Measurement at Millimeter Wave Frequencies in Tropical Vegetation," in *2017 IEEE 13th Malaysia International Conference on Communications (MICC)*, 2017, pp. 241–246.

[4] M. L. Laouira, A. Abdelli, J. B. Othman, and H. Kim, "An Efficient WSN Based Solution for Border Surveillance," *IEEE Transactions on Sustainable Computing*, vol. 6, no. 1, pp. 54–65, jan 2021.

[5] B. Montrucchio, E. Giusto, M. G. Vakili, S. Quer, R. Ferrero, and C. Fornaro, "A Densely-Deployed, High Sampling Rate, Open-Source Air Pollution Monitoring WSN," *IEEE Transactions on Vehicular Technology*, vol. 69, no. 12, pp. 15 786–15 799, dec 2020.

[6] S. Astapov, A. Riid, and J.-S. Preden, "Military Vehicle Acoustic Pattern Identification by Distributed Ground Sensors," in *2016 15th Biennial Baltic Electronics Conference (BEC)*. IEEE, oct 2016.

[7] G. Hernandez-Penaloza, A. Belmonte-Hernandez, M. Quintana, and F. Alvarez, "A Multi-Sensor Fusion Scheme to Increase Life Autonomy of Elderly People With Cognitive Problems," *IEEE Access*, vol. 6, pp. 12 775–12 789, 2018.

[8] D. Qiong and P. Hao, "Design and Implementation of Irrigation Water Saving Control System Based on WSN," in *2021 International Conference on Intelligent Transportation, Big Data & Smart City (ICITBS)*. IEEE, mar 2021.

[9] L. Shu, Y. Chen, Z. Sun, F. Tong, and M. Mukherjee, "Detecting the Dangerous Area of Toxic Gases with Wireless Sensor Networks," *IEEE Transactions on Emerging Topics in Computing*, vol. 8, no. 1, pp. 137–147, jan 2020.

[10] L. K. Ketshabetswe, A. M. Zungeru, M. Mangwala, J. M. Chuma, and B. Sigweni, "Communication Protocols for Wireless Sensor Networks: A

Survey and Comparison," *Heliyon*, vol. 5, no. 5, p. e01591, may 2019.

[11] J. G. D. Hester and M. M. Tentzeris, "A mm-wave Ultra-long-range Energy-autonomous Printed Rfid-enabled Van-atta Wireless Sensor: At the Crossroads of 5G and IoT," in *2017 IEEE MTT-S International Microwave Symposium (IMS)*, 2017, pp. 1557–1560.

[12] T. S. Bird, *Microstrip Patch Antenna*, 2015, pp. 137–147.

[13] C. A. Balanis, *Antenna Theory: Analysis and Design 4th Edition*. Wiley, January 2016, ch. Microstrip and Mobile Communications Antennas, pp. 783–847.

[14] H. Asplund, D. Astely, P. von Butovitsch, T. Chapman, M. Frenne, F. Ghasemzadeh, M. Hagström, B. Hogan, G. Jöngren, J. Karlsson, F. Kronestedt, and E. Larsson, "Chapter 13 - Performance of Multi-antenna Features and Configurations," in *Advanced Antenna Systems for 5G Network Deployments*, H. Asplund, D. Astely, P. von Butovitsch, T. Chapman, M. Frenne, F. Ghasemzadeh, M. Hagström, B. Hogan, G. Jöngren, J. Karlsson, F. Kronestedt, and E. Larsson, Eds. Academic Press, 2020, pp. 561–637.

[15] M. Appleby and F. Harrison, "47 - Cellular radio systems," in *Telecommunications Engineer's Reference Book*, F. Mazda, Ed. Butterworth-Heinemann, 1993, pp. 47–1–47–17.

[16] I. de Telecomunicações, "Project: Wireless sensor network for environmental monitoring," Nov. 2021. [Online]. Available: https://www.it.pt/Projects/Index/4576

[17] D. M. Sheen, D. L. McMakin, and T. E. Hall, "Detection of Explosives by Millimeter-wave Imaging," in *Counterterrorist Detection Techniques of Explosives*. Elsevier, 2007, pp. 237–277.

[18] A. N. Uwaechia and N. M. Mahyuddin, "A Comprehensive Survey on Millimeter Wave Communications for Fifth-Generation Wireless Networks: Feasibility and Challenges," *IEEE Access*, vol. 8, pp. 62 367–62 414, 2020.

[19] W. Hong, Z. H. Jiang, C. Yu, D. Hou, H. Wang, C. Guo, Y. Hu, L. Kuai, Y. Yu, Z. Jiang, Z. Chen, J. Chen, Z. Yu, J. Zhai, N. Zhang, L. Tian, F. Wu, G. Yang, Z.-C. Hao, and J. Y. Zhou, "The Role of Millimeter-Wave Technologies in 5G/6G Wireless Communications," *IEEE Journal of Microwaves*, vol. 1, no. 1, pp. 101–122, 2021.

[20] H. Wei, L. Shen, and D. Wang, "Current Situation and Development Trend of 5G Millimeter Wave," in *2020 Management Science Informatization and Economic Innovation Development Conference (MSIEID)*. IEEE, dec 2020.

[21] A. Ghosh, A. Maeder, M. Baker, and D. Chandramouli, "5G Evolution: A View on 5G Cellular Technology Beyond 3GPP Release 15," *IEEE Access*, vol. 7, pp. 127 639–127 651, 2019.

[22] Technical Specification Group Services and System Aspects, " TR 21.916 V1.0.0," 3rd Generatio Partnership Project, Tech. Rep., 2020.

[23] M. Weiser, "The Computer for the 21st Century," *Scientific American*, 1991.

[24] S. Chen, H. Xu, D. Liu, B. Hu, and H. Wang, "A Vision of IoT: Applications, Challenges, and Opportunities With China Perspective," *IEEE Internet of Things Journal*, vol. 1, no. 4, pp. 349–359, aug 2014.

[25] M. R. Palattella, M. Dohler, A. Grieco, G. Rizzo, J. Torsner, T. Engel, and L. Ladid, "Internet of Things in the 5G Era: Enablers, Architecture, and Business Models," *IEEE Journal on Selected Areas in Communications*, vol. 34, no. 3, pp. 510–527, 2016.

[26] M. Compare, P. Baraldi, and E. Zio, "Challenges to IoT-Enabled Predictive Maintenance for Industry 4.0," *IEEE Internet of Things Journal*, vol. 7, no. 5, pp. 4585–4597, may 2020.

[27] S. K. Panda, A. Blome, L. Wisniewski, and A. Meyer, "IoT Retrofitting Approach for the Food Industry," in *2019 24th IEEE International Conference on Emerging Technologies and Factory Automation (ETFA)*. IEEE, sep 2019.

[28] W. A. Jabbar, T. K. Kian, R. M. Ramli, S. N. Zubir, N. S. M. Zamrizaman, M. Balfaqih, V. Shepelev, and S. Alharbi, "Design and Fabrication of Smart Home With Internet of Things Enabled Automation System," *IEEE Access*, vol. 7, pp. 144 059–144 074, 2019.

[29] K. Agarwal, A. Agarwal, and G. Misra, "Review and Performance Analysis on Wireless Smart Home and Home Automation using IoT," in *2019 Third International conference on I-SMAC (IoT in Social, Mobile, Analytics and Cloud) (I-SMAC)*. IEEE, dec 2019.

[30] E. Anthi, L. Williams, M. Slowinska, G. Theodorakopoulos, and P. Burnap, "A Supervised Intrusion Detection System for Smart Home IoT Devices," *IEEE Internet of Things Journal*, vol. 6, no. 5, pp. 9042–9053, oct 2019.

[31] S. M. R. Islam, D. Kwak, M. H. Kabir, M. Hossain, and K.-S. Kwak, "The Internet of Things for Health Care: A Comprehensive Survey," *IEEE Access*, vol. 3, pp. 678–708, 2015.

[32] S. S. Vedaei, A. Fotovvat, M. R. Mohebbian, G. M. E. Rahman, K. A. Wahid, P. Babyn, H. R. Marateb, M. Mansourian, and R. Sami, "COVID-SAFE: An IoT-Based System for Automated Health Monitoring and Surveillance in Post-Pandemic Life," *IEEE Access*, vol. 8, pp. 188 538–188 551, 2020.

[33] P. Verma and S. K. Sood, "Fog Assisted-IoT Enabled Patient Health Monitoring in Smart Homes," *IEEE Internet of Things Journal*, vol. 5, no. 3, pp. 1789–1796, jun 2018.

[34] A. P. Singh, A. K. Luhach, X.-Z. Gao, S. Kumar, and D. S. Roy, "Evolution of Wireless Sensor Network Design from Technology Centric to User Centric: An Architectural Perspective," *International Journal of Distributed Sensor Networks*, vol. 16, no. 8, p. 155014772094913, aug 2020.

[35] M. U. Aftab, O. Ashraf, M. Irfan, M. Majid, A. Nisar, and M. A. Habib, "A Review Study of Wireless Sensor Networks and Its Security," *Communications and Network*, vol. 07, no. 04, pp. 172–179, 2015.

[36] K. Lin and T. Hao, "Experimental Link Quality Analysis for LoRa-Based Wireless Underground Sensor Networks," *IEEE Internet of Things Journal*, vol. 8, no. 8, pp. 6565–6577, apr 2021.

[37] ——, "Link Quality Analysis of Wireless Sensor Networks for Underground Infrastructure Monitoring: A Non-Backfilled Scenario," *IEEE Sensors Journal*, vol. 21, no. 5, pp. 7006–7014, mar 2021.

[38] A. R. Silva and M. Moghaddam, "Design and Implementation of Low-Power and Mid-Range Magnetic-Induction-Based Wireless Underground Sensor Networks," *IEEE Transactions on Instrumentation and Measurement*, vol. 65, no. 4, pp. 821–835, apr 2016.

[39] V. Kumar and V. K. Sinha, "Underwater Wireless Sensor Network Routing Protocols: The Survey," in *2020 2nd International Conference on Advances in Computing, Communication Control and Networking (ICACCCN)*. IEEE, dec 2020.

[40] J. Luo, Y. Chen, M. Wu, and Y. Yang, "A Survey of Routing Protocols for Underwater Wireless Sensor Networks," *IEEE Communications Surveys & Tutorials*, vol. 23, no. 1, pp. 137–160, 2021.

[41] M. Nain and N. Goyal, "Localization Techniques in Underwater Wireless Sensor Network," in *2021 International Conference on Advance Computing and Innovative Technologies in Engineering (ICACITE)*. IEEE, mar 2021.

[42] T. Vladimirova, X. Wu, and C. P. Bridges, "Development of a Satellite Sensor Network for Future Space Missions," in *2008 IEEE Aerospace Conference*. IEEE, mar 2008.

[43] T. Vladimirova, C. P. Bridges, J. R. Paul, S. A. Malik, and M. N. Sweeting, "Space-based Wireless Sensor Networks: Design Issues," in *2010 IEEE Aerospace Conference*. IEEE, mar 2010.

[44] S. Zafar, A. Bashir, and S. A. Chaudhry, "Mobility-Aware Hierarchical Clustering in Mobile Wireless Sensor Networks," *IEEE Access*, vol. 7, pp. 20 394–20 403, 2019.

[45] M. Iloridou and F.-N. Pavlidou, "Adaptive Global Reclustering in MWSNs," *IEEE Internet of Things Journal*, vol. 7, no. 6, pp. 4862–4871, jun 2020.

[46] J. Guo and H. Jafarkhani, "Movement-Efficient Sensor Deployment in Wireless Sensor Networks With Limited Communication Range," *IEEE Transactions on Wireless Communications*, vol. 18, no. 7, pp. 3469–3484, jul 2019.

[47] M. A. Jan, M. Usman, X. He, and A. U. Rehman, "SAMS: A Seamless and Authorized Multimedia Streaming Framework for WMSN-Based IoMT," *IEEE Internet of Things Journal*, vol. 6, no. 2, pp. 1576–1583, apr 2019.

[48] A. Yazici, M. Koyuncu, S. A. Sert, and T. Yilmaz, "A Fusion-Based Framework for Wireless Multimedia Sensor Networks in Surveillance Applications," *IEEE Access*, vol. 7, pp. 88 418–88 434, 2019.

[49] B. A. Y. Alqaralleh, S. N. Mohanty, D. Gupta, A. Khanna, K. Shankar, and T. Vaiyapuri, "Reliable Multi-Object Tracking Model Using Deep Learning and Energy Efficient Wireless Multimedia Sensor Networks," *IEEE Access*, vol. 8, pp. 213 426–213 436, 2020.

[50] C. Larsson, "The Internet of Things," in *5G Networks*. Elsevier, 2018, pp. 349–386.

[51] O. Cayirpunar, E. K. Urtis, and B. Tavli, "Mobile Base Station Position Optimization for Network Lifetime Maximization in Wireless Sensor Networks," in *2013 21st Signal Processing and Communications Applications Conference (SIU)*. IEEE, apr 2013.

[52] L. Shi, Y. Hu, J. Xu, Y. Shi, and X. Ding, "The Mobile Base Station Strategy for Wireless Networks With Successive Interference Cancellation," *IEEE Access*, vol. 7, pp. 88 570–88 578, 2019.

[53] G. E. Moore, "Cramming More Components onto Integrated Circuits, Reprinted from Electronics, Volume 38, Number 8, April 19, 1965, Pp.114 Ff." *IEEE Solid-State Circuits Society Newsletter*, vol. 11, no. 3, pp. 33–35, 2006.

[54] R. W. Keyes, "The Impact of Moore's Law," *IEEE Solid-State Circuits Society Newsletter*, vol. 11, no. 3, pp. 25–27, 2006.

[55] R. K. Cavin, P. Lugli, and V. V. Zhirnov, "Science and Engineering Beyond Moore's Law," *Proceedings of the IEEE*, vol. 100, no. Special Centennial Issue, pp. 1720–1749, 2012.

[56] P. Gelsinger, "Moore's Law – The Genius Lives On," *IEEE Solid-State Circuits Society Newsletter*, vol. 11, no. 3, pp. 18–20, 2006.

[57] S. Kumar, L. Wang, C. Wu, D. Henry, and A. Kurtz, "Preparing Students for an Embedded Everywhere World," 12 2006.

[58] M. Magno, F. Vultier, B. Szebedy, H. Yamahachi, R. H. R. Hahnloser, and L. Benini, "A Bluetooth-Low-Energy Sensor Node for Acoustic Monitoring of Small Birds," *IEEE Sensors Journal*, vol. 20, no. 1, pp. 425–433, jan 2020.

[59] D. G. Costa, "Visual Sensors Hardware Platforms: A Review," *IEEE Sensors Journal*, vol. 20, no. 8, pp. 4025–4033, apr 2020.

[60] C. Hao and C. Jiang, "Robust Wireless Sensor Network Against Strong Electromagnetic Pulse," *IEEE Sensors Journal*, vol. 21, no. 4, pp. 5572–5579, feb 2021.

[61] M. Matin and M. Islam, "Overview of Wireless Sensor Network," in *Wireless Sensor Networks - Technology and Protocols*. InTech, sep 2012.

[62] H. Yetgin, K. T. K. Cheung, M. El-Hajjar, and L. Hanzo, "A Survey of Network Lifetime Maximization Techniques in Wireless Sensor Networks," *IEEE Communications Surveys & Tutorials*, vol. 19, no. 2, pp. 828–854, 2017.

[63] "IEEE standard for telecommunications and information exchange between systems - LAN/MAN - specific requirements - part 15: Wireless medium access control (MAC) and physical layer (PHY) specifications for wireless personal area networks (WPANs)."

[64] V. K. Garg, "Wireless Personal Area Network — Bluetooth," in *Wireless Communications & Networking*. Elsevier, 2007, pp. 653–674.

[65] A. Nikoukar, S. Raza, A. Poole, M. Gunes, and B. Dezfouli, "Low-Power Wireless for the Internet of Things: Standards and Applications," *IEEE Access*, vol. 6, pp. 67 893–67 926, 2018.

[66] M. Wolf, "Standard Interfaces," in *Embedded System Interfacing*. Elsevier, 2019, pp. 23–40.

[67] F. U. Khan, M. Awais, M. B. Rasheed, B. Masood, and Y. Ghadi, "A Comparison of Wireless Standards in IoT for Indoor Localization Using LoPy," *IEEE Access*, vol. 9, pp. 65 925–65 933, 2021.

[68] "IEEE Standard for Wireless LAN Medium Access Control (MAC) and Physical Layer (PHY) specifications," *IEEE Std 802.11-1997*, pp. 1–445, 1997.

[69] "IEEE Standard for Telecommunications and Information Exchange Between Systems - LAN/MAN Specific Requirements - Part 11: Wireless Medium Access Control (MAC) and physical layer (PHY) specifications: High Speed Physical Layer in the 5 GHz band," *IEEE Std 802.11a-1999*, pp. 1–102, 1999.

[70] "IEEE Draft Standard for Information Technology - Telecommunications and information exchange between systems - Local and Metropolitan networks - Specific requirements - Part 11: Wireless LAN Medium Access Control (MAC) and Physical Layer (PHY) specifications - Amendment x : Technical corrections and clarifications," *IEEE Std P802.11ma/D3.0*, pp. 1–1026, 1999.

[71] "IEEE Standard for Information technology– Local and metropolitan area networks– Specific requirements– Part 11: Wireless LAN Medium Access Control (MAC) and Physical Layer (PHY) Specifications: Further Higher Data Rate Extension in the 2.4 GHz Band," *IEEE Std 802.11g-2003 (Amendment to IEEE Std 802.11, 1999 Edn. (Reaff 2003) as amended by IEEE Stds 802.11a-1999, 802.11b-1999, 802.11b-1999/Cor 1-2001, and 802.11d-2001)*, pp. 1–104, 2003.

[72] "IEEE Standard for Information technology– Local and metropolitan area networks– Specific requirements– Part 11: Wireless LAN Medium Access Control (MAC)and Physical Layer (PHY) Specifications Amendment 5: Enhancements for Higher Throughput," *IEEE Std 802.11n-2009 (Amendment to IEEE Std 802.11-2007 as amended by IEEE Std 802.11k-2008, IEEE Std 802.11r-2008, IEEE Std 802.11y-2008, and IEEE Std 802.11w-2009)*, pp. 1–565, 2009.

[73] "IEEE Standard for Information technology–Telecommunications and information exchange between systems—Local and metropolitan area networks–Specific requirements–Part 11: Wireless LAN Medium Access Control (MAC) and Physical Layer (PHY) Specifications–Amendment 4: Enhancements for Very High Throughput for Operation in Bands below 6 GHz." *IEEE Std 802.11ac(TM)-2013 (Amendment to IEEE Std 802.11-2012, as amended by IEEE Std 802.11ae-2012, IEEE Std 802.11aa-2012, and IEEE Std 802.11ad-2012)*, pp. 1–425, 2013.

[74] "IEEE Draft Standard for Information Technology – Telecommunications and Information Exchange Between Systems Local and Metropolitan Area Networks – Specific Requirements Part 11: Wireless LAN Medium Access Control (MAC) and Physical Layer (PHY) Specifications Amendment Enhancements for High Efficiency WLAN," *IEEE P802.11ax/D3.0, June 2018*, pp. 1–682, 2018.

[75] C. A. Trasvina-Moreno, A. Asensio, R. Casas, R. Blasco, and A. Marco, "WiFi Sensor Networks: A Study of Energy Consumption," in *2014 IEEE 11th International Multi-Conference on Systems, Signals & Devices (SSD14)*. IEEE, feb 2014.

[76] G. Huang, D. Chen, and X. Liu, "A Node Deployment Strategy for Blindness Avoiding in Wireless Sensor Networks," *IEEE Communications Letters*, vol. 19, no. 6, pp. 1005–1008, jun 2015.

[77] T. O. Olasupo and C. E. Otero, "A Framework for Optimizing the Deployment of Wireless Sensor Networks," *IEEE Transactions on Network and Service Management*, vol. 15, no. 3, pp. 1105–1118, sep 2018.

[78] C. E. Otero, W. H. Shaw, I. Kostanic, and L. D. Otero, "Multiresponse Optimization of Stochastic WSN Deployment Using Response Surface Methodology and Desirability Functions," *IEEE Systems Journal*, vol. 4, no. 1, pp. 39–48, mar 2010.

[79] T. O. Olasupo and C. E. Otero, "The Impacts of Node Orientation on Radio Propagation Models for Airborne-Deployed Sensor Networks in Large-Scale Tree Vegetation Terrains," *IEEE Transactions on Systems, Man, and Cybernetics: Systems*, vol. 50, no. 1, pp. 256–269, jan 2020.

[80] D. Deif and Y. Gadallah, "Wireless Sensor Network Deployment Using Stochastic Optimization Techniques - a Comparative Study," in *2015 International Conference on Computing and Network Communications (CoCoNet)*. IEEE, dec 2015.

[81] R. E. Mohamed, A. I. Saleh, M. Abdelrazzak, and A. S. Samra, "Survey on Wireless Sensor Network Applications and Energy Efficient Routing Protocols," *Wireless Personal Communications*, vol. 101, no. 2, pp. 1019–1055, may 2018.

[82] H. Luo, K. Wu, Z. Guo, L. Gu, and L. M. Ni, "Ship Detection with Wireless Sensor Networks," *IEEE Transactions on Parallel and Distributed Systems*, vol. 23, no. 7, pp. 1336–1343, jul 2012.

[83] A. Ali, Y. K. Jadoon, S. A. Changazi, and M. Qasim, "Military Operations: Wireless Sensor Networks based Applications to Reinforce Future Battlefield Command System," in *2020 IEEE 23rd International Multitopic Conference (INMIC)*. IEEE, nov 2020.

[84] A. J. AL-Mousawi and H. K. AL-Hassani, "A Survey in Wireless Sensor Network for Explosives Detection," *Computers & Electrical Engineering*, vol. 72, pp. 682–701, nov 2018.

[85] O. Bouhamed, H. Ghazzai, H. Besbes, and Y. Massoud, "A UAV-Assisted Data Collection for Wireless Sensor Networks: Autonomous Navigation and Scheduling," *IEEE Access*, vol. 8, pp. 110 446–110 460, 2020.

[86] L. Shu, M. Mukherjee, X. Xu, K. Wang, and X. Wu, "A Survey on Gas Leakage Source Detection and Boundary Tracking with Wireless Sensor Networks," *IEEE Access*, vol. 4, pp. 1700–1715, 2016.

[87] M. Bal, "An Industrial Wireless Sensor Networks Framework for Production Monitoring," in *2014 IEEE 23rd International Symposium on Industrial Electronics (ISIE)*. IEEE, jun 2014.

[88] J. Lentz, S. Hill, B. Schott, M. Bal, and R. Abrishambaf, "Industrial Monitoring and Troubleshooting Based on LoRa Communication Technology," in *IECON 2018 - 44th Annual Conference of the IEEE Industrial Electronics Society*. IEEE, oct 2018.

[89] I. F. Akyildiz and M. C. Vuran, "Applications of Wireless Sensor Networks," in *Wireless Sensor Networks*. John Wiley & Sons, Inc., 2010, pp. 38–74.

[90] J. Wang, Y. Xiao, T. Li, and C. L. P. Chen, "A Survey of Technologies for Unmanned Merchant Ships," *IEEE Access*, vol. 8, pp. 224 461–224 486, 2020.

[91] Y. Zhang, L. Sun, H. Song, and X. Cao, "Ubiquitous WSN for Healthcare: Recent Advances and Future Prospects," *IEEE Internet of Things Journal*, vol. 1, no. 4, pp. 311–318, aug 2014.

[92] A. Alaiad and L. Zhou, "Patients' Adoption of WSN-Based Smart Home Healthcare Systems: An Integrated Model of Facilitators and Barriers," *IEEE Transactions on Professional Communication*, vol. 60, no. 1, pp. 4–23, mar 2017.

[93] V. R. Shinde, P. P. Tasgaonkar, and R. D. Garg, "Environment Monitoring System through Internet of Things(IT)," in *2018 International Conference on Information , Communication, Engineering and Technology (ICICET)*. IEEE, aug 2018.

[94] L. K. Hema, D. Murugan, and R. M. Priya, "Wireless Sensor Network Based Conservation of Illegal Logging of Forest Trees," in *2014 IEEE National Conference on Emerging Trends In New & Renewable Energy Sources And Energy Management (NCET NRES EM)*. IEEE, dec 2014.

[95] J. Joshi, S. Mukherjee, R. Kumar, P. Awasthi, M. Deka, D. S. Kurian, S. Mittal, and B. Birdi, "Monitoring of Earth Air Tunnel (EAT) a smart cooling system using Wireless Underground Sensor Network," in *2016 International Conference on Wireless Communications, Signal Processing and Networking (WiSPNET)*. IEEE, mar 2016.

[96] P. Fernandez-Martinez, S. Martin-Anton, and D. Segovia-Vargas, "Design of a wideband vivaldi antenna for 5g base stations," in *2019 IEEE International Symposium on Antennas and Propagation and USNC-URSI Radio Science Meeting*. IEEE, jul 2019.

[97] P. Liu, J. Zhang, S. Lu, and J. Lin, "Design and Achievement of Miniaturization in Wi-fi Base Station Antenna," in *Proceedings of 2014 3rd Asia-Pacific*

Conference on Antennas and Propagation. IEEE, jul 2014.

[98] L. Hong, W. An, and S. Li, "A Broadband Solar Antenna Element for Base Station," in *2018 IEEE International Conference on Signal Processing, Communications and Computing (ICSPCC)*. IEEE, sep 2018.

[99] Y.-L. Chen and Q.-X. Chu, "A Novel Filter Antenna for Base Station," in *2019 IEEE-APS Topical Conference on Antennas and Propagation in Wireless Communications (APWC)*. IEEE, sep 2019.

[100] Texas Instruments Incorporated, "2.4-ghz inverted f antenna, swru120d," April 2007–Revised January 2019.

[101] R. Bourtoutian, C. Delaveaud, and S. Toutain, "Differential Antenna Design and Characterization," in *2009 3rd European Conference on Antennas and Propagation*, 2009, pp. 2398–2402.

[102] N. Pires, T. Parra, A. K. Skrivervik, and A. A. Moreira, "Design and Measurement of a Differential Printed Antenna for a Wireless Sensor Network Node," *IEEE Antennas and Wireless Propagation Letters*, vol. 16, pp. 2228–2231, 2017.

[103] P. Nepa, G. Manara, S. Mugnaini, G. Tribellini, S. Cioci, G. Albasini, and E. Sacchi, "Differential Planar Antennas for 2.4/5.2 GHz WLAN Applications," in *2006 IEEE Antennas and Propagation Society International Symposium*. IEEE, 2006.

[104] S. Gahgouh, H. Ragad, and A. Gharsallah, "Small Size Cubic Antenna Design for WSN," in *2017 18th International Conference on Sciences and Techniques of Automatic Control and Computer Engineering (STA)*. IEEE, dec 2017.

[105] K. Kim, J. Ahn, Y. Yoon, and K. Hwang, "Pattern Reconfigurable Antenna for Wireless Sensor Network System," *Electronics Letters*, vol. 48, no. 16, pp. 984–985, aug 2012.

[106] D. Guan, Y. Zhang, Z. Qian, Y. Li, W. Cao, and F. Yuan, "Compact Microstrip Patch Array Antenna With Parasitically Coupled Feed," *IEEE Transactions on Antennas and Propagation*, vol. 64, no. 6, pp. 2531–2534, 2016.

[107] K. Bangash, M. M. Ali, H. Maab, and H. Ahmed, "Design of a Millimeter Wave Microstrip Patch Antenna and Its Array for 5G Applications," in *2019 International Conference on Electrical, Communication, and Computer Engineering (ICECCE)*, 2019, pp. 1–6.

[108] J. Xu, W. Hong, Z. H. Jiang, and H. Zhang, "Wideband, Low-Profile Patch Array Antenna With Corporate Stacked Microstrip and Substrate Integrated Waveguide Feeding Structure," *IEEE Transactions on Antennas and Propagation*, vol. 67, no. 2, pp. 1368–1373, 2019.

[109] P. A. Dzagbletey and Y. Jung, "Stacked Microstrip Linear Array for Millimeter-Wave 5G Baseband Communication," *IEEE Antennas and Wireless Propagation Letters*, vol. 17, no. 5, pp. 780–783, 2018.

[110] M. Wang, H. Wang, J. Cao, J. Zhou, G. Liang, L. Wang, and S. Jiang, "A Ka-Band High-Gain Dual-Polarized Microstrip Antenna Array for 5G Application," in *2019 International Conference on Microwave and Millimeter Wave Technology (ICMMT)*, 2019, pp. 1–3.

[111] S. J. Yang, Y. M. Pan, L. Shi, and X. Y. Zhang, "Millimeter-Wave Dual-Polarized Filtering Antenna for 5G Application," *IEEE Transactions on Antennas and Propagation*, vol. 68, no. 7, pp. 5114–5121, 2020.

[112] S. M. Sarwar, M. F. F. Chowdhury, and H. S. Das, "A Dual Band Shark Fin Integrated Vehicle Antenna For 5G and Wi-Max Applications," in *2019 IEEE International Conference on Telecommunications and Photonics (ICTP)*, 2019, pp. 1–4.

[113] H.-D. Lu, L.-M. Si, and Y. Liu, "Compact Planar Microstrip-fed Quasi-yagi Antenna," *Electronics Letters*, vol. 48, no. 3, p. 140, 2012.

[114] T. C. Edwards and M. B. Steer, "Fundamentals of Signal Transmission on Interconnects," in *Foundations of Interconnect and Microstrip Design*. John Wiley & Sons, Ltd, dec 2013, pp. 1–29.

[115] R. Douville and D. James, "Experimental Study of Symmetric Microstrip Bends and Their Compensation," *IEEE Transactions on Microwave Theory and Techniques*, vol. 26, no. 3, pp. 175–182, mar 1978.

[116] C. A. Balanis, *Antenna Theory: Analysis and Design, 3rd Edition*. John Wiley & Sons, 2005, vol. 72.

[117] S.-J. Wang, L. Li, and M. Fang, "A Novel Compact Differential Microstrip Antenna," *Progress In Electromagnetics Research Letters*, vol. 57, pp. 97–101, 2015.

[118] B. Wadell, *Transmission Line Design Handbook*. Boston: Artech House, 1991.

[119] B. L. Shrestha, H. C. Wood, and S. Sokhansanj, "Modeling of Vegetation Permittivity at Microwave Frequencies," *IEEE Transactions on Geoscience and Remote Sensing*, vol. 45, no. 2, pp. 342–348, feb 2007.

[120] K. McGrattan, R. McDermott, S. Hostikka, J. Floyd, and M. Vanella, *Fire Dynamics Simulator*, sixth edition ed., 2018.

[121] S. S. Faria, N. Leonor, C. A. Fernandes, J. Felicio, C. Salema, and R. F. S. Caldeirinha, "Radiowave Propagation Modelling in the Presence of Wildfires: Initial Results," in *2020 14th European Conference on Antennas and*

Propagation (EuCAP). IEEE, mar 2020.

[122] K. M. Mphale and M. L. Heron, "Plant Alkali Content and Radio Wave Communication Efficiency in High Intensity Savanna Wildfires," *Journal of Atmospheric and Solar-Terrestrial Physics*, vol. 69, no. 4-5, pp. 471–484, apr 2007.

[123] Pycom, "Lopy4, datasheet v1.1," Nov. 2021. [Online]. Available: https://docs.pycom.io/datasheets/development/lopy4/

DECLARATION

Declaro, sob compromisso de honra, que o trabalho apresentado nesta dissertação, com o título *" Small Antennas for 5G and IoT "*, é original e foi realizado por Tiago Emanuel da Silva Oliveira (2192599) sob orientação de Professor Rafael F. S. Caldeirinha (rafael.caldeirinha@ipleiria.pt) e Professor João R. Reis (joao.reis@ipleiria.pt).

Leiria, November of 2021

Assinado por: **Tiago Emanuel da Silva Oliveira**
Num. de Identificação: 14131218
Data: 2022.01.19 18:12:01+00'00'

Tiago Emanuel da Silva Oliveira